A MULTIWAVELENGTH DETECTOR AND HYDRODYNAMIC CHROMATOGRAPHY SYSTEM FOR THE DETERMINATION OF PARTICLE SIZE AND SIZE DISTRIBUTION

by

Charles Robert Knipe Jr.

Dissertation submitted to the Graduate Faculty of the Virginia Polytechnic Institute and State University in partial fulfillment of the requirements for the degree of

DOCTOR OF PHILOSOPHY

in

Chemistry

APPROVED:

R. E. Dessy, Chairman

A. F. Clifford

J. E. McGrath

J. G. Mason

J. F. Wolfe

December, 1983

Blacksburg, Virginia

A Multiwavelength Detector and Hydrodynamic Chromatography System for the Determination of Particle Size and Size Distribution

by

Charles Robert Knipe Jr.

(ABSTRACT)

The knowledge of particle size and size distribution are important parameters for understanding the behavior of numerous colloid systems. These areas include for example, clays, viruses, paints and blood. Until recently this information could be obtained only by the use of expensive, slow and complex instrumentation.

Hydrodynamic chromatography provides a means of investigating particles in the submicron and micron region. The separation mechanism of this method is based upon the flow parameters with which the solute particles interact as they pass through a packed column. In the past the interpretation of these chromatograms has been based upon the mathematical modeling of the column parameters.

We have developed a new multiwavelength detector system to be used in conjunction with hydrodynamic chromatography which provides size and concentration information of the eluant directly. The result is a rugged system that

provides size and size distribution information rapidly and at low cost.

to Janet

Acknowledgements

I am grateful to many people who have contributed greatly to this project. I want to especially thank my parents for their continued support in all aspects of my personal development. I also want to thank my wife, Janet, for her loving support and unselfish sacrifices on my behalf.

I would like to thank Union Carbide for their financial support for this work, and Stan Hager and James Hatfield from Union Carbide who supplied valuable information and industrial samples. I am indebted to Martin Langhorst of Dow Chemical for supplying the hydrodynamic chromatography column. The chemistry glass and electronic shops provided valuable expertise for some of the logistical problems. Steve Dueball provided the software for the plotting routines and the communication to the laser printer.

I want to express my appreciation to my fellow graduate students and Professor Dessy for providing a unique atmosphere for research and the exchange of ideas. The members of the group provided an essential stabilizing force for which I am thankful.

Table of Contents

	Page
Abstract	ii
Acknowledgements	v
Table of Contents	vi
List of Figures	viii
List of Tables	x
I. Introduction	1
II. Historical	5
A. Size Analysis by Light Scattering	5
B. Hydrodynamic Chromatography	10
C. Detector Systems	14
III. Detector Fabrication	16
A. Background	16
B. Photodiode Connection and Packaging	16
C. Aperture and Filter Construction	17
D. Array Testing and Performance	25
IV. Detector Support Components	36
A. Electronics	36
B. Optics	45
C. Computer Network	48
D. Software	51
V. Light Scattering	54
A. Theory	54
B. Size Analysis of Monodispersed Systems	59

page

C. Bimodal Systems 61

D. Use of Linear Parameter Estimation . . . 65

E. Non-negative Least Squares 70

F. Size Determination in a Flowing System . 71

IV. Hydrodynamic Chromatography 79

A. Theory 79

B. Column Evaluation 81

C. Monodispersed Samples 84

D. Bimodal Samples 93

E. Polydispersed Sample 93

VII. Summary 100

VIII. References 104

IX. Software Appendix 107

X. Vita 134

List of Figures

Figures		page
1.	$(\tau/c)_o$ versus size curve	9
2.	Isotronic package	18
3.	Internal lay-out of array	19
4.	Pin-out of array	20
5.	Aperture mask positive	22
6.	Exploded view of array	26
7.	Optical test set-up	27
8.	Photodiode spectral response	28
9.	Transmittance of Epo-tec 301 epoxy	29
10.	Transmittance of interference filter (640nm.).	30
11.	Overlap of the interference filter transmittances	33
12.	Diode response with only one diode exposed	34
13.	Electronic circuitry	39
14.	Operational amplifier P.C. board positive	40
15.	Header board P.C. board positive	41
16.	Operational Amplifier connections to the A/D	43
17.	Overview of the electronic cabling	44
18.	Optical lay-out	46
19.	Computer Network	49
20.	Q ratio versus size	58
21.	Turbidity versus concentration (0.166μ)	62
22.	Turbidity versus concentration (0.50μ)	63
23.	Turbidity versus concentration (1.16μ)	64

Figure page

24. 1.16μ sample, flow rate = 1.6 mls./min. . . . 75

25. 1.16μ sample, flow rate = 2.0 mls./min. . . . 76

26. 1.16μ sample, flow rate = 2.4 mls./min. . . . 77

27. 1.16μ sample, flow rate = 3.2 mls./min. . . . 78

28. Size exclusion chromatography 80

29. Hydrodynamic chromatography 82

30. Chromatographic set-up 83

31. R_f versus diameter 85

32. Chromatogram of monodispersed 0.73μ 88

33. Chromatogram of monodispersed 0.325μ 89

34. Chromatogram of monodispersed 0.166μ 90

35. Chromatogram of monodispersed 0.50μ 91

36. Size analysis of monodispersed 0.50μ 92

37. Chromatogram of bimodal mixture (0.325μ-0.73μ) 94

38. Size analysis of bimodal mixture (0.325μ-0.73μ) 95

39. Chromatogram of Union Carbide 14FR10 latex . . 97

40. Size analysis of Union Carbide 14FR10 latex . 98

41. Comparison of techniques 99

List of Tables

Table		page
1.	ADC Channel Assignments	42
2.	Monodispersed Sample Analysis	60
3.	Bimodal Mixtures (1.16μ - 0.5μ)	66
4.	Bimodal Mixtures (1.16μ - 0.16μ)	67
5.	Trimodal Mixture (1.16μ - 0.50μ - 0.166μ) . . .	72
6.	Comparison of R_f Values	86

INTRODUCTION

A recurring problem for scientists in many fields is the measurement and characterization of particles in the micron and submicron size region (0.1 to 5.0 microns). Chemists are interested in monitoring polymers and colloidal dispersions in investigations of physical and chemical properties as well as controlling size for commercial applications. Biologists often need to characterize naturally occurring polymers, microscopic structures (viruses, cells) and do aggregation and agglutination studies. Many others need to characterize the constituents of our atmosphere. Pollution monitoring, meteorology and communications (satellite, missile guidance, etc.) are all highly dependent upon the size and composition of elements in our atmosphere.

The most common tools in operation which can yield this information are: transmission electron microscopy(TEM), disc centrifuge, gel permeation chromatoography(GPC), and light scattering. TEM can give directly particle size and concentration; however, it suffers from numerous drawbacks. One of the major problems is the lengthy sample preparation and analysis time required. Samples cannot be examined in situ and results

are affected by the preparation method. After such preparation, analysis by a skilled operator can take hours to days if photographs are taken and analyzed. The technique does not provide information on the chemical make-up of the sample, and also requires expensive equipment and specially trained personnel. The disc centrifuge suffers from long analysis times (hours) and inability to do in situ measurements. Centrifugation can detect particles only larger than 0.25 microns.

Gel permeation chromatography is applied primarily to particles from 50 to 500 angstroms and can do analysis in from 10 minutes to several hours. Again, analyses can not be done in situ, but the instrumentation is readily available and reasonably priced. It has been only recently that a form of GPC has been used to investigate larger sized particles (0.1 to 5 microns). Hamish Small introduced the concept of hydrodynamic chromatography (HDC) at Dow Chemical in 1974 (1). However, due to the column technology at the time, long analysis times were required. Since then many advances have been made in column packings and the analysis time has been reduced. This technique still suffers from lack of resolution.

Light scattering methods vary with the detection scheme used, but are valid over a large size range and in general are a non-intrusive, rapid method of analysis.

One of the simplest, yet most informative methods, is to determine the extinction of incident radiation by the sample at a prescribed angle. A primary disadvantage of this method is that the results give an average size for polydispersed samples. Theoretically if one were to monitor a large enough number of wavelengths one could determine absolutely the number of each size present. To make matters more manageable this detection scheme could be coupled with a separation scheme such as HDC to help limit the polydispersity. This concept has already been proposed by A. Hamielic of McMasters University for simultaneous particle size determination and determination of the refractive index of the particles (2).

In order to make better use of the light scattering method a multiwavelength detection system is required. There are numerous multiwavelength schemes available. The choices are (1) a system that mechanically scans a wavelength region and time multiplexes the signal or (2) one involving dispersive optics and spatially separates the wavelength information over several detectors. The first is usually slow, the latter expensive. It was decided to investigate a new detector system which is both low in cost and rugged. This system involves using a white light source, and a new detector which consists of a package of individual photodiodes each covered by a unique

interference filter.

This research project falls primarily into three catagories:

I. To investigate the characteristics of the new detector system and examine its attributes.

II. To show the utility of this system for particle sizing in both static and flowing systems.

III. To investigate the applicability of this detection system for absolute particle size analysis in conjunction with hydrodynamic chromatography.

HISTORICAL

A. Size Analysis by Light Scattering

The interest in the interaction of light with discrete particles is centuries old. It has been only over the last 150 years that these interactions have been understood well enough to quantify the observations. Early researchers such as Tyndall, Govi, and Rayleigh were interested in the color and polarization produced by different aerosols. Rayleigh is generally recognized as the one who set down the mathematical relationships between the incident light and particles (3). These relationships, however, are valid only when the diameter of the particles are much smaller than the wavelength of incident light hitting it. In 1908 Gustav Mie published his work relating dielectric spheres with diameters of approximately the same size as the incident radiation to their scattering properties (4). Much of the work on the characterization of aerosols and hydrosols has been based on this theory.

Of the various methods for particle size analysis by light scattering, transmission methods are the most common and widely used. The applicability of using transmission

for particle sizing based upon Mie theory was investigated by LaMer and Barnes using monodisperse sulfur sols (5,6). Application of Mie theory to latex analysis was originally done by Tabibian, Heller, Epel (7), Bateman, Weneck, and Eschler (8), and Dezelic and Kratohvil (9). These early methods were based upon measurement of turbidity and concentration to determine the particle size.

The turbidity (τ) of a solution is defined as

$$\tau = 1/l \ln (I_o/I) \quad 2\text{-}1$$

where l is the path length of the transmission cell, I_o and I are the intensities of the incident and transmitted beams, respectively (10). Assuming a monodisperse sample of nonabsorbing isotropic spheres, Mie theory predicts the turbidity to be

$$\tau = N\pi r^2 Q_{sca}(\alpha,m) \quad 2\text{-}2$$

In this equation N is the particle concentration, r is the particle radius and Q_{sca} is the scattering coefficient. Q_{sca} is a function of m, the ratio of the refractive index of the scattering particle to the refractive index of the medium, and $\alpha = 2\pi r/\lambda_m = \pi D/\lambda_m$, where λ_m is the wavelength of the incident radiation in the medium.

If c is the concentration of scattering particles in grams per cubic centimeter and ρ is their density, then $c = 4/3\pi r^3 \rho N$ and equation 2-2 can be written as

$$\tau = (3Qc)/(4r\rho) = (3Qc)/(2\rho D) \quad 2\text{-}3$$

multiplying both sides of equation 2-3 by λ_m/π yields

$$(\lambda_m \tau)/\pi = (3Qc\lambda_m)/(2\rho\pi D) \quad 2\text{-}4$$

substituting $\alpha = \pi D/\lambda_m$ into equation 2-4

$$(\lambda_m \tau)/\pi = (3Qc)/(2\rho\alpha) \quad 2\text{-}5$$

rearranging 2-5, we obtain

$$(\tau/c)_o = (Q/\alpha)\ (3\pi/2\rho\lambda_m) \quad 2\text{-}6$$

The quantity $(\tau/c)_o$ is known as the specific turbidity. The zero subscript indicates that the ratio (τ/c) has to be extrapolated to $c = 0$ to satisfy the Mie theory requirement that there are no multiple scattering or mutual interactions of the particles (10).

A theoretical curve of $(\tau/c)_o$ versus α can be produced at the appropriate values of m and λ_m. (See Figure

1.) By comparision of the experimental results for the specific turbidity with the theoretical curve, the size parameter α can be obtained. Since the theoretical curves are not always single valued it is often necessary to determine the specific turbidity at several wavelengths to decide the particle size unambiguously.

Maron et al. conducted their experiments at wavelengths ranging from 350 to 1000 nanometers (10). Each study produced similar results, verifying the validity of this wavelength region for transmission measurements applied to particle size analysis.

The specific turbidity method suffers from the fact that both turbidity and concentration information is required. Dobbins and Jizmagian have shown that particle diameter and concentration can be obtained by measuring transmittances at two well separated wavelengths (11).

From equation 2-2 the turbidity ratio at two wavelengths is

$$\tau/\tau' = Q(\lambda)/Q'(\lambda') \qquad 2\text{-}7$$

Theoretical curves of the relative scattering coefficients versus particle size can be produced. From the experimentally measured turbidity ratio, the size can be determined. The wavelengths used are governed by the size re-

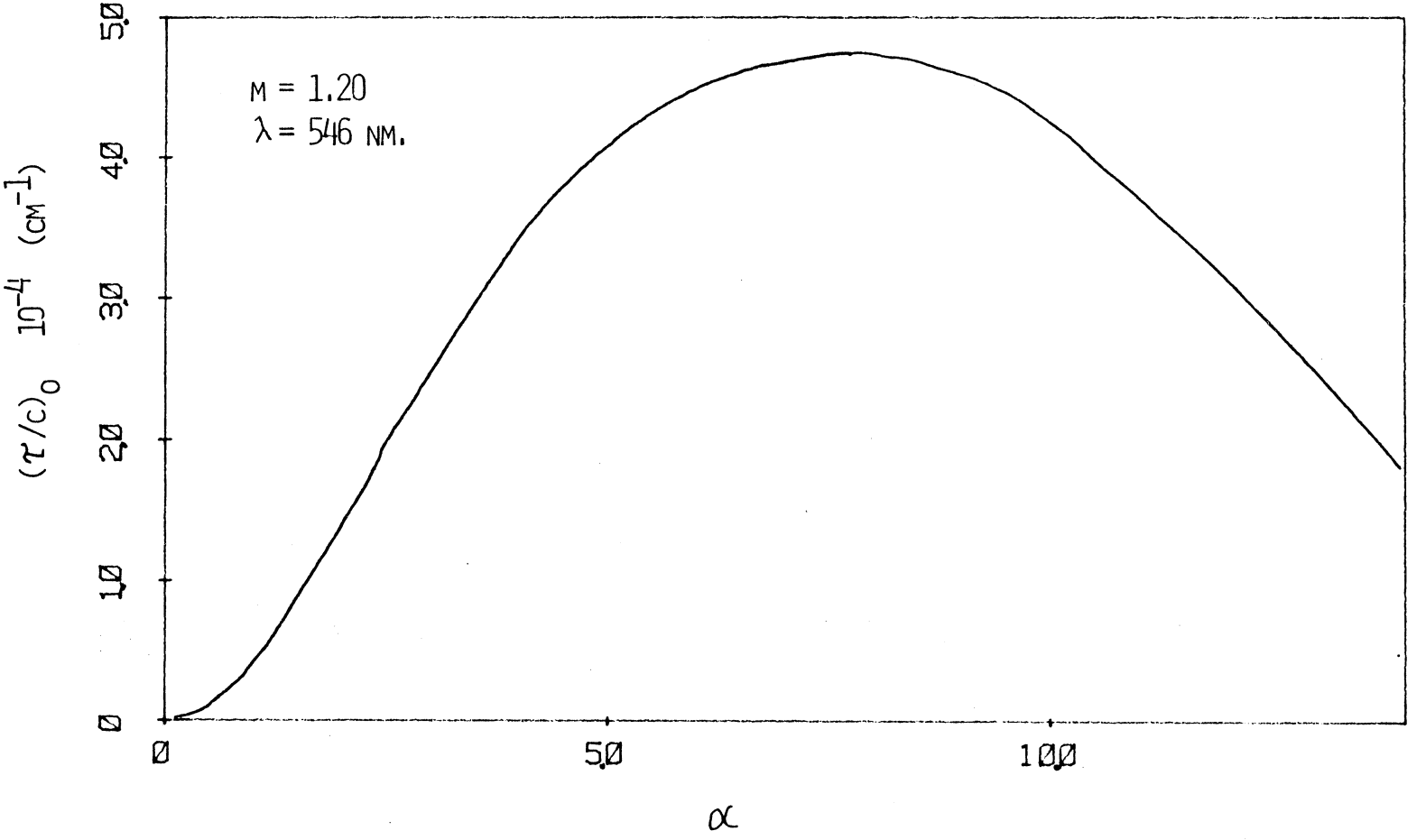

Figure 1. $(\tau/c)_o$ versus size

gion being investigated and the ratio of the refractive index of the particle to the refractive index of the medium (m). This method yields only an average size. Therefore it is of limited use in polydispersed systems. However if enough is known about the sample, a mathematical model of the distribution can be developed and used in conjunction with the transmission data. Yamamoto and Tanaka have made use of this method to analyze aerosols over Chesapeake Bay (12). Even in situations where the refractive index is not accurately known, transmission methods are valuable. Cashdollar et al. have shown the applicability of transmission methods to smoke particles that are not spherical and the refractive index can only be approximated. They were able to determine particle size and concentration, by monitoring three wavelengths and assuming a log-normal distribution function (13).

B. Hydrodynamic Chromatography

Over the last several decades chemists and biochemists have been very successful in using gel permeation chromatography to separate components by their molecular weight (size). The technique was originally used to

separate biological materials by passing them through a bed of cross-linked dextran gel. Separation by size takes place because the smaller molecules can fit into the small pores as they pass through the column. They are thus retained longer than the larger particles which are excluded from the pores and elute first. Since these gels are relatively soft and cannot be used under pressure, they require long analysis times. Semirigid organic gels such as cross-linked polystyrene or cross-linked styrene-divinylbenzene are more commonly used for the analysis of synthetic organic polymers . Rigid packings of inorganic material (silica) are also available for HPLC. The beads can be unmodified, as with controlled pore glass (CPG), or they may be modified with organic substituents. The advantages of rigid packings are their ease of packing homogeneously, versatility, and ability to handle high temperatures and pressures (14).

Traditionally gel permeation chromatography has been limited to separations in the size region of 60 to 10^5 angstroms. In 1974 Hamish Small proposed using standard chromatographic instrumentation to separate colloidal dispersions in the submicron range (1). Separations occurring in this size region are based on slightly different principles than in traditional gel permeation chromatography. Since colloidal sized particles will be ex-

cluded from the pores of the packing material, separation is due to the hydrodynamic forces which the particles experience as they flow through the packed bed, thus the term hydrodynamic chromatography. An alternative has been size analysis by flow through lengths of capillary tubing (15). Capillary hydrodynamic chromatography is limited to particles 1.0 micron in diameter and larger due to the flow velocities and tubing diameters necessary for separations to be observed.

Small's initial work was based on a combination of four to six columns each about three feet in length. These columns contained styrene/divinylbenzene copolymer and spherical glass packing. Major contributors to the flow characteristics are the ionic nature of the solution and packing material. The optimal packing material for latex particles is a cationic exchange resin. McGowan and Langhorst have been successful in performing separations on this material with columns of 50 cm., reducing analysis time from 90-120 to 5-10 minutes (16).

The only detection schemes that have been utilized with this technique are refractive index detectors and UV absorption monitors at one wavelength (usually at 254 nm.). Because of the lack of specificity of the detectors, various band spreading functions of the column, and extra-columnar effects it has been necessary to apply num-

erous math functions to analyze the results. Tung developed a mathematical model to determine the molecular weight distribution from gel permeation chromatograms (17). The measured chromatogram can be expressed as

$$F(v) = \int W(y)G(v,y)dy \quad 2\text{-}8$$

where F(v) is the observed fucnction, G(v,y) is the instrumental spreading function, and W(y) is the input distribution. The function G(v,y) represents the convolving function of the instrument imposed on the sample (W(y)). Various functions have been developed to define G(v,y). Original work assumed the instrumental spreading function, G(v,y), to be log-normal, gaussian or some variation of these (18,19,20). Stoisits applied a least-squares method to calculate relative amounts of a mixture of two monodispersed samples (21). The method suffers because it requires prior knowledge of the particle sizes present in the mixture. To date no function has been found capable of handling both continuous and discontinuous distribution functions well (22). The problem is compounded in hydrodynamic chromatography because the column parameters are not consistent. Samples with particles greater than 0.5 microns will be deposited on the column, changing the axial dispersion (G(v,y)) in the column. Therefore there

is a need for a system that can relate F(v) to W(y) in absolute terms.

C. Detector Systems

To date the only detection systems applied to hydrodynamic chromatography have been refractive index detectors and single wavelength UV absorbance monitoring systems. To gain as much information as possible about the chromatograph eluant a multiwavelength detector is needed. Great strides in this area have been made in the last decade due to transducer development and miniaturization (23). One possiblity for multiwavelength monitoring is the use of a single detector used in a time multiplex mode. This method suffers from two serious drawbacks,(1) registration of the scanning mechanism and (2) speed of the scan. The second and more promising option is to use dispersive optics in association with multiple detectors. Multiple detector systems have been applied to liquid chromatographic systems in various ways. These have included bucket brigade transducers (Reticon devices), charge-coupled detectors (TV cameras), and Vidicon tubes (24,25,26). The advantage of these detectors is their ability to record large amounts of spectral information rapidly. However, for the spectral information to be ac-

curate they depend upon calibrated and sensitive dispersive optics. Another detector system has been produced utilizing discrete photodiodes each covered with a narrow bandpass interference filter. These offer several advantages. They are rugged, require less constrained optics, look at known wavelengths and can be easily interchanged depending upon the analysis to be done.

DETECTOR FABRICATION

A. Background

The detector system developed for this work consists of discrete photodiodes placed in a dual in-line package (DIP). Each individual photodiode is covered by a 10 nanometer bandpass interference filter. The result is a multiple filter photometer housed in an integrated circuit package. Due to the lack of commercial expertise in this area, this required the development of a detector of my own design.

B. Photodiode Connection and Packaging

The active elements of the detector system were RCA C30850 N-type silicon photodiodes (27). The diode wafers were 1.5 millimeters square with a phot-sensitive surface ofl millimeter diameter. The photo-sensitive area was surrounded by a 0.12 millimeter conductive ring. This conductive ring served as a connection to the anode of the photodiode. The underside of the photodiode served as a connection to the cathode of the photodiode.

Connection to the anode ring of the photodiode required special connection techniques and equipment. RCA Ltd. of Canada was contracted to make the specialized connections to the photodiodes. Dual in-line packages were supplied to RCA along with a description of the necessary connections. RCA-Canada supplied the photodiodes and the technical expertise. The photodiodes were conductively epoxied to a common strip that was insulated from the carrier package. The common conductor served as a ground plane. Connection to the anode ring was made by ultrasonically wire bonding a fine gold wire to it. The other end of the wire was similarly bonded to a conductive area near the photodiode. From this patch, another gold wire was connected to a post of the DIP package.

The dual in-line packages used were Isotronic PI 4105-s-3's. The package was of the solid side wall variety with 18 pins. The packages and pins were KOVAR coated to insure reliable electrical connections. The photodiode placement and connections are shown in Figures 3 and 4.

C. Aperture and Filter Construction

Each of the individual photodiodes in the DIP package

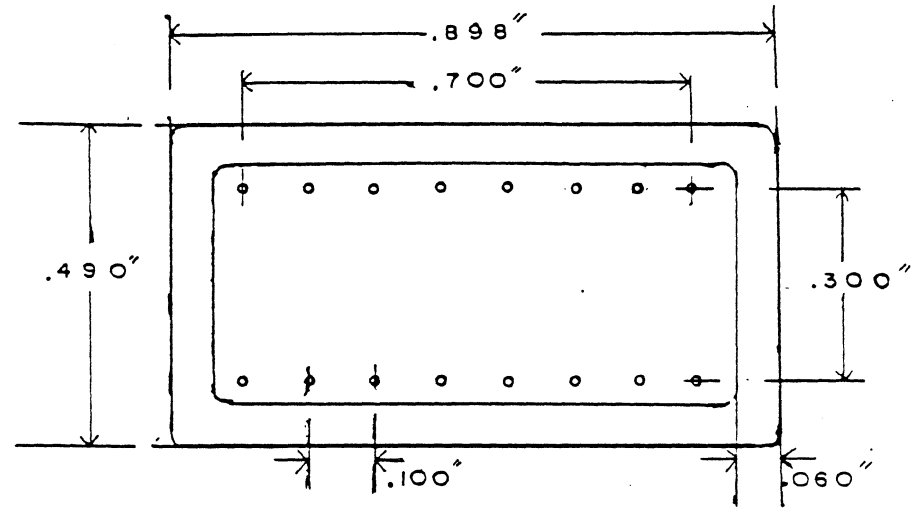

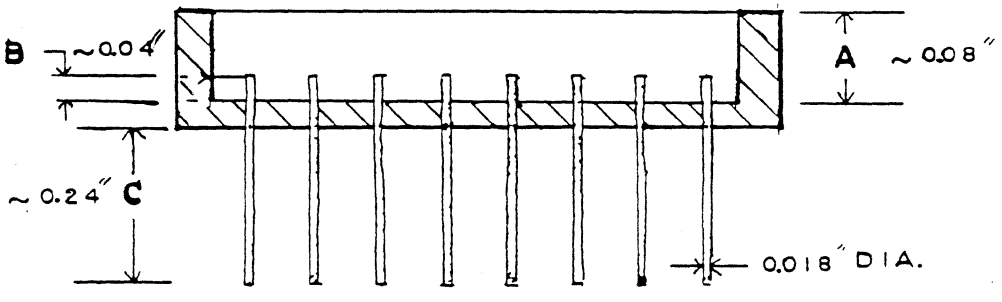

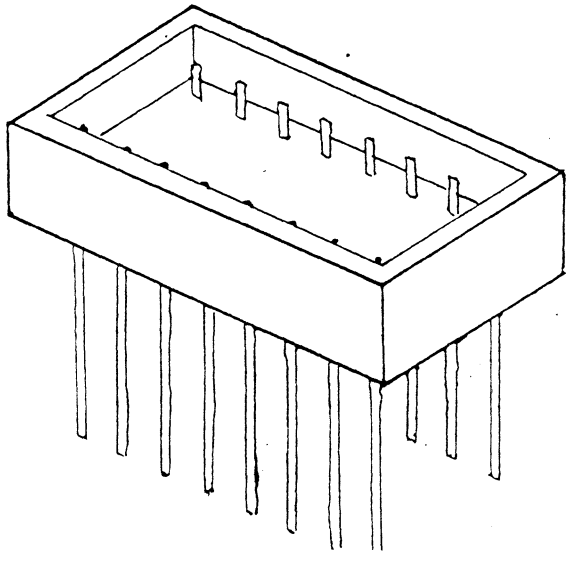

Isotronic Package

Figure 2.

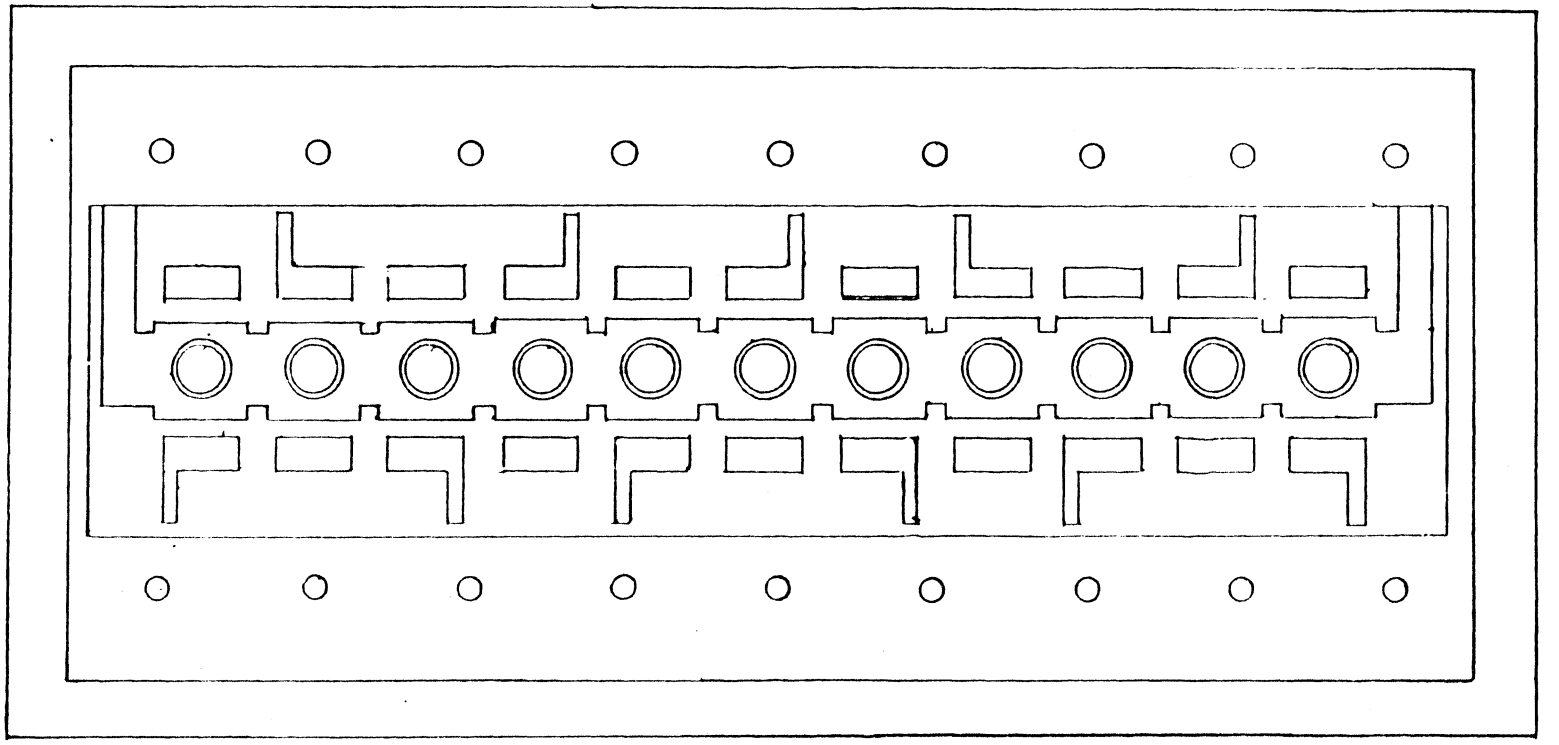

Figure 3. Internal lay-out of array

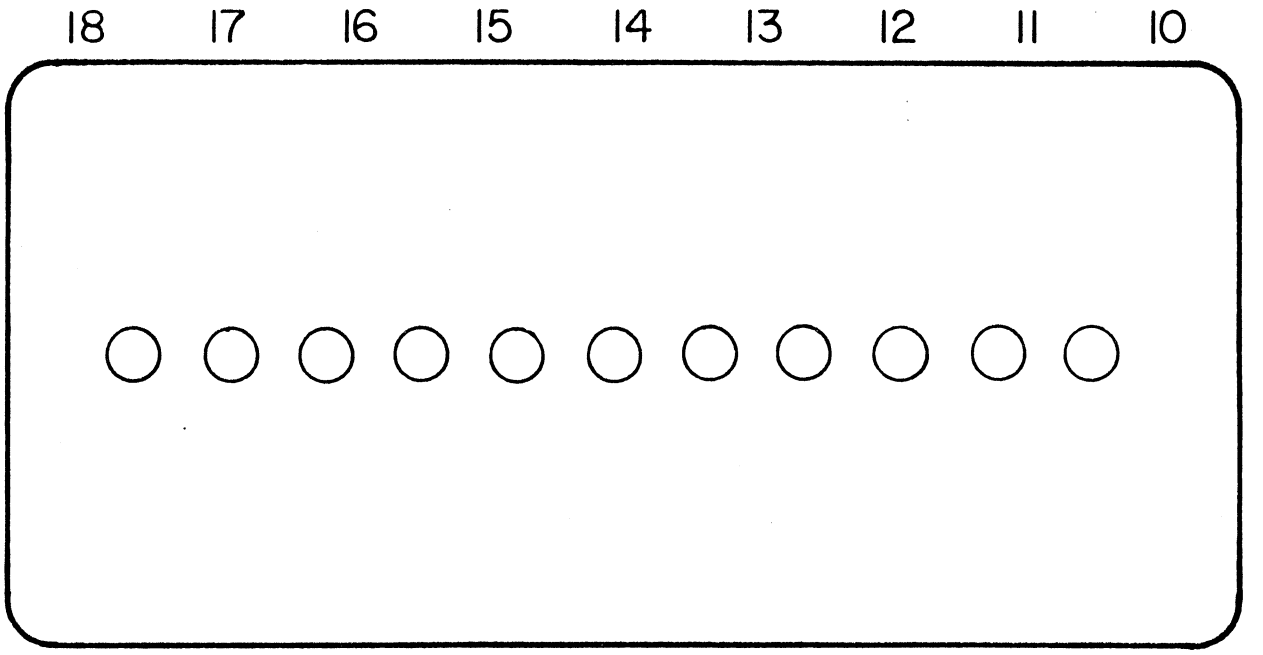

1	D1	460nm.	7	D9		13	D8	
2	N.C.		8	N.C.		14	D6	
3	D3		9	D11		15	D4	520nm.
4	D5		10	Gnd.		16	N.C.	
5	N.C.		11	D10	680nm.	17	D2	
6	D7	600nm.	12	N.C.		18	Gnd.	

Figure 4. Pin out of photodiode array

was covered by two optical components, (1) an aperture, and (2) a narrow bandpass interference filter. The aperture was necessary to define the field of view for each individual diode and prevent unwanted radiation from reaching the diode. To optimize the output of the diode, it was necessary to have the aperture large enough, so that as much of the photosensitive area was illuminated as possible. However the opening could not be so large that it overfilled the diode and allowed unwanted radiation to strike the diode. This was especially important due to the close proximity of the diodes to one another.

The aperture mask was produced on photographic slide medium. A positive of the desired mask was layed out using black layout tape and printed circuit board template material on lined vellum. The design was approximately nine times larger than the actual size. Dimension marks were made on the layout to indicate the final measurements. (See Figure 5.) The positive was photoreduced to the proper dimensions, producing a photographic negative. The negative had transparent apertures of the proper size and position, corresponding to the photoactive areas of the diode array. The film was optically transparent from the visible through the near IR region.

Because of the flexible nature of the negative material it was necessary to mount it on a support medium.

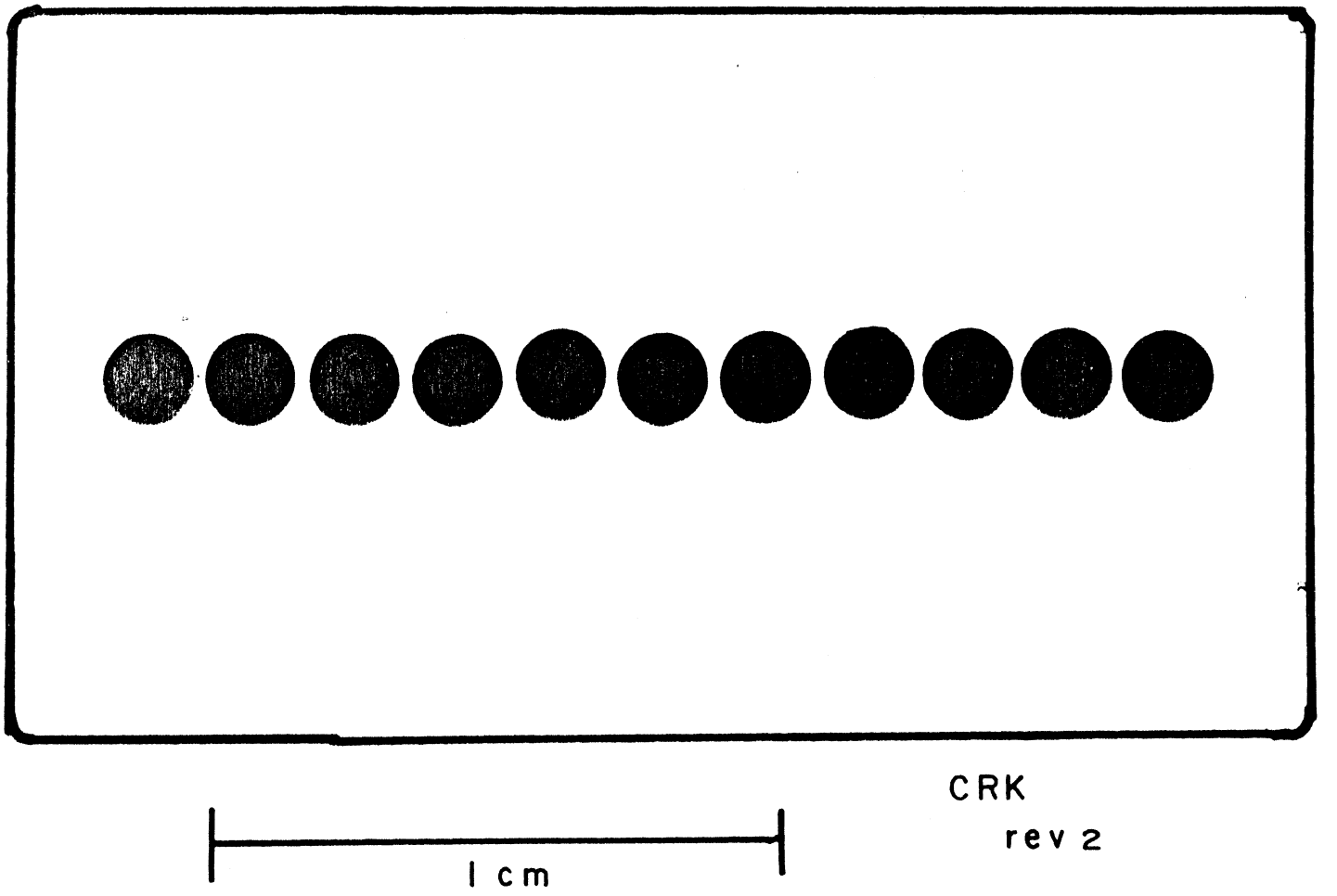

Figure 5. Aperture mask positive

For this glass slides were chosen, which were transparent in the region of interest, inexpensive, readily available, and easy to work with. Microscope slides were trimmed to size with a glass cutter. The aperture masks were mounted on the glass slides using optically transparent epoxy. The epoxy used was Epo-tec 301 obtained from Epoxy Technology. Small amounts of the epoxy were placed on the mask. A glass slide was then placed on top, applying pressure to get an even distribtion of the epoxy and remove any air bubbles. The mask and glass slide were sandwiched between Teflon sheets and a weight was applied. With the weight in place the epoxy was allowed to cure overnight. The Teflon sheets were used to prevent the mask or glass slide from being attached to the table or weight, if any excess epoxy were to seep out around the edges.

Once the mask was attached to a glass slide the narrow bandpass interference filters were mounted. The filters were bonded to the underside of the photographic film. This produced a glass-mask-filter interface. Again Epo-tec 301 transparent epoxy was used to attach the filters. A brass jig was machined to help position the filters properly on the mask. The mask had small comb-like teeth, which accepted the filters and spaced them appropriately. The filters were approximately 1.75

millimeters square and varied in thickness. To manipulate the filters while epoxying them to the mask, dental instruments along with a glass placement tool were used. The tool was connected to a faucet aspirator attachment at one end. The other end was drawn out to a capillary point, used to pick up and position the filters. There was a "finger hole" located near the capillary end used to control the vacuum. Covering the hole created a vacuum, with which to pick up the filters. Uncovering the hole broke the vacuum and the filter was released. The filters were applied to the mask with their more reflective side facing the glass slide. This helped to reflect some of the incident radiation, reducing the heating of the filter. Using this orientation also reduced the number of possible internal reflections in the device itself.

The arrays were allowed to dry overnight in a nitrogen filled glove bag. Due to the hydrophilic nature of the dielectric material of the filters, moist air could have caused the layers to separate and peel off. The glass-mask-filter unit was then epoxied in place over the photodiode array package. Epo-tec 320 optically opaque epoxy (also from Epoxy Technology) was used for this purpose. The glass-mask-filter unit was aligned on the array package by centering the first and last photodiodes under apertures which had no filters covering them. The units

were left to dry overnight and a second coat of opaque epoxy was applied along the edge of the glass slide.

D. Array Testing and Performance

The spectral response of the components used in the arrays were evaluated throughout the fabrication process. A Heath model EU-701-50 tungsten lamp with focusing mirror was used as a continuum source. The output of the source was focused onto a Heath EU-700/E monochromator. The monochromator was under computer control to generate spectral scans. The photodiodes were tested first and subsequently used as the detector to test the other components.

Figure 8 shows the spectral response of the RCA photodiodes. These results agree favorably with published spectra for N-type photodiodes. The diodes show poor response below 400 nanometers with acceptable output throughout the visible region. Transmission curves of the epoxies used (Epo-tec 301 and 320) indicated appropriate characteristics throughout this wavelength region.

Scans of the interference filters revealed them to have a 10 nanometer bandpass centered about their stated wavelength. Initially scans were done only in the vicinity of the bandpass region. Tests were done with the

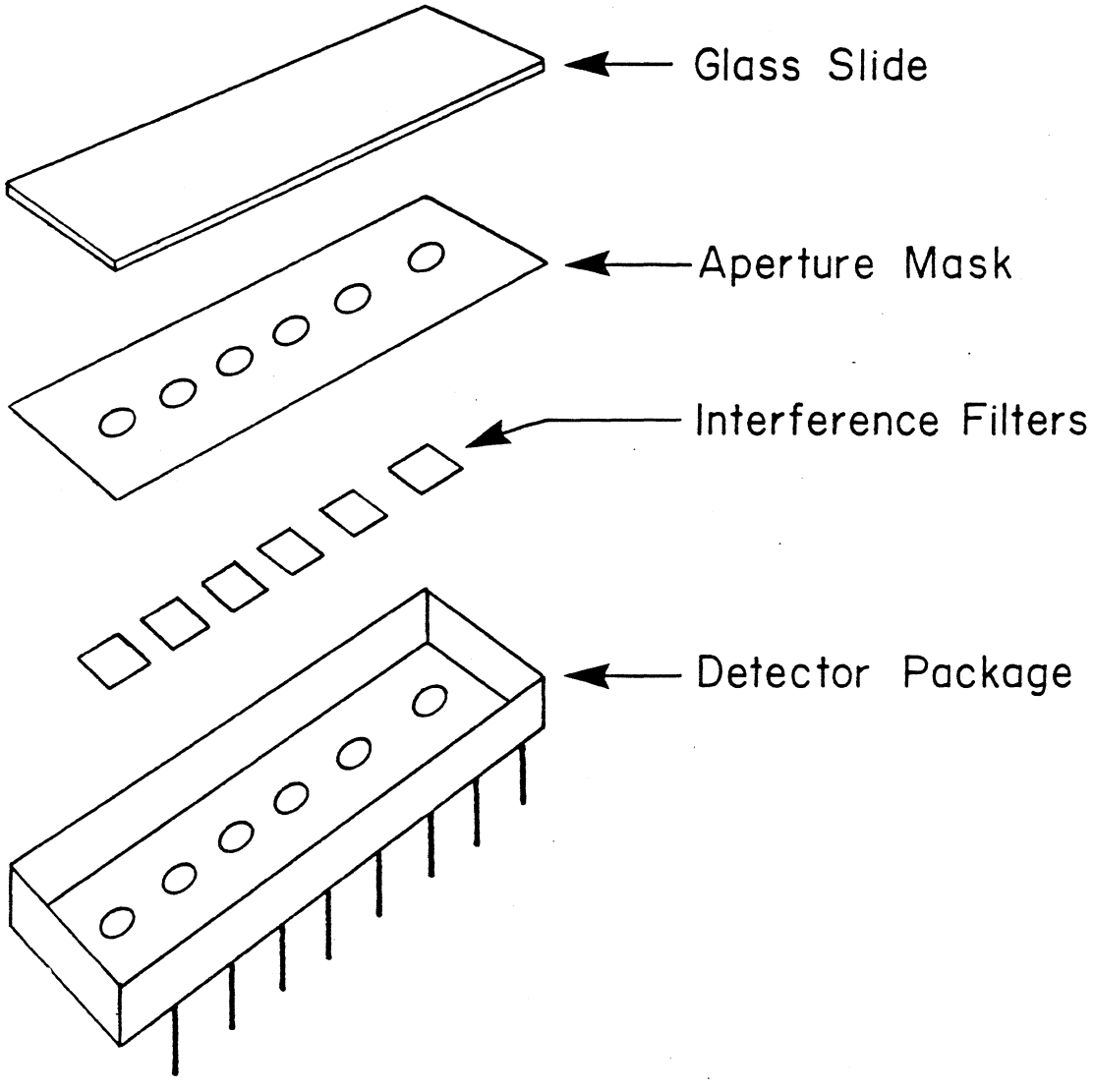

Exploded view of array

Figure 6.

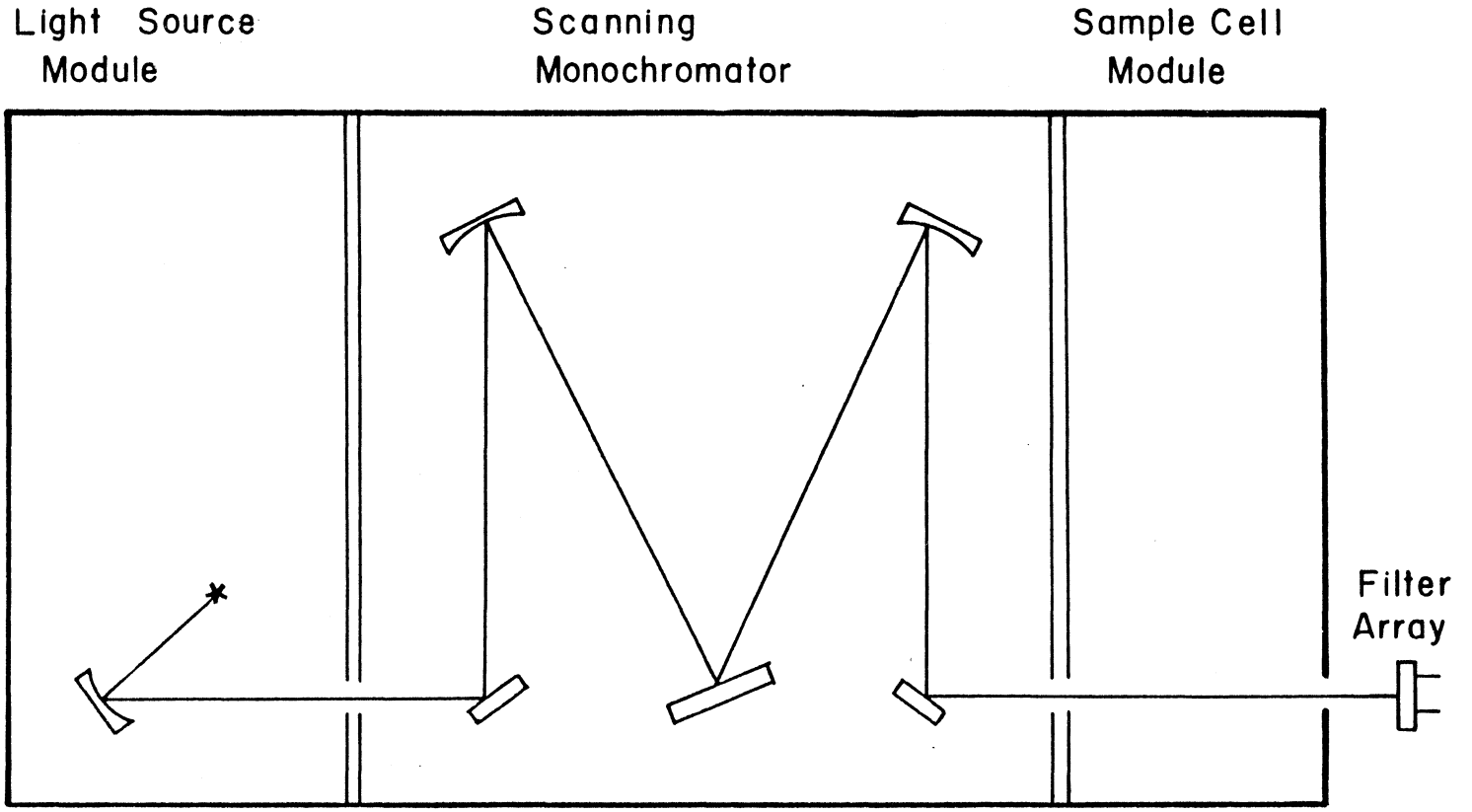

Figure 7. Optical test set up

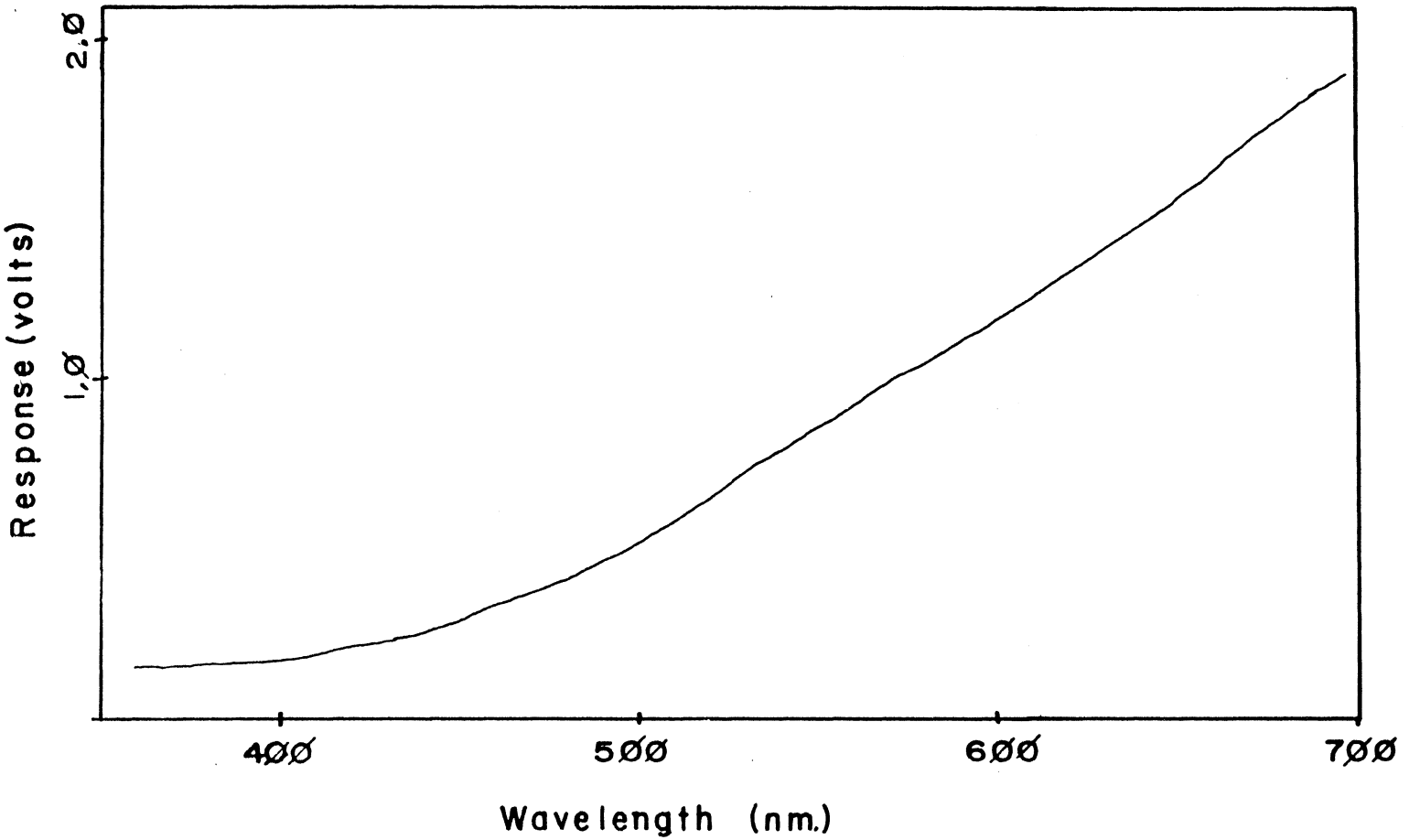

Figure 8. Photodiode spectral response

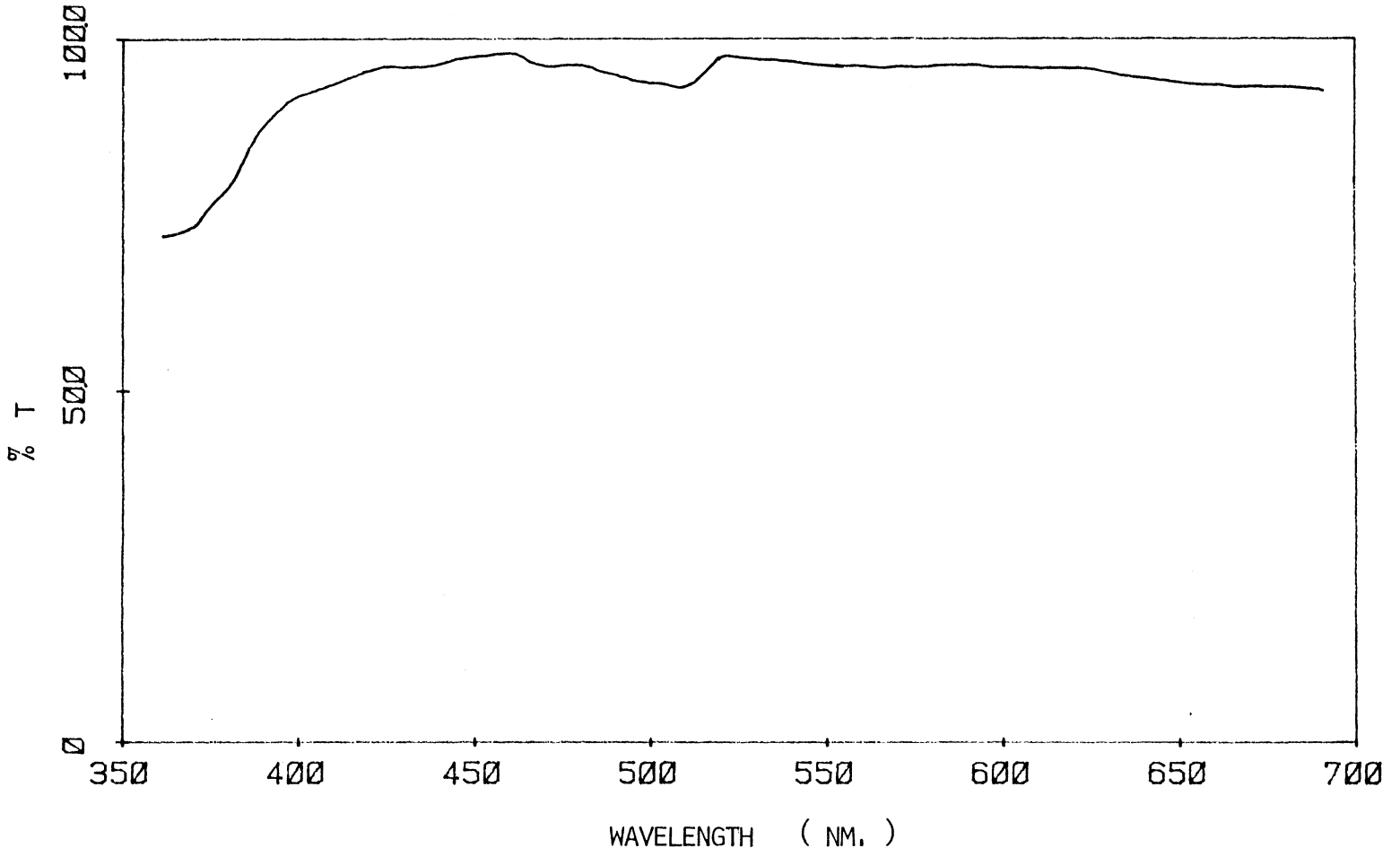

Figure 9. Transmittance of Epo-tec 301 epoxy

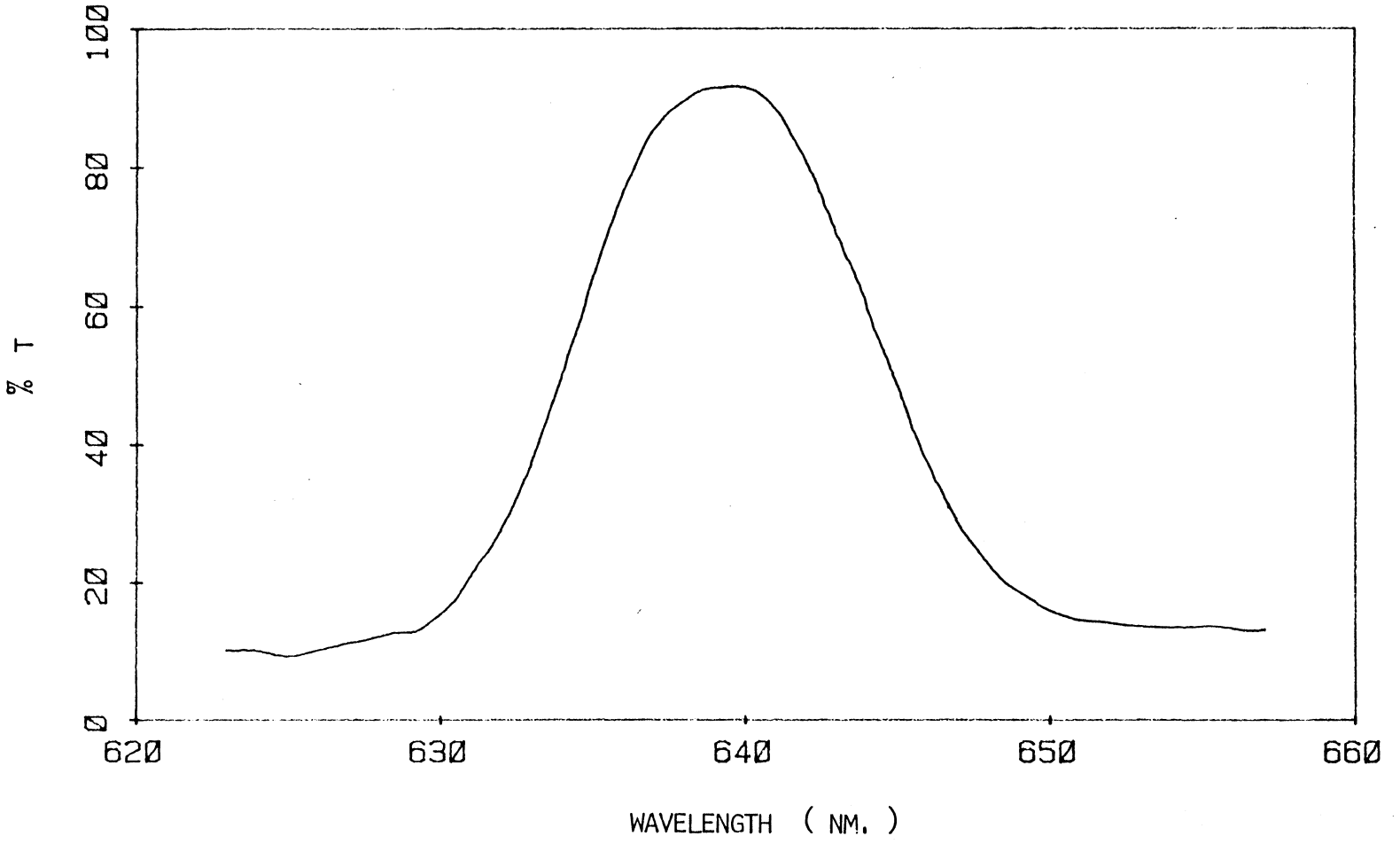

Figure 10. Transmittance of interference filter (640nm.)

filters using a white light source. The results indicated that more radiation was incident upon the detectors than could be explained by the bandpass transmission of the filters. The filters were found to be of the multilayer type instead of the Fabrey-Perot type. Fabry-Perot filters consist of two semireflecting surfaces separated by a dielectric layer. Incident radiation constructively and destructively interfere as it passes through the filter. Full reinforcement occurs when the separation of the surfaces is a multiple of the wavelength. That is, $2d = m\lambda/n$, where d is the thickness of the dielectric layer, n is its refractive index at wavelength λ (in vacuum), and m is the order transmitted (28). With these filters, the user needs only to make sure that the wavelengths at some of the other orders not interfere with the measurements.

Multilayer filters have slightly different transmittance characteristics from those of the Fabret-Perot filters. These filters are also based upon constructive and destructive interference. They are constructed of multiple layers of alternating high refractive index and low refractive index material. Several of these stacks are present and separated by an "absentee" layer of one half the wavelength to be transmitted (29). These filters show a greater transmittance and narrower half-peak widths than Fabrey-Perot filters. However they show a greater

transmittance in unwanted parts of the spectrum. It is this greater transmittance that was observed about 150 nanometers from the passband. This explains the need for additional filters positioned in the source beam of the optical layout described in Chapter 4.

The major problem found after the first array was made was the optical crosstalk amoung the diodes. If all but one of the apertures were masked off, the neighboring diodes still responded to incident radiation. Electronic crosstalk was first investigated. If the crosstalk were electrical in nature it would most likely be on the amplifier boards, but grounding and disconnecting neighboring circuits had no effect upon the observed output. Any other electical interaction would therefore have to originate at the arrays. Since the currents generated by the diodes is so small (nanoamperes), it is doubtful that this was the source of the noise.

The response distribution of the diodes showed a bell shape curve, where the response drops off the greater the distance from the illuminated diode. This suggested that there was leakage of light or reflections internal to the array. First the diameters of the apertures were reduced to narrow the field of view. There was little improvement. To reduce internal reflections most of the internal areas of the array were painted matte black, but again

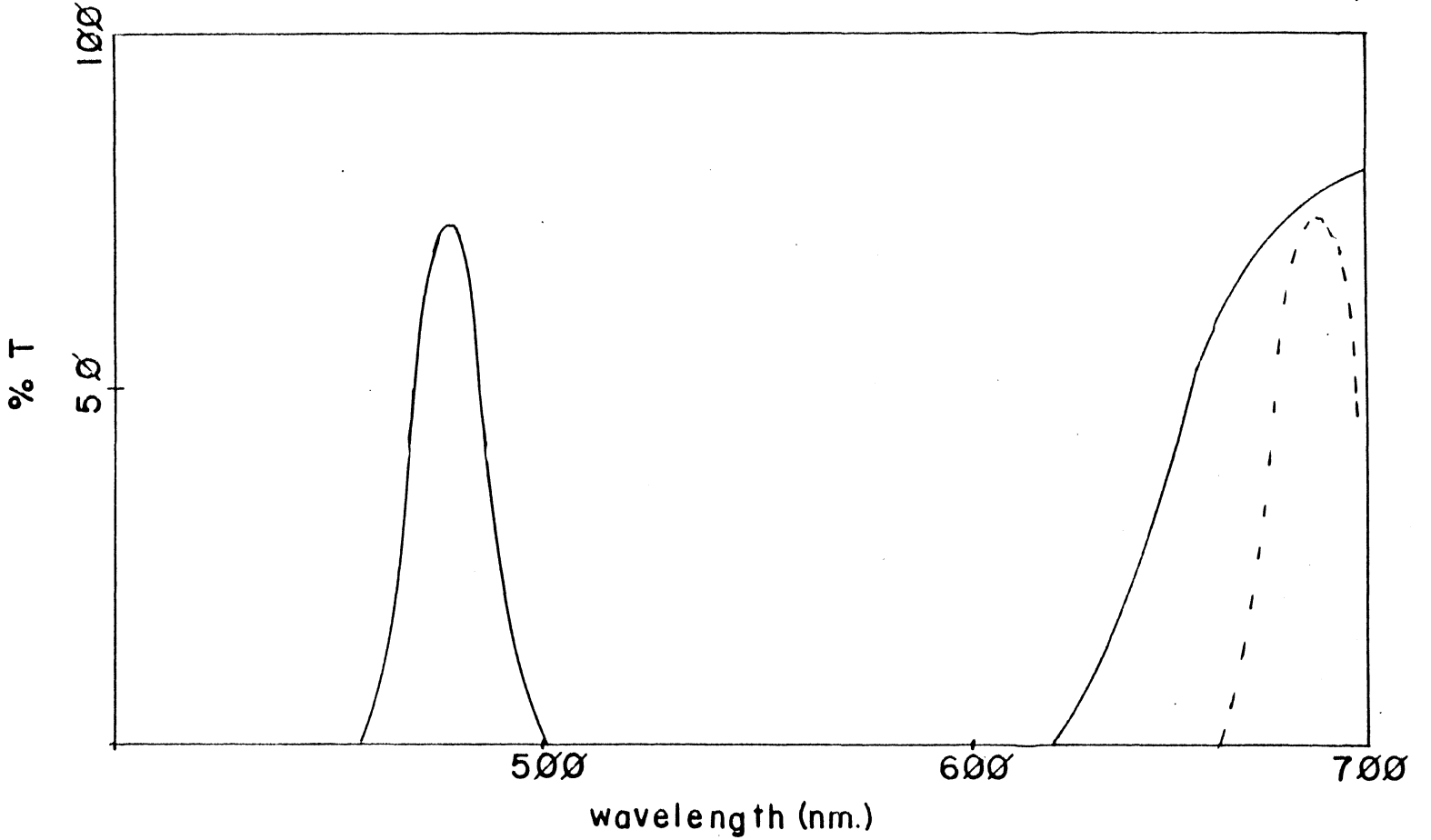

Figure 11. Overlap of the interference filter transmittances

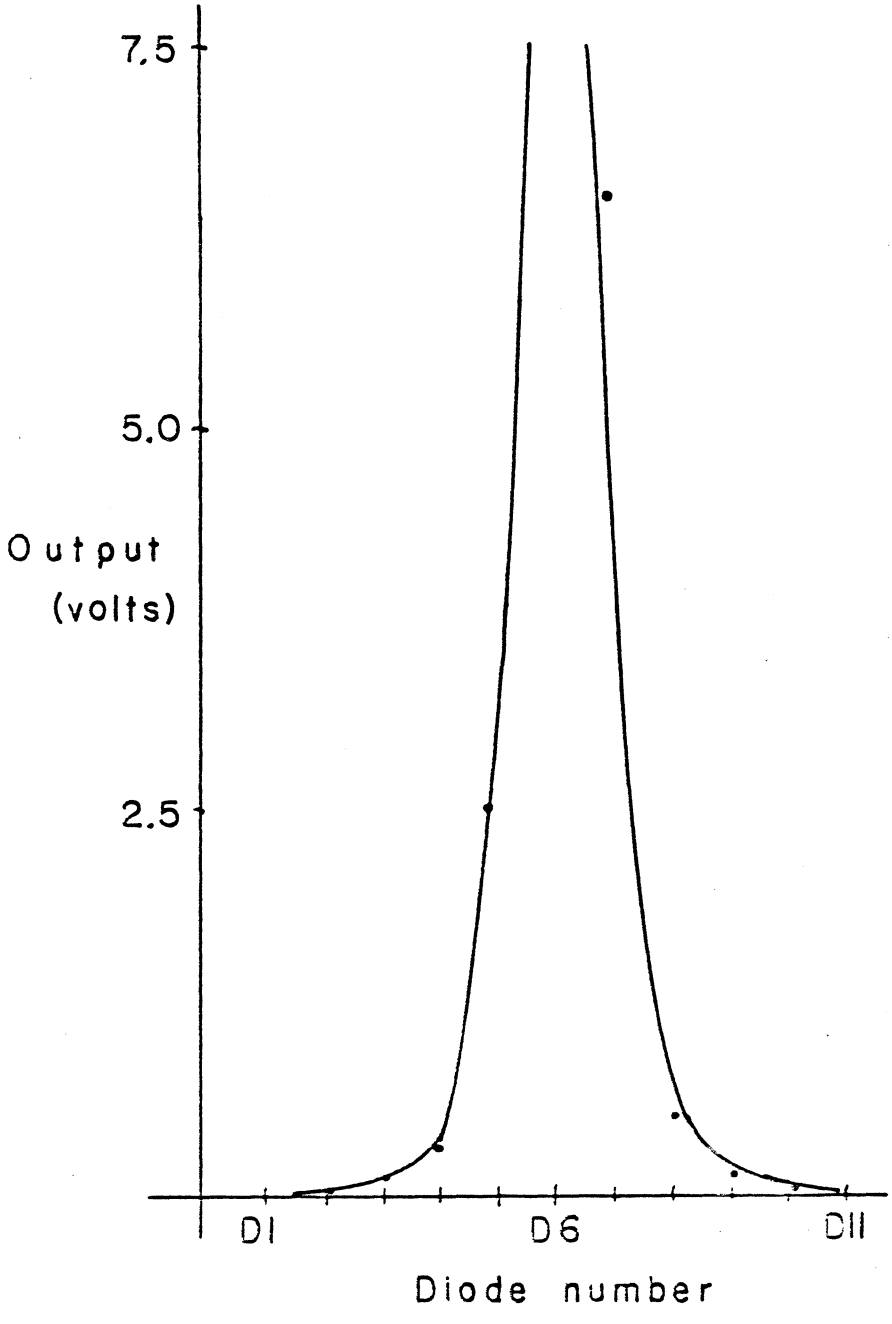

Diode response with only one diode exposed

Figure 12.

there was little improvement. The most successful technique was to paint the edges of the filters matte black. This helped significantly, so apparently there was a large amount of light leakage out the sides of the filters. The situation was thus improved, but not to the point of eliminating the crosstalk totally. This also restricted use of the two diodes on either side of an illuminated diode. Such limitations allowed for the production of an array utilizing only four filters and diodes instead of the hoped for nine. Other methods were tried to improve the condition, such as epoxying opaque "blinders" between the filters. These attempts were unsuccessful.

DETECTOR SUPPORT COMPONENTS

A. Electronics

The detector arrays were designed around a set of RCA C30850 silicon photodiodes. The photodiodes were operated in the photovoltaic mode. That is, there was no externally applied voltage to the p-n junction. In this mode, incident radiation generates a current which is proportional to the light power incident on the active surface. Since the active area of the diode was small, and the bandwith of the interference filters narrow, the photocurrent produced was small. The currents were generally on the order of nanoamperes. This required an amplification circuit with high input impedance so that it would not load down the diode.

A two stage operational amplifier circuit was designed to provide for large amplification and noise immunity. The RCA CA3140 operational amplifiers were chosen for their very high input impedance and low input currents.

The first stage of the circuit was a current-to-voltage converter. The cathode of the photodiode and the non-inverting input of the amplifier were

connected to ground. The anode of the photodiode was connected to the inverting input of the amplifier. The feedback resistor of the amplifier determined the gain at this stage. The voltage produced at the output of the amplifier was related to the photocurrent by

$$v_o = i_{hv} R_f$$

where i_{hv} is the photocurrent and R_f is the value of the feedback resistor.

Output from the first stage was directed to a second stage operational amplifier. This stage was designed for additional amplification and filtering of high frequency noise from the signal. The gain from the second stage was G=R3/R2, where R3 is the feedback resistor and R2 is the input resistor of the second stage. A capacitor was also placed in the feedback loop of the amplifier. This had no effect upon the gain of the system, but does limit the frequency response of the circuit. Since the signals of interest were D.C., or of very low frequency, this did not present a problem.

Associated with each stage of the circuit were offset controls. These allowed for the stages to be independently zeroed to account for any dark current or leakage current which might be associated with the circuit. The overall equation for the circuit can be expressed as

$$v_{out} = i_{hv} R1 (R3/R2)$$

The resistor values chosen are shown in Figure 13. The net gain of the circuit is 10^{10}. At this gain, a photocurrent of 1 nanoampere produces a 0.1 volts signal at the output. The decision was made to provide each individual diode with its own circuit. The primary reason for this was the noise associated with field-effect-transistor multiplexors, and the small currents being investigated.

The printed circuit board schematics are shown in Figures 14 and 15. A single board will handle six individual photodiodes. Two of these boards are necessary to record the output of a single array. An aluminum housing was constructed to house the boards. A bus system was included for power, ground and output lines and to allow for interchangeability of the boards. bThe output lines were wired to a Cannon 7414 DD50P header for connection to the analog-to-digital converter board in the satellite processor.

Ribbon cable headers were placed on the amplifier boards to provide connection to the arrays. A printed circuit board was designed to hold the array and, provide connection to the amplifier boards via a ribbon cable. A zero insertion force (ZIF) socket was used to hold the arrays. This allowed for fast and easy interchangeability of the arrays.

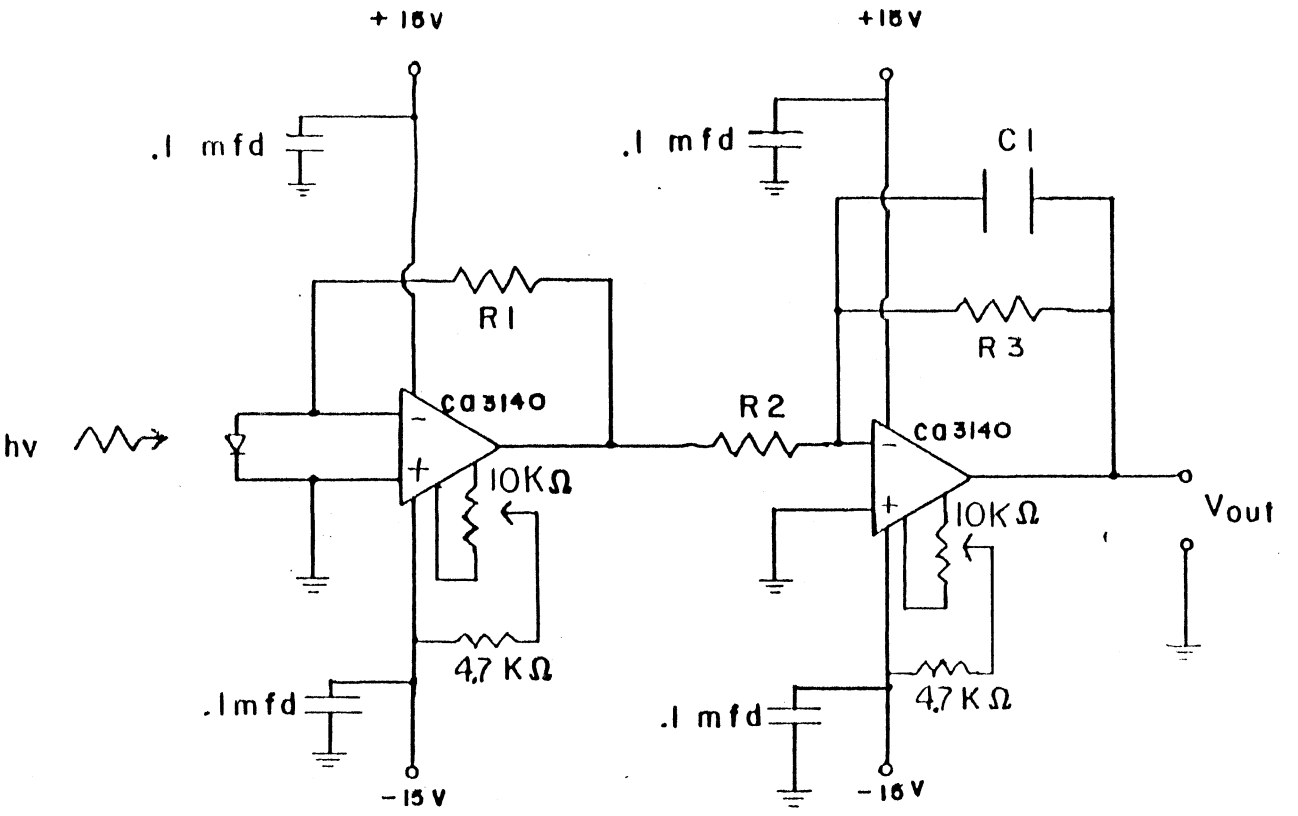

R1 = 100 Meg Ω
R2 = 10 KΩ
R3 = 1 Meg Ω
C1 = 0.1 mfd

$$V_{out} = I_{hv} \cdot R1 \cdot \frac{R3}{R2}$$

Figure 13. Electronic circuit

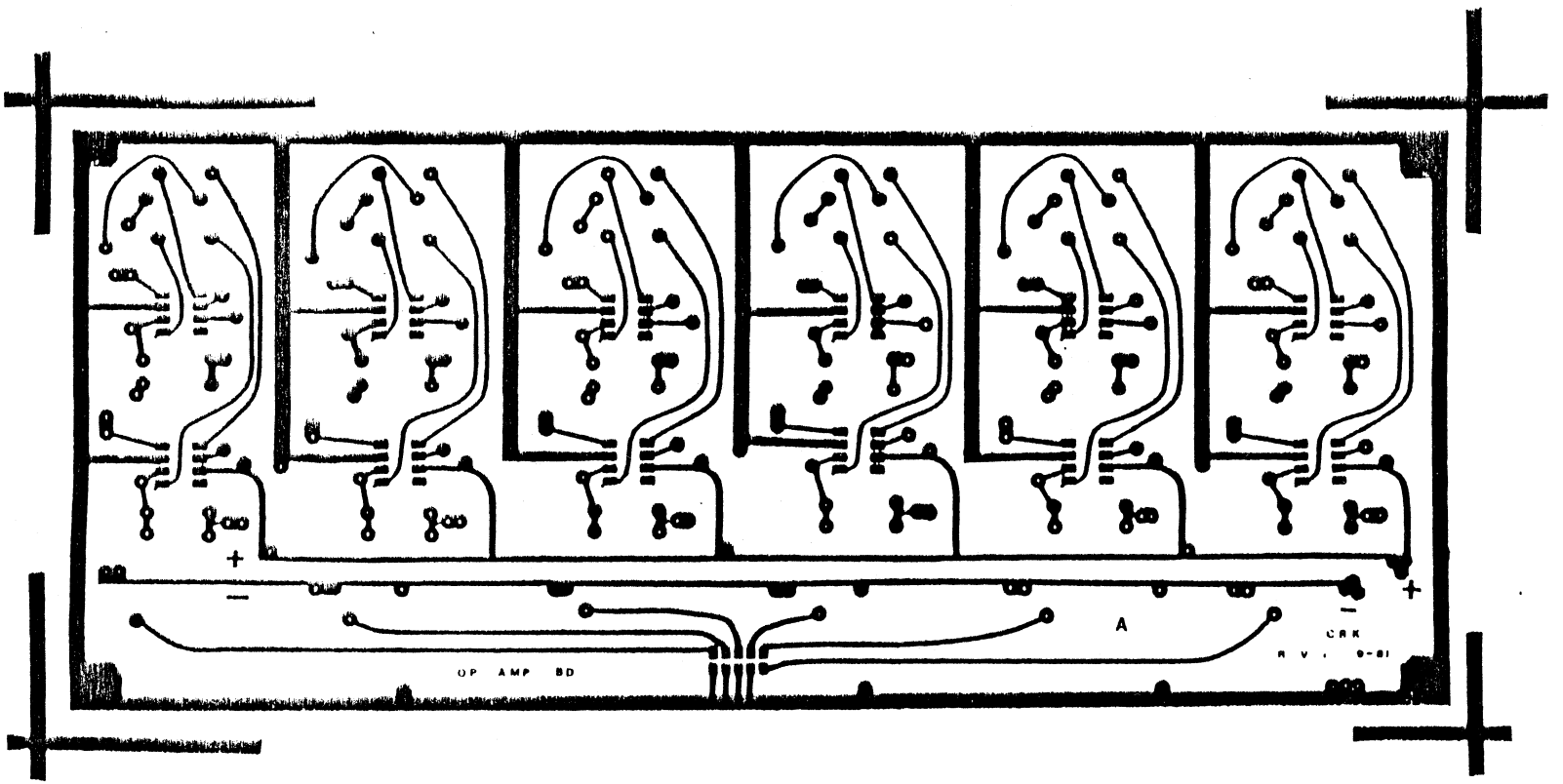

Figure 14. Operational amplifier printed circuit board positive

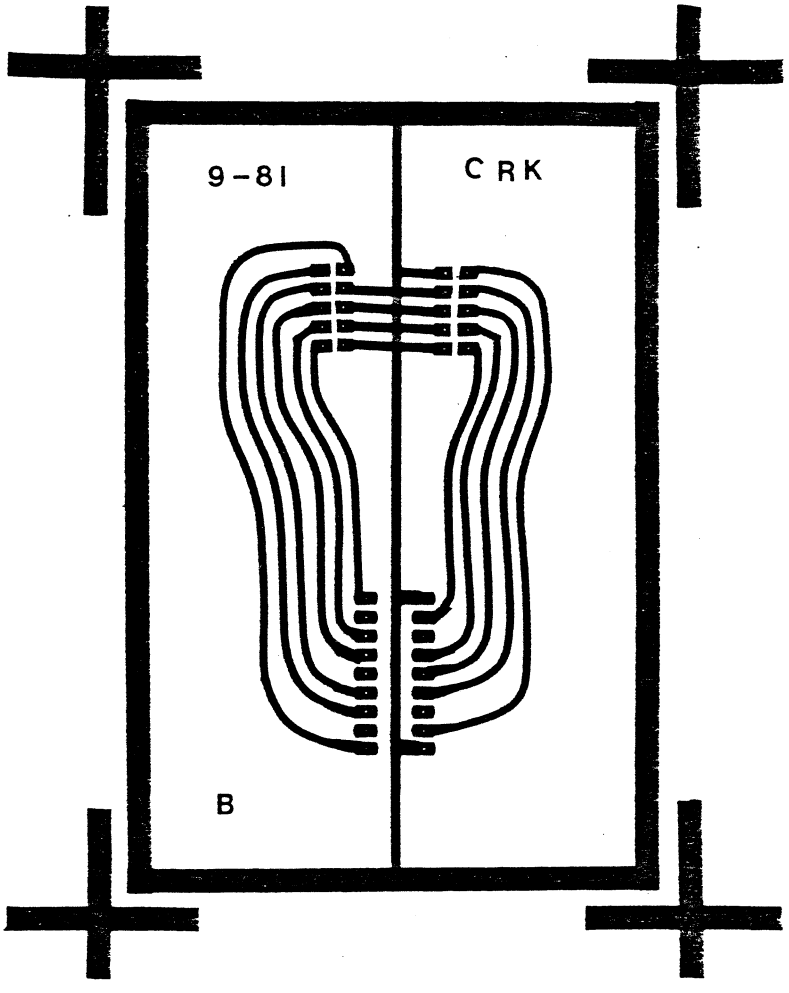

Header printed circuit board
positive

Figure 15.

Table 1

ADC Channel Assignments

Diode Number	Wavelength	ADC Channel
D1	460 nm.	5
D4	520 nm.	7
D7	600 nm.	2
D10	680 nm.	10

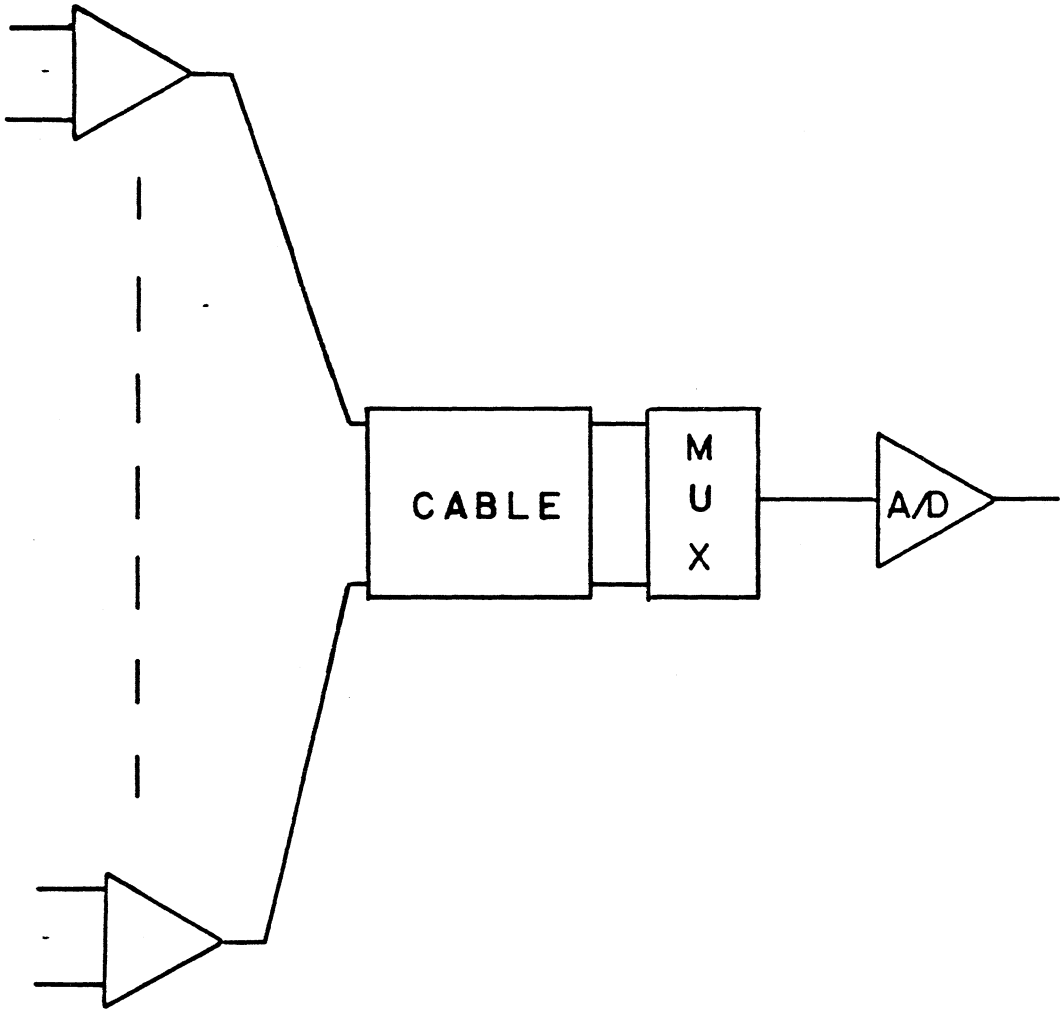

Amplifier connections to the A/D converter

Figure 16.

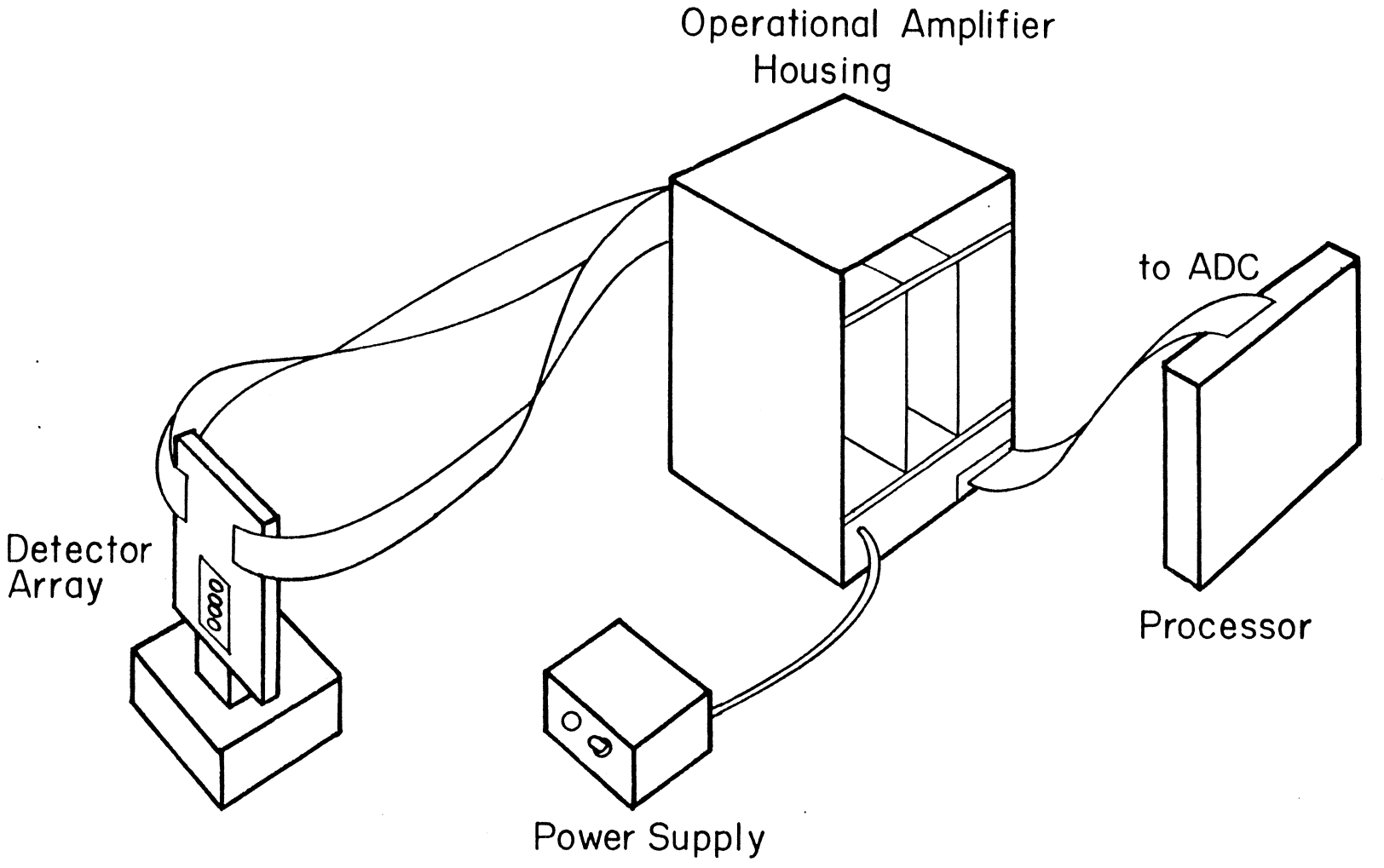

Figure 17. Overview of the electronic cabling

B. Optics

The optical layout follows traditional designs used in UV-VIS spectrophotometer systems. The light source was a tungsten filament lamp. The unit used was a Heath model EU-701-50 which includes a focusing mirror with a 40.0 mm focal length. The optical beam has a rectangular profile determined by the filament length and width. The beam passed through an infrared suppressor filter and a neutral density filter before exiting from the source housing. The infrared suppressor filter was a Corion FR-400-F circular filter eliminating radiation above 710 nanometers. A neutral density filter (1.3 O.D.) was included to reduce the intensity of the source to prevent saturation of the diodes. A liquid filter made from $CuSO_4$ $5H_2O$ was placed in the beam such that it intercepted half of the beam. The half of the beam with which it interacted, was the portion of the beam incident on the section of the array with bandpass filters at the shorter wavelengths. This was necessary because of the transmission characteristics of the interference filters as discussed in Chapter 3. The liquid filter had a cut-off at approximately 630 nanometers.

The beam was split into two separate paths using another neutral density filter (Melles Griot BK-7, 50 mm.

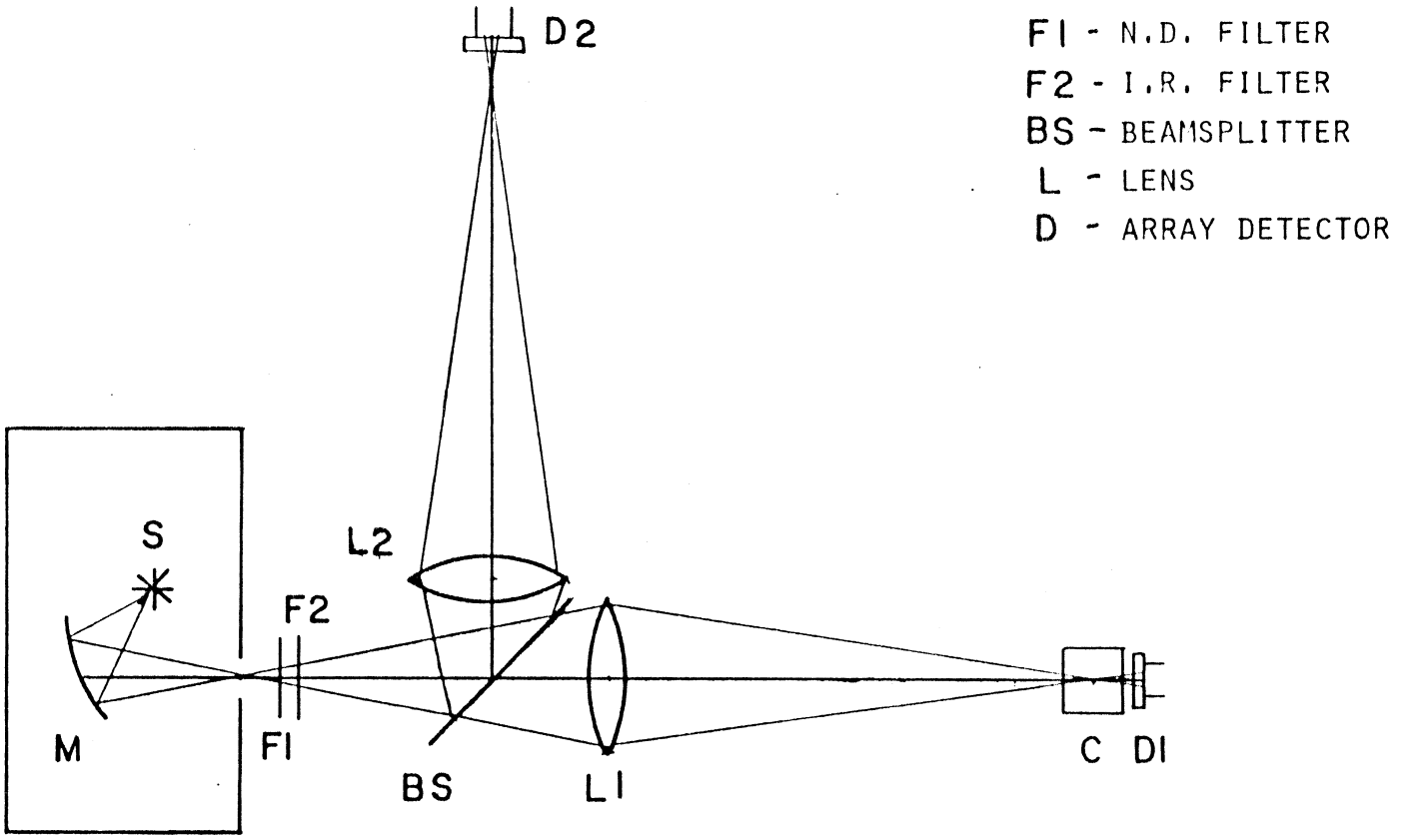

Figure 18. Optical Lay-out

square) as a beam splitter. Setting the filter at 45° to the incident beam, 33% of the radiation will pass through the filter, 33% will be reflected and 33% will be absorbed. This produces two perpendicular beams of equal intensity.

Both beams pass through a symmetric convex spherical glass lens. Each lens had a 47 mm diameter and 80.0 mm focal length. The beam that continued straight through the beam splitter passed through a sample cell and then struck the sample filter array. The perpendicular beam struck a filter array with no cell in the path. The array set at right angles to the source output acted as a power monitor. This array determined source fluctuations and source drift, which then could be corrected. Identical arrays were used in both beams so that the individual spectral characteristics could be determined. Thus, if the color temperature of the lamp were to change, this could be compensated for.

The two concave lenses were placed 85mm from the focal point of the source and 115mm from the detectors. This allowed for a magnification of the source beam to fill the windows of the diodes in the arrays. The source beam was 1 by 15 mm. The beam was magnified to 1.6 by 24 mm, which filled the window of the diodes. The magnification was defined as

$$M = s''/s$$

where s" is the distance from the lens to the detector and s is the distance from the output of the source to the lens.

To check the spectral response of some of the components, the optics described above were slightly modified. The Heath lamp unit was used in conjunction with a Heath EU-700/E scanning monochromator. This was then coupled with the Heath EU-701-11 sample cell module. The monochromator was automatically scanned under computer control. However, this unit was capable of scanning in only one direction (high to low wavelengths), and had to be manually set between runs.

C. Computer Network

The computer system consisted of a multilayer star structure (Figure 19). The satellite computers were LSI-11 processors with 16 kilobytes of dynamic memory. The satellite processors communicated with the host computers by an RS232-C asynchronous line. There were two levels of host computers. The one level consisted of a PDP 11/02 processor with 28 kilobytes of memory and four double density (500kb) floppy disk drives. The second

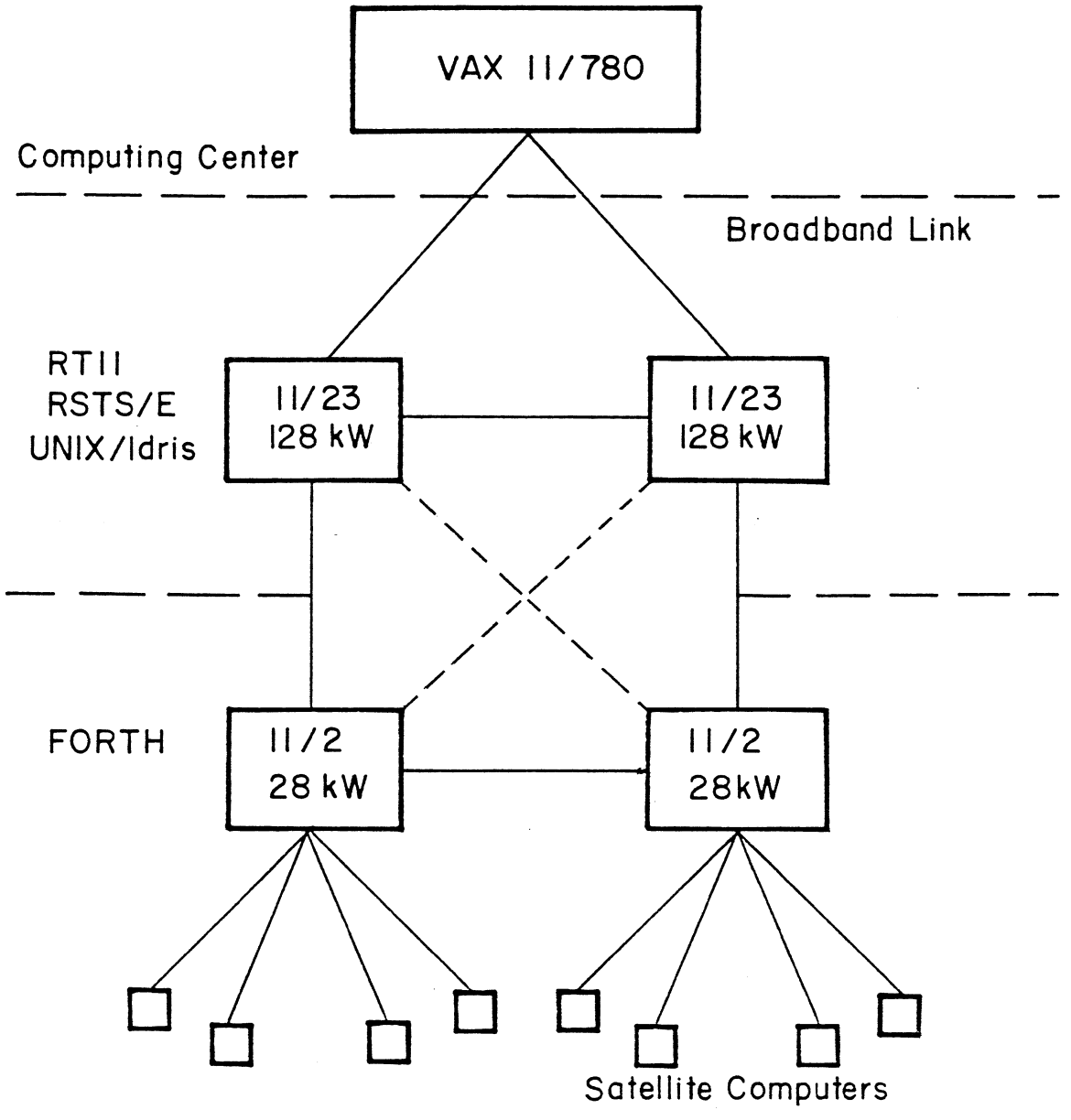

Computer network

Figure 19.

host level had PDP 11/23 processors with 96 kilobytes of memory and two 2.5 Mbyte disk drives.

The satellite processors were set up to allow for maximum flexiblity. Besides the processor, memory, and serial boards the rest of the backplane was open for individual needs. These processors were primarily for data acquisition and instrument control. Due to the need for rapid data collection the satellite processors ran a threaded linked list language called FORTH. This provided a means for programing in a higher level language, while maintaining execution speeds close to that of assembly language. FORTH required very little memory space and could run on smaller processors.

The Polyforth operating system ran on the 11/02 host processors. This provided support for multiusers, multitasking programing. The communication lines provided for three terminals, three inter-host lines, and four satellite stations. Program development and program and data file storage were done at this level. The next level, the 11/23's ran more standard operating systems. These included RT-11, RSTS/E, Idris and Unix. The languages available were Fortran, Basic, C, APL and Pascal. There was an additional level available. The laboratory computers and terminals could be connected to the campus computer center through a broadband hookup. The computer

center had several Digital Equipment Corporation VAX machines and an IBM 3240. Additional software packages were available at this level such as SAS. This also allowed access to the IBM 6670 laser printer for high quality hardcopy.

D. Software

Software development fell into two areas. Programs were written in FORTH for data acquisition, monochromator control, and turbidity calculations. The scattering efficiency, matrices and particle size calculation programs were written in Fortran under RSTS/E.

The monochromator controller expects +5 volt pulses to drive the motors of the grating. Approximately 600 pulses correspond to a one angstrom change in the output wavelength. The FORTH word NANOMETERS outputs 6000 decimal pulses, which decrements the monochromator by one nanometer.

The data acquisition program was RUN-DATA. The program collected five data points from a single diode in rapid succession, and stored the average value in the data array for that diode. This resulted in a five point box-car average. This sequence continued through the

diodes of interest. A stall loop was inserted to control the rate of data collection. The stall loop was set such that one scan of the diodes was completed three times per second. RUN-DATA halted after collecting 500 scans (2 minutes 46 seconds). The data arrays were stored on a floppy disk by the word STORE-DATA. Each data array resides in a separate block on disk (1 block= 512 words).

The turbidities were calculated by TAU-POINTS. Supplying the program with the block number, background reading, and solvent blank value, an array of the turbidities was produced (Y-VALUE). The resulting array could be typed out or plotted directly to give a turbidity versus time curve. To determine particle size it was necessary to evaluate the turbidity ratios. The word RATIO-TEST calculated the turbidities at two wavelengths (using TAU-POINTS) and returned the turbidity ratio values.

To go from the turbidity values to paricle size it was necessary to calculate the scattering efficiencies theoretically (Q_{sca}). The program to calculate Q_{sca} was obtained from IBM, using the algorithm developed by J. Dave (30). The program was written in Fortran and labeled Scat.sav. Initially tables were produced for the Q values over the particle size range from 0.1 to 1.12 microns at the various wavelengths being used. Tables of the Q ratios were also prepared so that the turbidity values could

be related to size immediately if the upper host computer was not on line. The Fortran program Ratio.sav would produce size values directly given the turbidity ratio, wavelengths used, and the particle size range under investigation.

The software to decompose the mixtures to obtain the concentration information was also written in Fortran. The Linear Parameter Estimation program was based on the algorithm described by Brubaker (31). The Non-negative Least Squares Package (NNLS) was obtained from D. Leggett of Dow Chemical, Freeport Texas. Both of these programs expect turbidity values and yield the concentration vectors.

LIGHT SCATTERING

A. Theory

The method of determining particle size by transmission in this project was based upon evaluation of the turbidity of the sample and relating it back to size. Using the equation

$$\tau = l\ N\ C_{ext} \qquad 5\text{-}1$$

where l is the path length of the sample cell, N is the concentration of particles per unit volume and C_{ext} is the extinction cross section of the particles, τ (turbidity) can be related back to particle size (11).

The theory and equations presented here assume only single scattering and elastic interactions. Single scattering requires that the scattering particle is unaffected by neighboring particles and that the scattered radiation proceeds uninhibited through the rest of the sample. This assures that the turbidity will be directly proportional to the concentration of particles. The scattering is assumed to be elastic (no shift in frequency between incident and scattered radiation) which precludes

looking at samples that exhibit Raman or Brillouin scattering or fluorescence. Since the scattering particles are assumed to be randomly dispersed in solution and an incoherent beam is being used, polarization effects will not be involved with the measurement.

The extinction cross section is the summation of the scattering cross section and the absorption cross section displayed by the particles (32).

$$C_{ext} = C_{sca} + C_{abs} \qquad 5\text{-}2$$

The samples investigated in this work showed no absorption in the wavelength region used. Therefore $C_{abs}=0$ and equation 5-2 becomes, $C_{ext}=C_{sca}$. The extinction of the incident beam is due totally to scattering. Thus the subscript, sca, will be used instead of the more general subscript, ext. This does not diminish the validity of the theory or method, but does simplify the calculations.

Dividing the scattering cross section, C_{sca}, by the geometrical cross section of the particles yields a scattering efficiency value, $Q_{sca}=C_{sca}/((\pi/4)D^2)$. Assuming a path length of l=1cm. an equation can be written

$$\tau = (\pi/4)\ D^2\ Q_{sca} \qquad 5\text{-}3$$

Again, Q_{sca} is a function of m, the relative refractive index of the sample to that of the solvent and α, a dimensionless size parameter related to the wavelength ($\alpha=\pi D/\lambda_m$). In the case of Rayleigh scattering, Q_{sca} can be readily calculated. Rayleigh scattering assumes that the particles are much smaller than the wavelength of the incident radiation ($r < (1/20)\lambda$) (33).

The determination of Q_{sca}, where the particles are approximately the same size or larger than the wavelength of the radiation is much more complex. This is known as the Mie scattering region. In 1908 Mie derived an expression for Q_{sca} for spherical particles in this size region. Van de Hulst describes this derivation in detail (32). Though the theory has been known since 1908 it has been difficult to apply, due to the complexity of the mathematics. In 1957 Heller and Pangonis produced tables for calculating Q_{sca} at various values of m and r(radius) (34). This provided approximate values of Q_{sca}, but interpolation of the tables was required for their practical application. With the advent of computers the tedious calculations could be done directly and with no interpolation necessary. It was not until 1968 that J. Dave developed a linear program and appropriate algorithms to do these calculations (30).

The importance of these calculations becomes clear when we see how the particle size is determined from the turbidity measurements. In equation 2-2, N, r and Q_{sca} are all unknowns, while τ is experimentally measured. If turbidities are determined at two wavelengths, two equations can be written

$$\tau_1 = N\ (\pi/4)\ D^2\ Q_{sca}(\lambda_1) \qquad 5\text{-}4$$

$$\tau_2 = N\ (\pi/4)\ D^2\ Q_{sca}(\lambda_2) \qquad 5\text{-}5$$

Dividing equation 5-4 by 5-5 we get

$$\tau_1 / \tau_2 = Q(\lambda_1) / Q(\lambda_2) \qquad 5\text{-}6$$

From tables of $Q_{sca}(\lambda_i)$ versus diameter, a curve of $Q_{sca}(\lambda_1)/Q_{sca}(\lambda_2)$, (Q ratio) versus diameter can be obtained (11). Relating the turbidity ratio (found experimentally) to the Q ratio versus diameter curve, the diameter of the sample can be determined. The program RATIO does this automatically. Supplying the program with the turbidity ratio, the Q ratio is optimized for best fit and the diameter is printed out.

However in some size regions the Q ratio is not single valued. To determine the size unambiguously it is necessary to be able to determine turbidity ratios at sev-

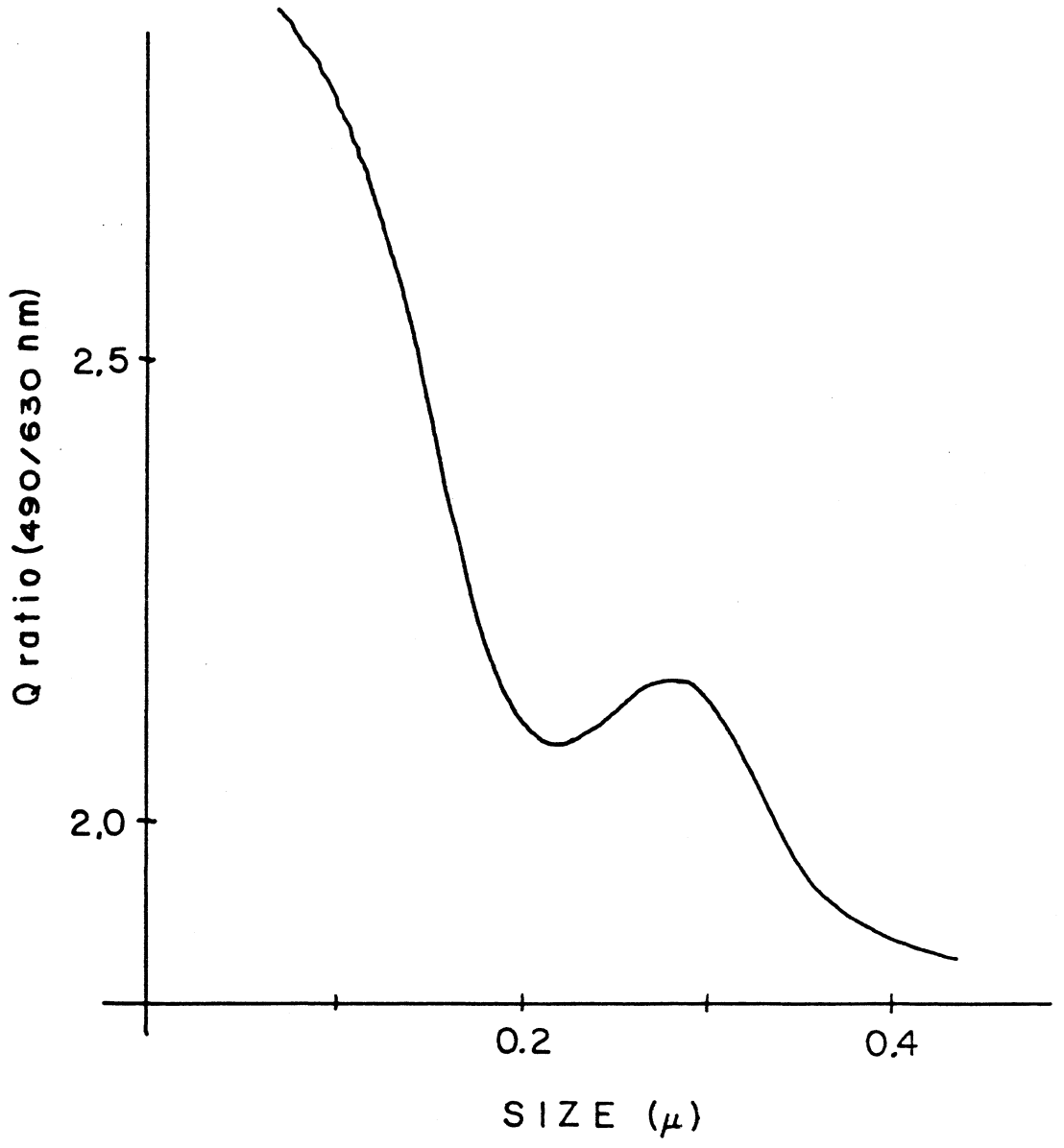

Figure 20. Q ratio versus size

eral wavelengths.

B. Size Analysis of Monodispersed Systems

To insure the validity of the theory for actual analysis, experiments were performed using controlled samples. The experimental set-up consisted of a continuous source, source filters, beam splitter, lenses, a quartz cuvet, and the detector array as described in Chapter 4. The only difference between this arrangement and that used in the final application was the use of a cuvet instead of the flow cell.

The monodispersed samples were obtained from Polysciences, Warrington Pa. They were polystyrene latex spheres supplied as a 2.5% by weight sample in aqueous solution. The sizes covered the range from 0.166μ to 1.16μ with a size variation as listed in Table 2.

The turbidity analysis involved taking a background reading, a measurement of a blank, and a measurement of the sample. The blank consisted of the solvent used with the sample, placed in a cuvet. For all of these measurements values were recorded at at least two wavelengths. The turbidity was calculated at each wavelength by

$$\tau = \ln [(\text{blank} - \text{dark}) / (\text{sample} - \text{dark})] \quad 5\text{-}7$$

Table 2.

Size Data for Monodispersed Polystyrene Sample

Polyscience's Value	Multiwavelength Array	Perkin-Elmer Spectrophotometer
1.16 μ	1.20 μ	1.17 μ
0.73 μ	0.78 μ	0.84 μ
0.50 μ	0.55 μ	0.57 μ
0.166 μ	0.16 μ	0.18 μ

The τ values were submitted to the Fortran program RATIO which calculated the size of the sample from the turbidity ratios. The results are tabulated in Table 2.

The system was also checked for its ability to yield concentration information. Concentration curves were also prepared to indicate for what concentration range this method was valid. These curves were linear up to concentrations of 0.01 weight percent.

The samples were also analyzed using a commercial spectrophotometer. A Perkin-Elmer Lambda 3 UV-VIS spectrophotometer was used scanning the region from 750 nanometers to 400 nanometers. Particle sizes were calculated at the same wavelengths as those used by the filter array. The results are listed in Table 2. The multiwavelength array and the commercial spectrophotometer give similar results.

C. Bimodal Systems

The monodispersed samples represent a specialized case not applicable to all analysis. Bimodal blends were made up to investigate the applicability of this method to more polydispersed systems. The experimental conditions were the same as those for the monodispere experiments.

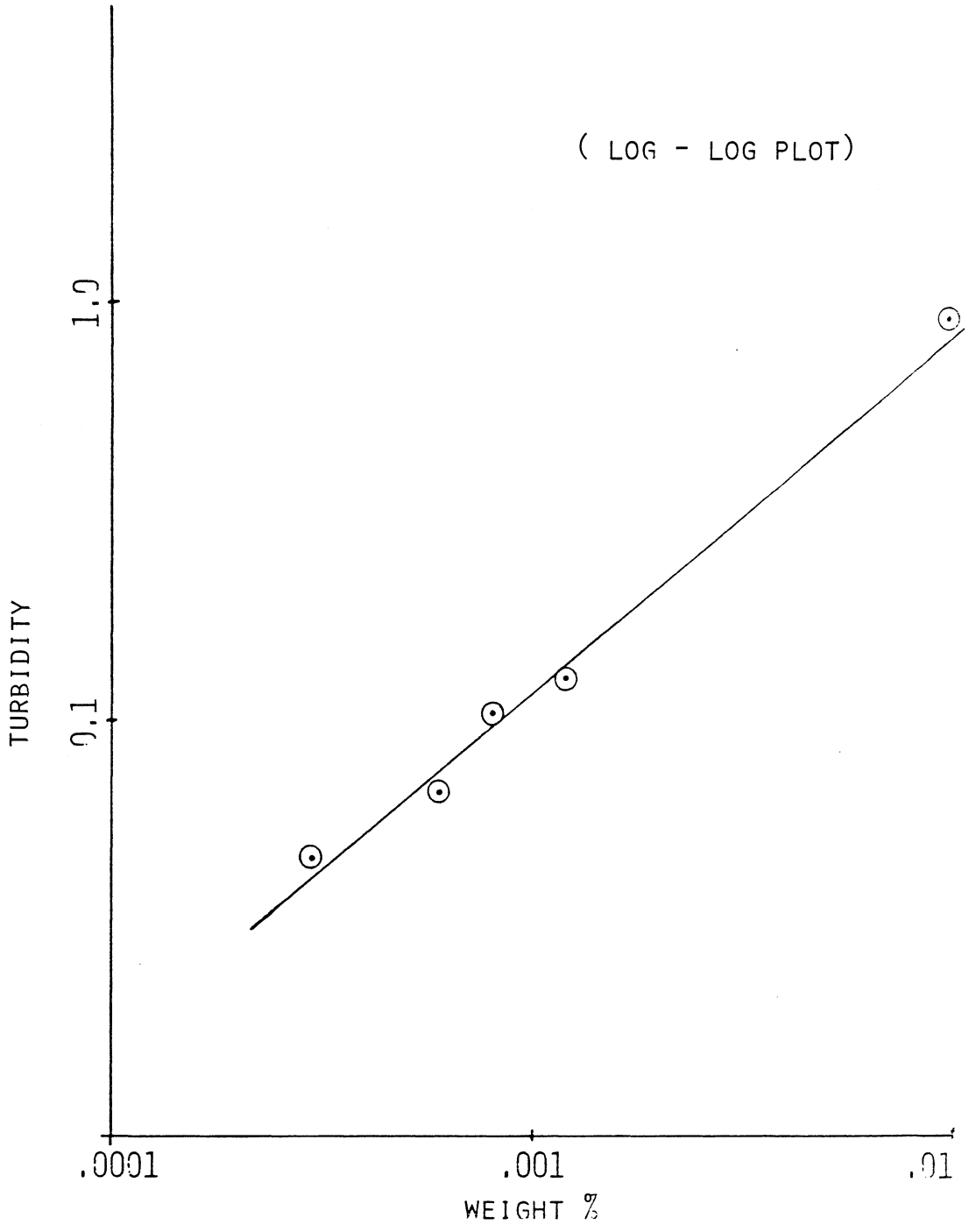

Figure 21. Turbidity vs. Concentration (0.166μ)

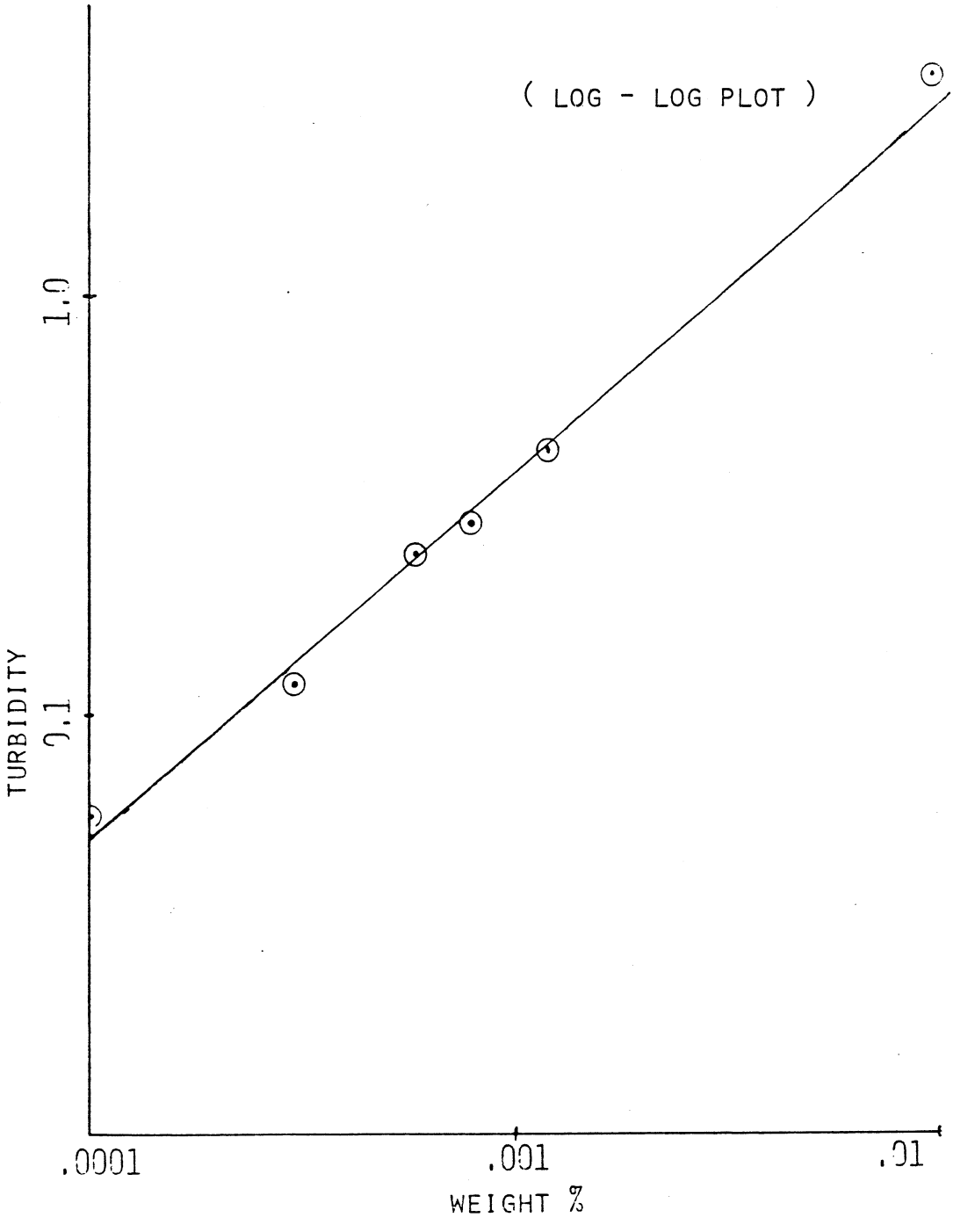

Figure 22. Turbidity vs. Concentration (0.5μ)

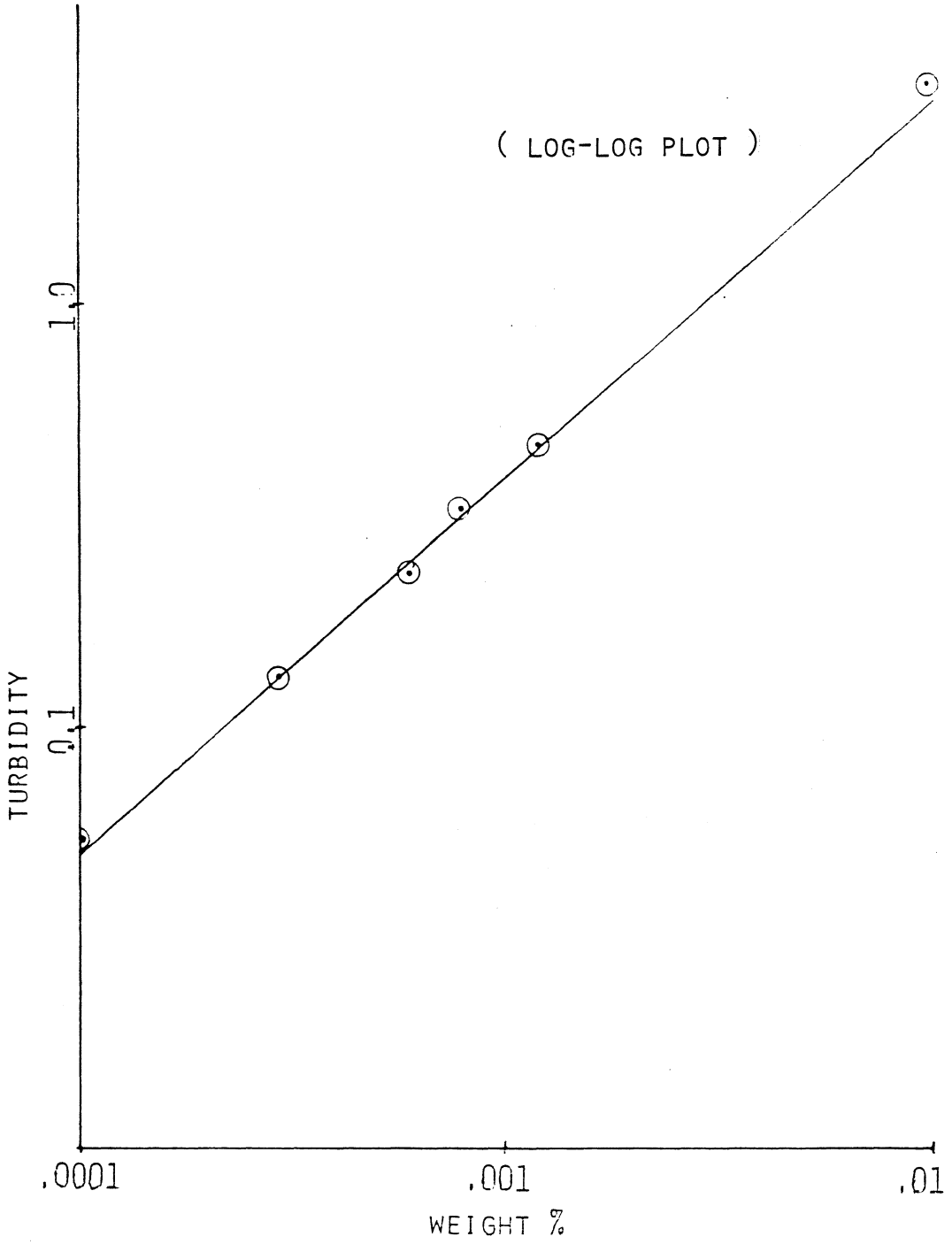

Figure 23. Turbidity vs. Concentration (1.16μ)

The monodispersed standards from Polysciences were used to prepare the bimodal blends. Preparation consisted of diluting the standards in water to appropriate concentration levels (0.001 weight percent) to produce stock solutions of monodispersed samples. Known volumes of the stock solutions were combined, producing the bimodal blends. Mixtures were made using various combinations of the monodispersed stock solutions. Aliquots were pipetted from the stock solutions and combined in a cuvet. The ratios of the volumes used were 1:5, 5:1, to provide a range of mixtures.

The size and concentration of the particles in the stock solutions were determined with the filter array. The concentration values can be determined by solving simultaneously

$$\tau_1 = N_a(\pi/4)D^2Q_{1a} + N_b(\pi/4)D^2Q_{1b} \qquad 5\text{-}8$$

$$\tau_2 = N_a(\pi/4)D^2Q_{2a} + N_b(\pi/4)D^2Q_{2b} \qquad 5\text{-}9$$

where τ is measured experimentally and the scattering efficiencies are calculated.

D. Use of Linear Parameter Estimation

Table 3.

Bimodal Mixtures of

Monodispersed Polystyrene Standards

	1.16 μ	0.50 μ
Stock Conc. =	6.75×10^{10}	9.40×10^{11}
5 : 1	5.59×10^{10} (1%)	1.59×10^{11} (1%)
1 : 5	1.05×10^{10} (6%)	7.66×10^{11} (8%)

(vol. : vol.) units = particles per unit volume.

Table 4.

Bimodal Mixtures of

Monodispersed Polystyrene Standards

	1.16 μ	0.16 μ
Stock Conc. =	6.75×10^{10}	6.00×10^{13}
5 : 1	5.73×10^{10} (2%)	8.54×10^{12} (14%)
1 : 5	9.35×10^{9} (17%)	5.33×10^{12} (7%)

(vol. : vol.) units = particles per unit volume.

Even though the calculations for the bimodal mixtures are amenable to hand calculations, an automated method is preferred. Linear parameter estimation (LPE) was chosen because of its ease of use and flexibility to handle more complex mixtures if necessary (31). Equation 5-3 can be expanded to n equations for a mixture of n components.

$$\tau_1 = N_a(\pi/4)Q_{1a} + \ldots\ldots + N_n(\pi/4)Q_{1n}$$
$$\ldots = \ldots\ldots\ldots\ldots\ldots\ldots\ldots\ldots$$
$$\tau_n = N_a(\pi/4)Q_{na} + \ldots\ldots + N_n(\pi/4)Q_{nn}$$

These equations can be reduced to

$$[T] = [H]\,[N] \qquad 5\text{-}10$$

where

$$[T] = \begin{bmatrix} \tau_1 \\ . \\ . \\ . \\ \tau_i \end{bmatrix} \qquad [H] = \begin{bmatrix} C_{scal1} & \ldots & C_{scalj} \\ . & \ldots & . \\ . & \ldots & . \\ . & \ldots & . \\ C_{scai1} & \ldots & C_{scaij} \end{bmatrix} \qquad [N] = \begin{bmatrix} N_1 \\ . \\ . \\ . \\ N_j \end{bmatrix}$$

Multiplying each side of equation 5-10 by $[H]^t$ yields

$$[H]^t\,[T] = [H]^t\,[H]\,[N] \qquad 5\text{-}12$$

Each side of equation 5-12 can be multiplied by $([H]^t[H])^{-1}$ to give

$$([H]^t[H])^{-1}[H]^t[T]=([H]^t[H])^{-1}[H]^t[H][N] \quad 5\text{-}13$$

Equation 5-13 reduces to

$$[N] = ([H]^t[H])^{-1} [H]^t [T] \quad 5\text{-}14$$

In equation 5-14, matrix [T] consists of experimentally measured values. Matrix [H] consists of standard values of the scattering cross sections of the particles at the specified wavelengths. Equation 5-14 yields the concentrations of the components from these results. The algorithm was tested on the bimodal mixtures. It produced values equivalent to those obtained by hand calculations.

When a trimodal mixture was analyzed, negative concentrations were obtained. Negative concentrations are not meaningful for the interpretation of this data. Leggett describes two sources which can cause this type behavior (36). Either the mathematical model is not appropriate to the system or the instrument is not capable of the necessary resolution. Due to the well behaved nature of the system being investigated, it is doubtful that

the mathematical description, $\tau = \Sigma(\pi/4)D^2NQ_{sca}$, is inappropriate in this case. Lack of resolution is the most probable cause.

E. Non-negative Least Squares

Solving a set of simultaneous equations with nonnegative least squares is very similar to the linear parameter estimation scheme outlined in the previous section. The only difference is that in this situation the matrix being solved for can contain no negative values. The problem can be stated as

$$\text{minimize} \quad \| H\,N - \tau \| \qquad N \geq 0 \qquad 5\text{-}15$$

where the matrices H, N, and τ are the same as those defined in the previous section. The solution to this problem requires forming several holding matrices and iteratively solving for N where $N \geq 0$. In the computation of N, if a negative value is produced, this element is replaced by zero and N is recalculated. The software used in this study was obtained from Dr. D. Leggett of Dow Chemical Co., Freeport Texas. The algorithms used are based on those described by Lawson and Hanson (37).

The nonnegative least squares (NNLS) programs were first compared with the linear parameter estimation technique. The bimodal data that was analyzed previously was submitted to the NNLS program. The results were identical to those that the LPE program produced.

Next trimodal data was submitted for analysis. In this case no negative values were produced. However the results did not show significant correlation to the concentrations present. The NNLS gave a zero value concentration, with the two other concentrations being far from the amount that was predicted to be there.

F. Size Determination in a Flowing System

The above experiments were conducted under static conditions. This allowed for the independent testing of the optics and arrays for use in particle sizing. The real interest was the application of this detector for liquid chromatography. Because of the spatial separation of the individual photodiodes in the array, this presented special problems. The size was determined by using the turbidity ratio as determined from the photodiodes. For this information to be accurate the individual diodes need to view the exact same portion of the sample bolus as it

Table 5.

Trimodal Mixture of

Monodispersed Polystyrene Standards

	1.16μ	0.50μ	0.166μ
Actual Concentration	2.25×10^{10}	3.13×10^{11}	2.00×10^{13}
LPE	1.98×10^{10} (12%)	6.30×10^{11} (100%)	-1.88×10^{-15}
NNLS	1.50×10^{10} (33%)	6.98×10^{11} (123%)	0

(concentration = number of particles / unit volume)

flows through the detector cell. This necessitates that the bolus changes little or not at all as it passes in front of the array.

The flow system was studied using the same optical and electronic design as in the previous experiments. The cuvet was replaced by a Helma 174 flow cell. The cell had a rectangular optical window 4mm wide by 20mm high. The optical path length was 10mm. The cell was connected to the output of a Spectra-Physics 3500 liquid chromatograph but without a column. Monodispersed samples were injected into the flow stream with a Valco high pressure injection valve. The sample bolus was monitored by two of the diodes in the array. The two diodes used were the two at the extremes of the array. Data was taken at the rate of one point per second. The shape of the curves produced by the diodes were compared. The curves showed similar shape under all conditions. The pumps were run at various flow rates as well as with and without the flow feedback turned on. This verified that the bolus in fact did not change as it passed in front of the filter array. Flow rates ranged from 0.80 to 3.60 mls/min.

The experiments were conducted using various sizes of the monodispersed standards. Using the turbidity ratio technique the sizes were calculated and found to agree with the results obtained under static conditions. This

required taking into account the temporal relationship of the data produced. This was handled by offsetting one of the data sets so that the peak maxima corresponded to one another. The ratio of the peak maxima gave size values within 10% of the supplier's values.

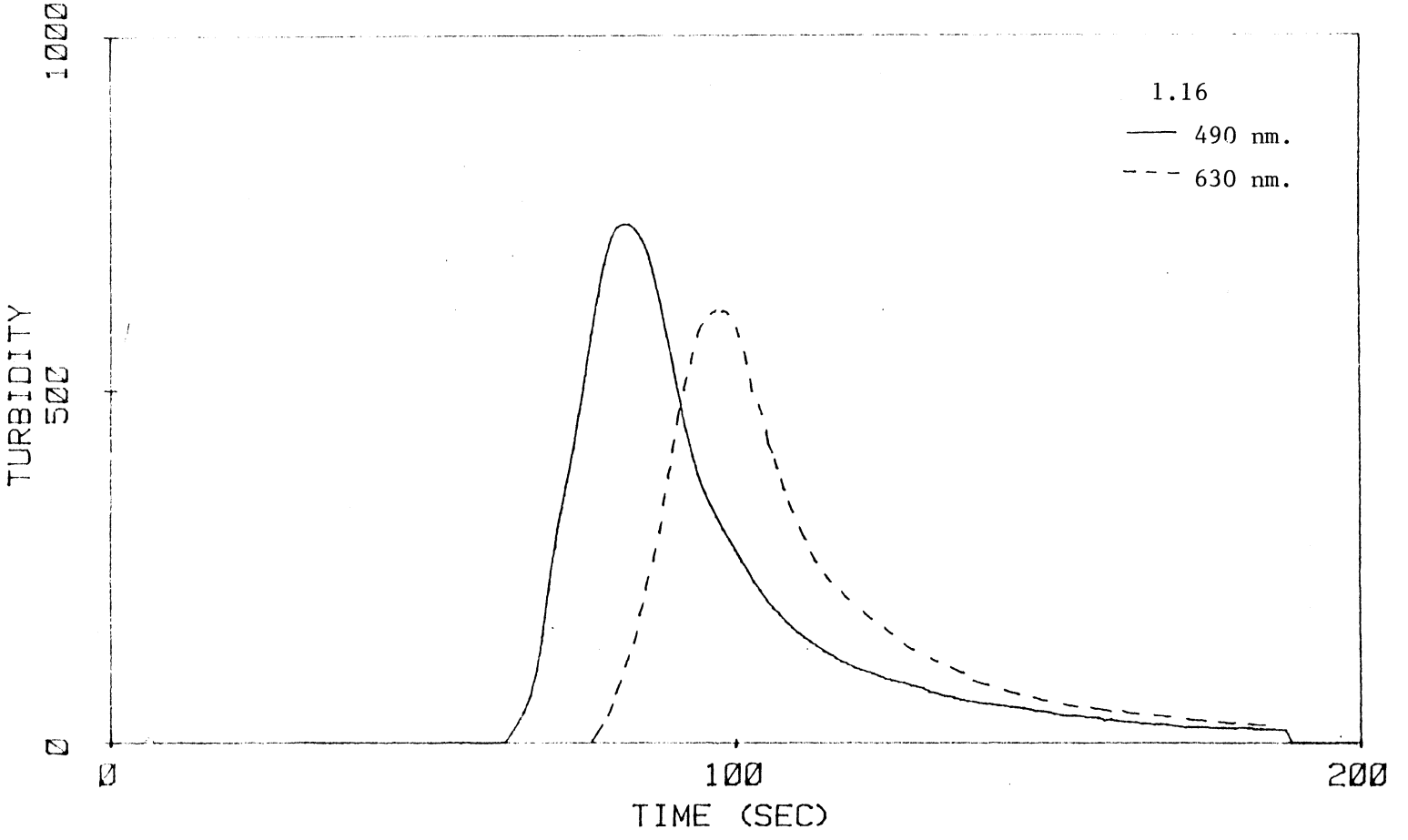

Figure 24. Flow rate = 1.6 mls./min.

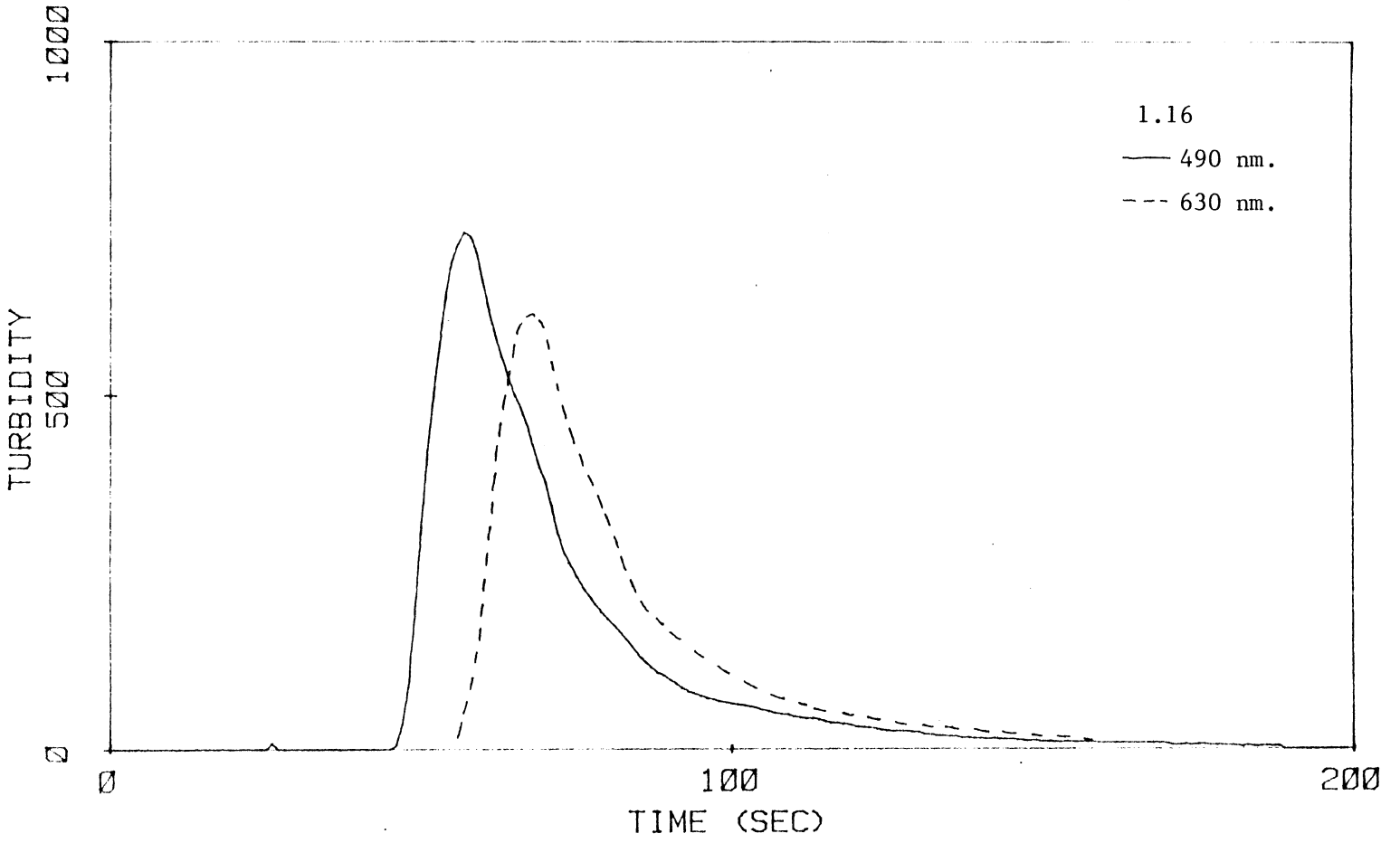

Figure 25. Flow rate = 2.0 mls./min.

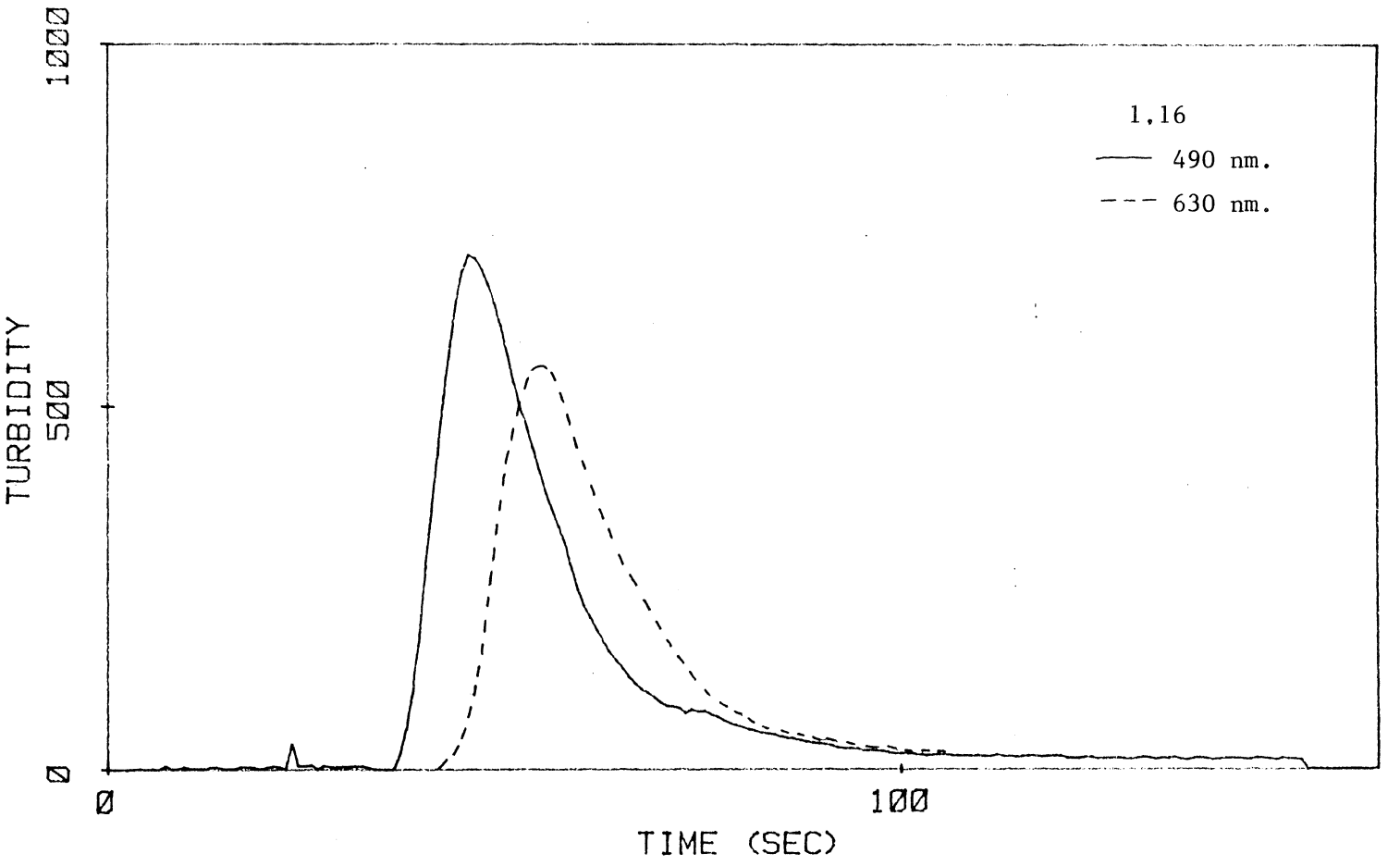

Figure 26. Flow rate = 2.4 mls./min.

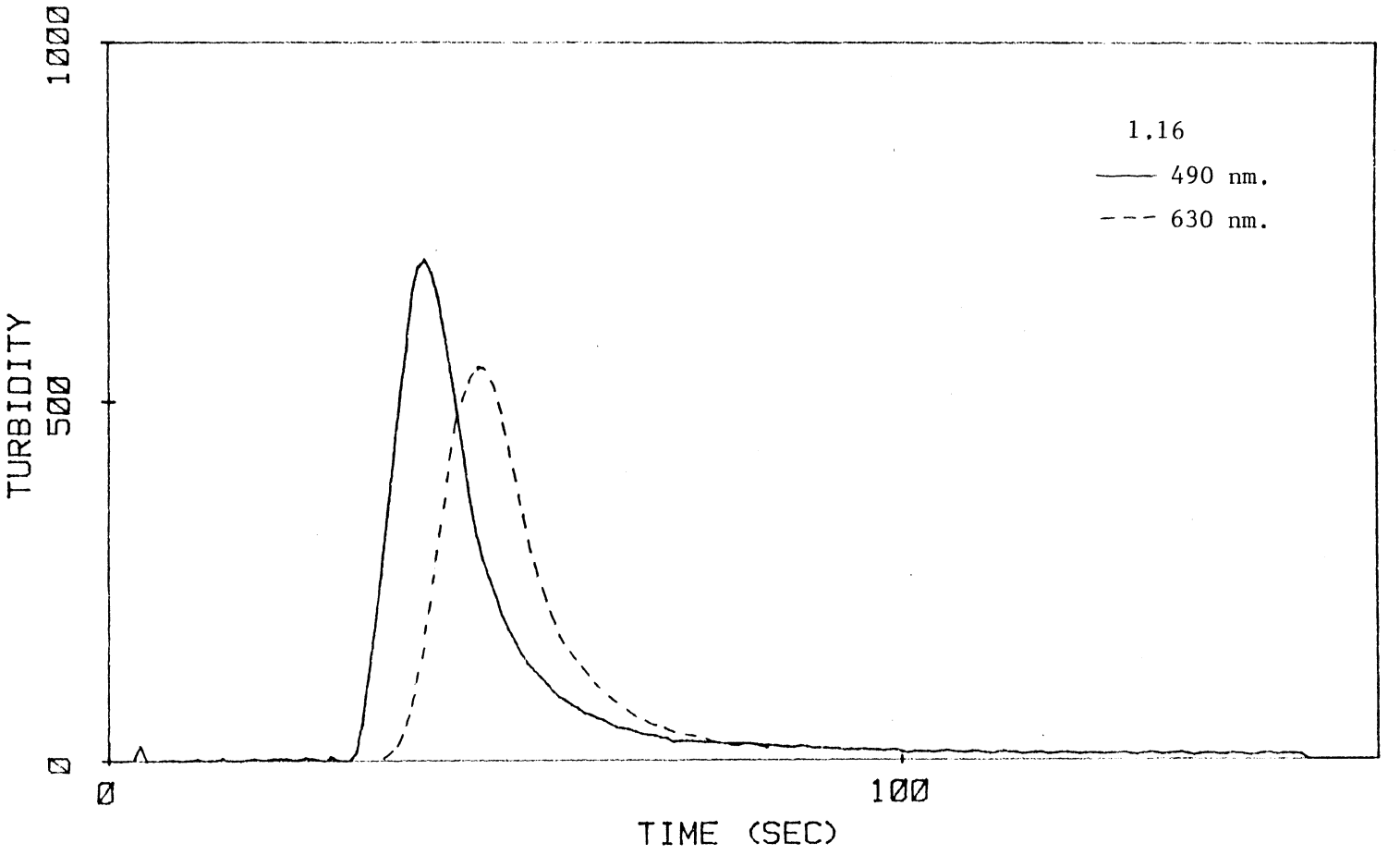

Figure 27. Flow rate = 3.2 mls./min.

Hydrodynamic Chromatography

A. Theory

In 1974 Hamish Small developed a method for the separation of colloids in the micron and submicron size region (1). The original experimental set up included columns packed with solid, nonporous particles. It was immediately obvious that the separation mechanism of these columns was different from that of traditional gel permeation chromatography. In gel permeation chromatography, separation relies primarily on a chemical or physical interaction between the solute and the stationary phase. Small's system was based upon the different eluant velocities the solute experiences as it flows through the interstitial volume of the packed bed.

The columns were composed of styrene/divinylbenzene and glass spheres. Similar behavior was observed between the styrene/divinylbenzene and the glass packed columns. This indicates that the separation is primarily dependent upon the flow phenomena in the column not the composition of the packing material, thus the term hydrodynamic chromatography. The flow in the interstitial void volume is similar to the Poiseuille flow observed in a capillary.

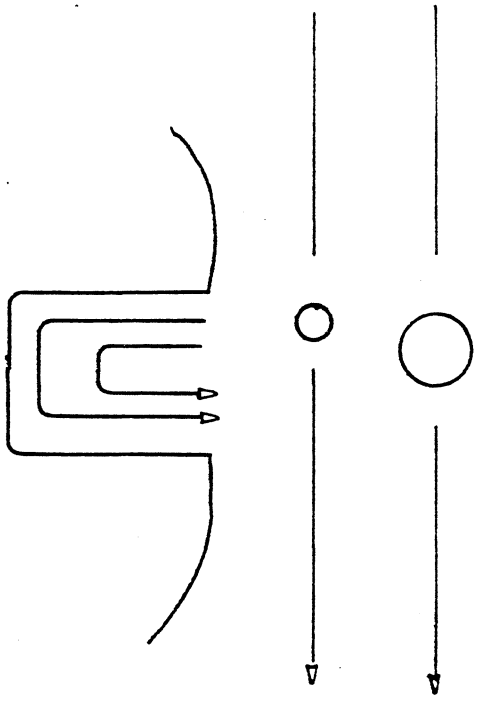

SIZE EXCLUSION CHROMATOGRAPHY

Figure 28.

The larger solute particles cannot approach the surface of the packing material as closely as the smaller particles. Therefore the larger particles experience the higher flow velocities while the smaller particles can get closer to the packing-eluant interface where the flow is slower. The larger particles elute first while the smaller particles elute later due to these "wall" effects.

In an attempt to make hydrodynamic chromatography a feasible method for routine analysis it is necessary to reduce the analysis time from 90-120 to 5-10 minutes. Recently McGowan and Langhorst have developed a method to analyze colloids in 5-10 minutes (16). This has been accomplished by developing better packing procedures and optimizing the packing material. They have produced 50 cm. columns using 15μ, cation exchange resins.

B. Column Evaluation

Martin Langhorst graciously provided me with a state of the art HDC column. The column was a 50 cm. stainless steel tube, 1/2" o.d. and 10mm. i.d. with Valco column end fittings. The first experiments were aimed at evaluating the column for its ability to separate particles by size. The experimental set up used the optical design described

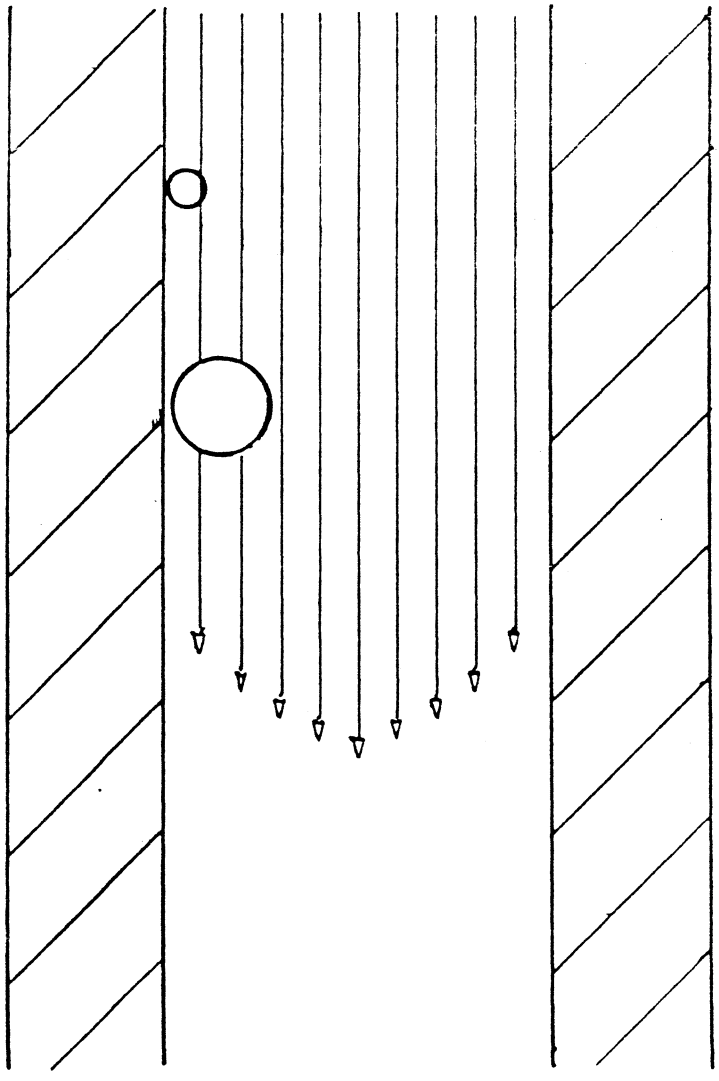

Hydrodynamic Chromatography

Figure 29.

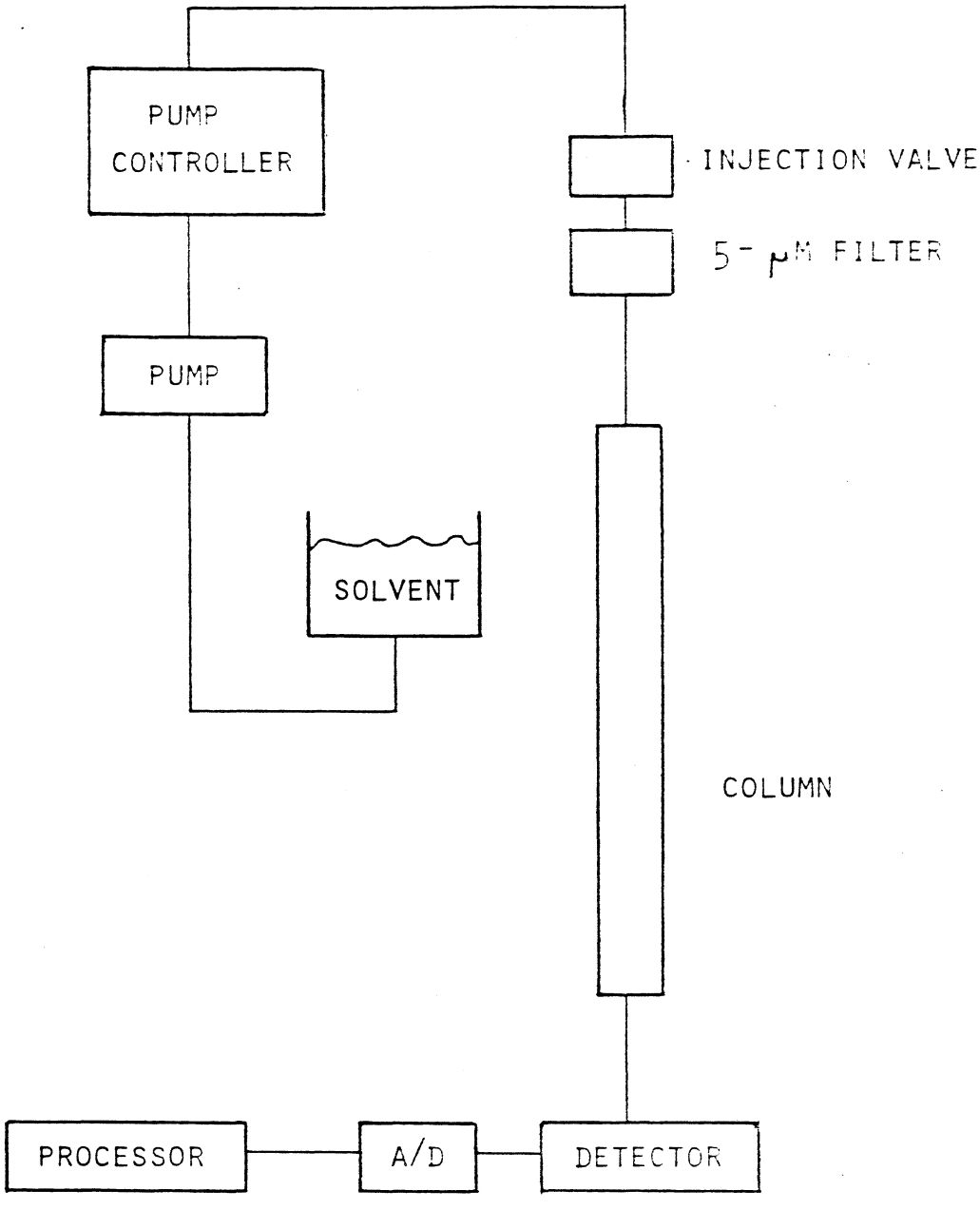

Chromatographic Set-up

Figure 30.

in Chapter 4. The chromatograph was a Spectra-Physics model 3500. The pump was run in the flow feed-back mode to maintain a constant flow rate. The flow rate was set at approximately 1.5 ml./min. The solvent used was distilled water, 0.002M Na_2HPO_4, 0.2% Triton X-100 (non-ionic surfactant), and 0.005% Thimerosal (antibacterial). Samples were injected via a Valco six port high pressure injection valve. The pressure across the column was approximately 200 psi. Monodisperse polystrene latex standards from Polysciences of Warrington Penna. were used. Sodium dichromate was added to the solutions to act as a marker.

Table 6 shows the R_f values for the various standards. The plot of R_f versus particle diameter, indicates a linear relationship between the two (Figure 31). Thus from the R_f values the particle diameter can be determined from this calibration curve. Comparision of these values with those of Langhorst and McGowan show excellent agreement (Table 6).

C. Monodispersed Samples

The R_f values determined from the monodispersed standards were based upon the time at the peak maximum. These

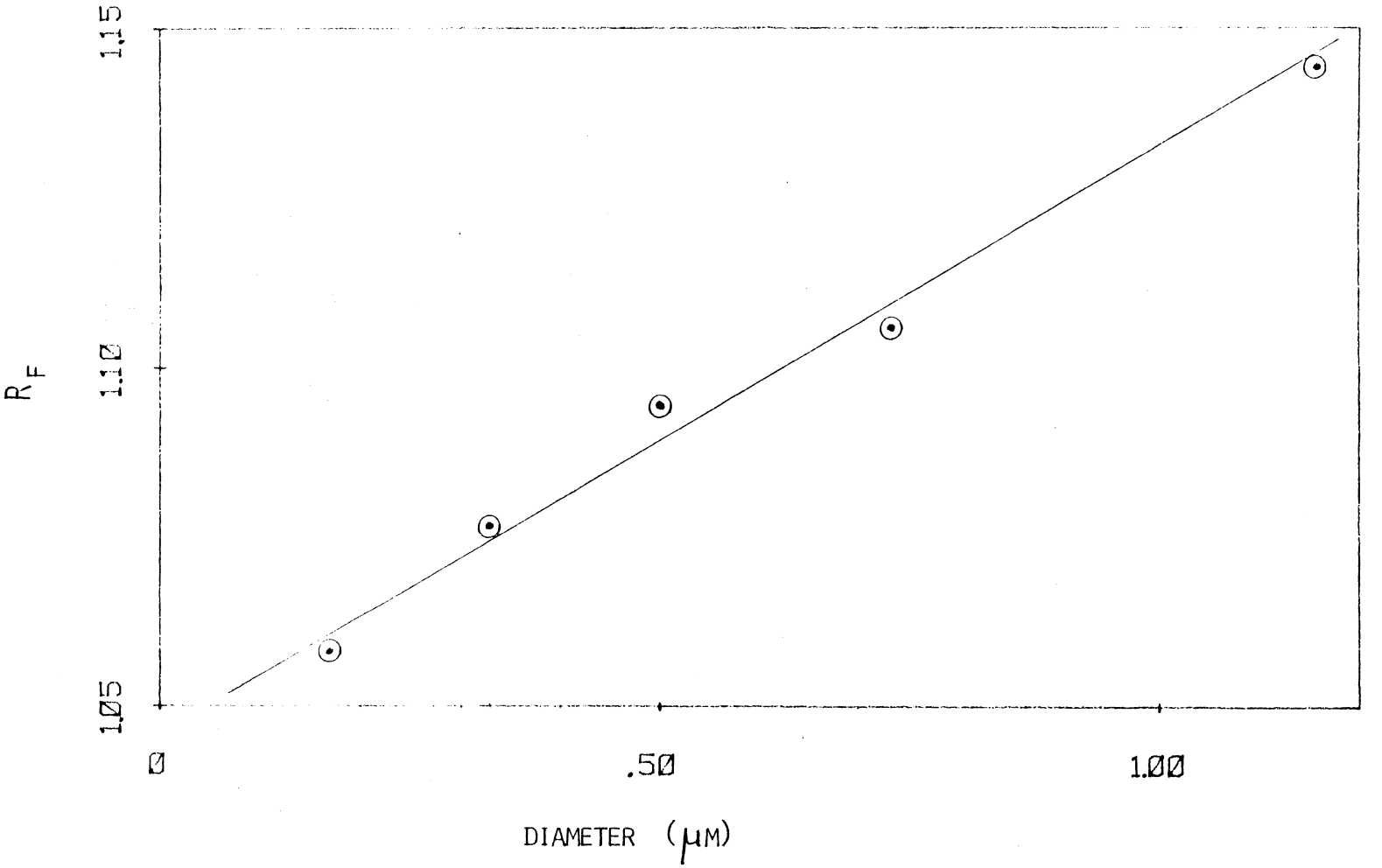

Figure 31. R_f versus particle diameter

Table 6.

Comparison of R_f Values

Dow Chemical Co.[16]		Va. Tech.	
Size	R_f	Size	R_f
0.109μ	1.038	0.166μ	1.058
0.312μ	1.071	0.325μ	1.076
0.500μ	1.088	0.500μ	1.095
0.760μ	1.106	0.730μ	1.107
1.100μ	1.132	1.160μ	1.145

standards showed significant peak broadening with respect to the R_f values. A small change in the R_f value produced a large shift in the diameter when evaluated from the R_f versus diameter calibration curve. Analysis of even monodispersed standards purely by R_f values would indicate a very polydispersed sample. For example Figure 35 shows the chromatogram for a 0.5μ monodispersed sample at a single wavelength. From the R_f values this sample represents a polydispersed sample from 0.2μ to 0.85μ. These band broadening aspects of the chromatographic process are to be expected and cannot be totally eliminated. In this case the band broadening can severely limit useful interpretation of the chromatographic results.

Employing the multiwavelength detector, size evaluation could be conducted directly on the eluant. Analysis of the same 0.5μ monodispersed sample at different wavelengths is shown in Figure 36. The histogram shown was produced by evaluating the tau ratios determined directly from the multiwavelength detector. The tau ratios were related to particle size by the program Ratio.sav. Concentrations were calculated from the diameter and turbidity values. A histogram was produced from the multiwavelength detector turbidity values. This method indicated a slight polydispersity, but gave a reasonable indication of the composition of the injected sam-

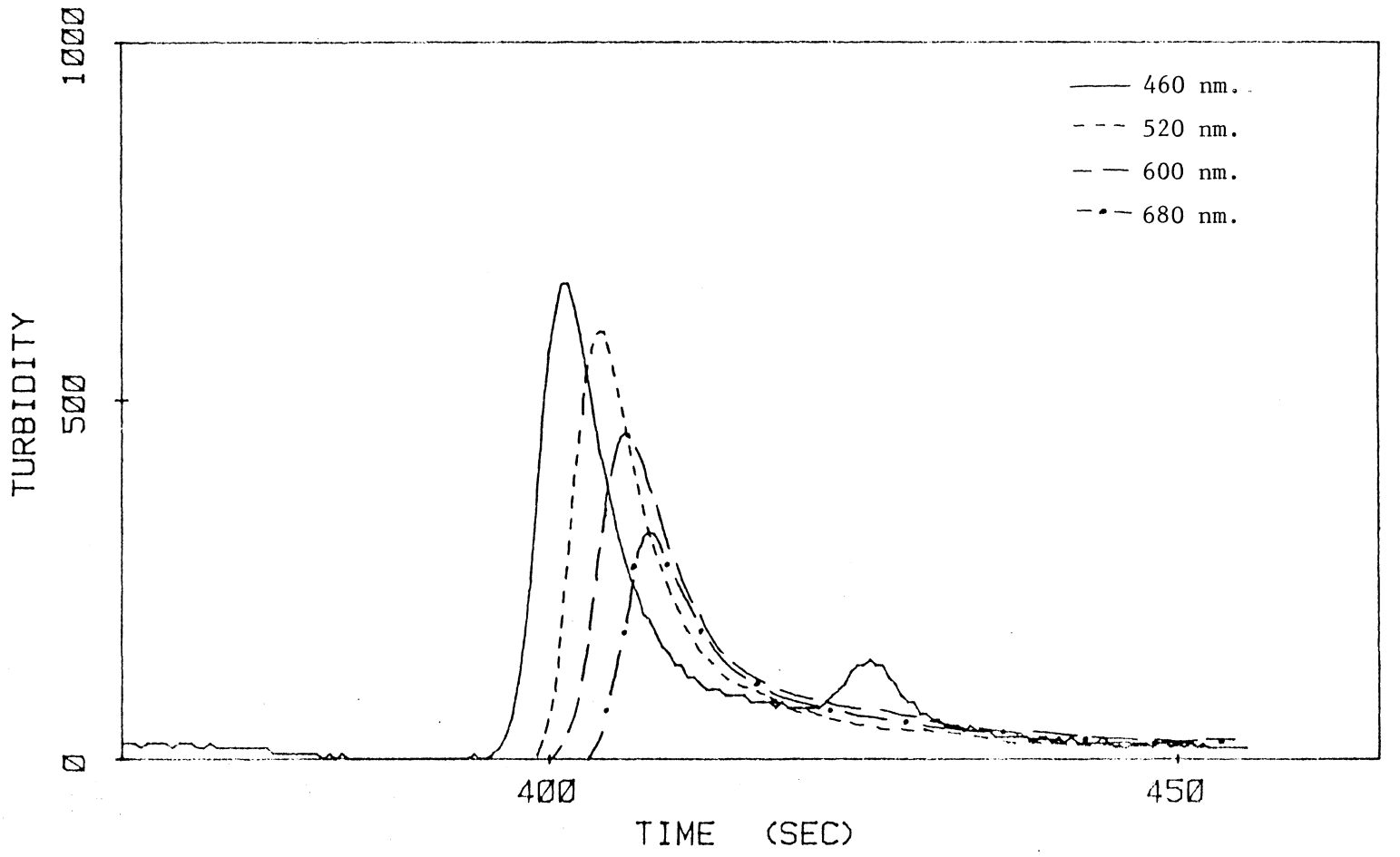

Figure 32. Chromatogram of monodisperse 0.73μ

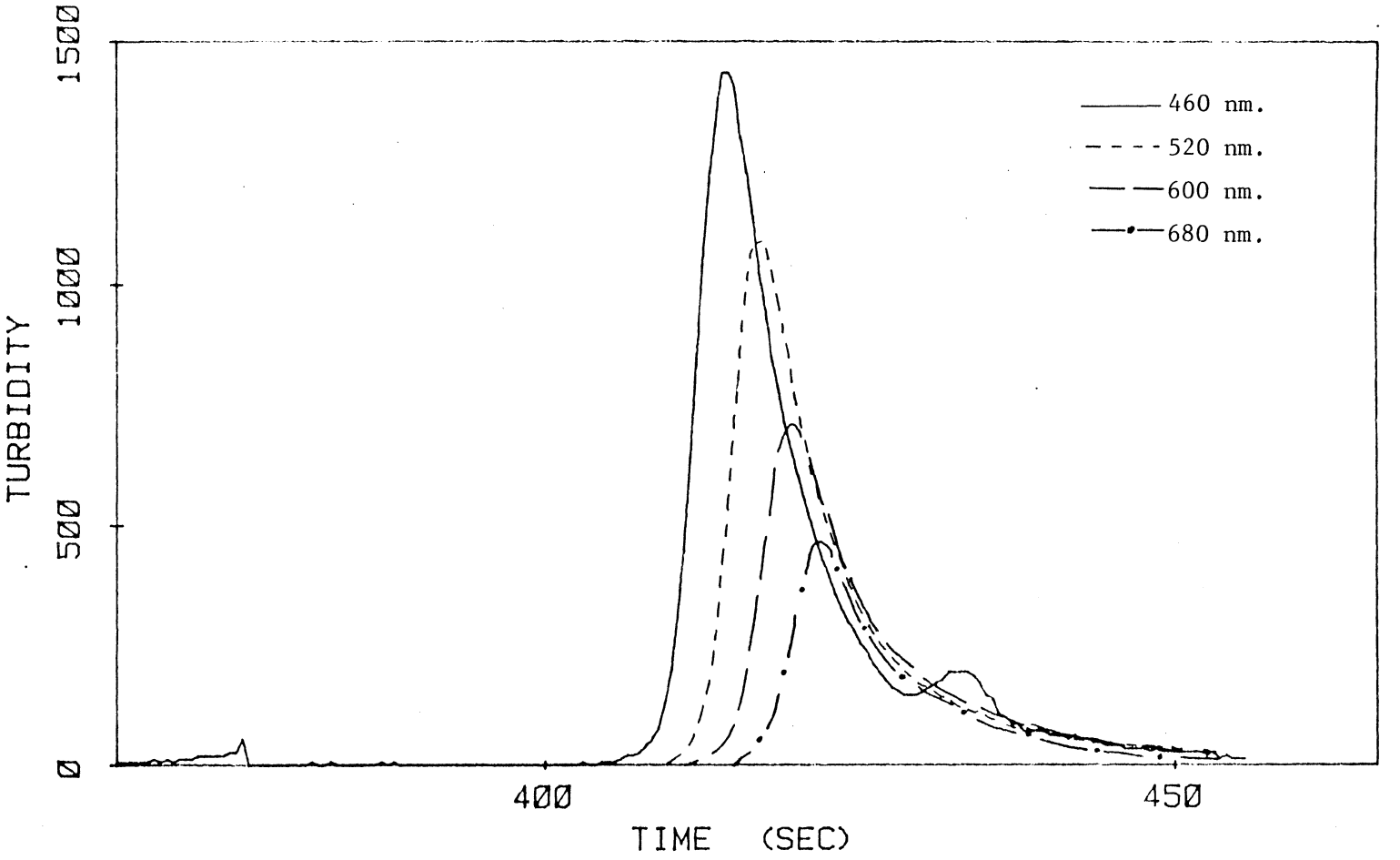

Figure 33. Chromatogram of monodisperse 0.325 μ

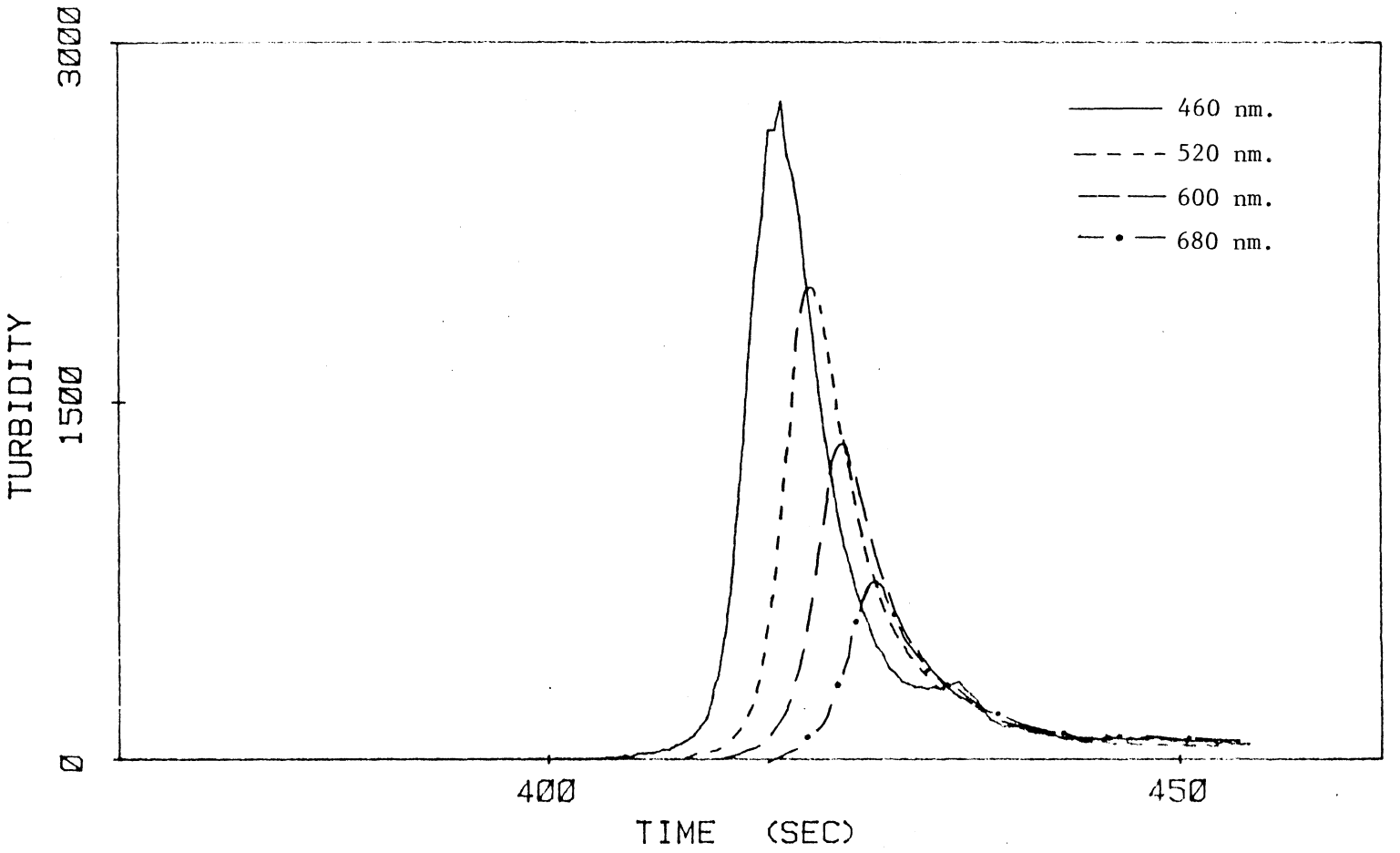

Figure 34. Chromatogram of monodisperse 0.166 μ

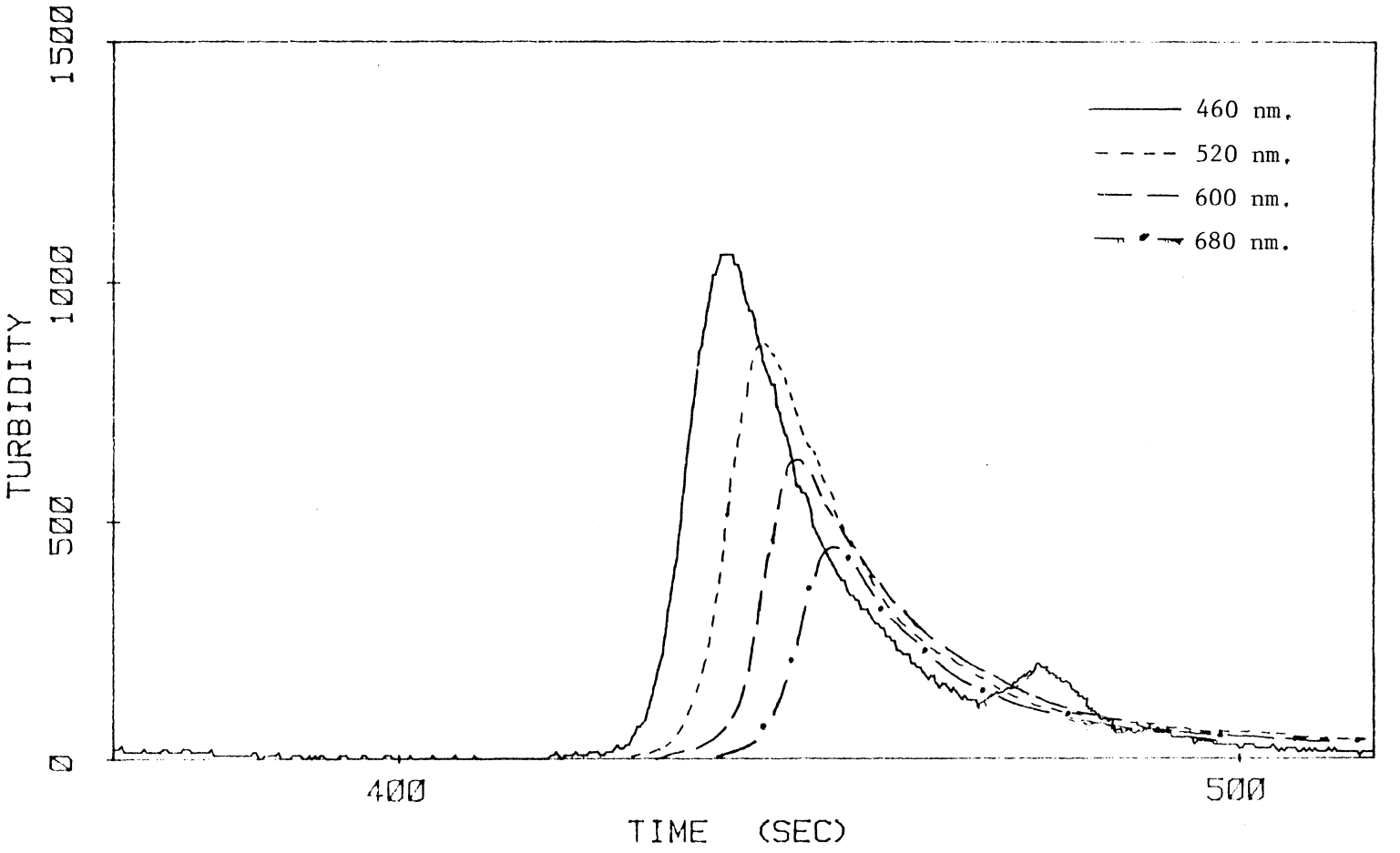

Figure 35. Chromatogram of monodisperse 0.50μ

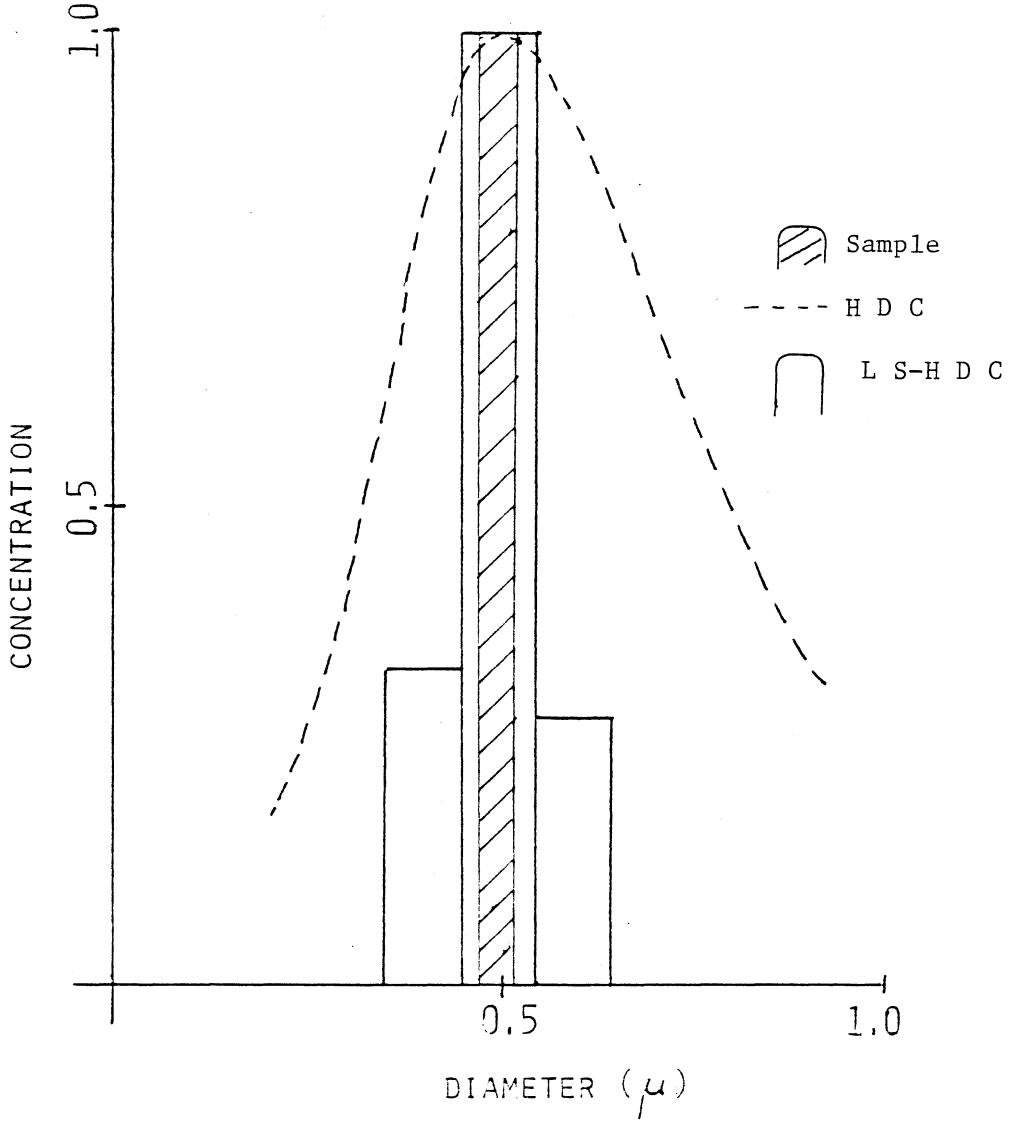

Size analysis of monodisperse 0.50

Figure 36.

ple. Using this method of size determination eliminated the need for a marker. In addition, flow rate variations do not effect size determinations directly with the multiwavelength system; but would in the case of R_f values.

D. Bimodal Samples

Bimodal blends were studied by both the R_f and multiwavelength systems. The blends were made from monodispersed standard solutions. Again the R_f values indicate that the samples were more polydisperse than they actually were. Figure 37 shows a chromatogram of a 1:1 by volume mixture of 0.325μ (0.01 wt.%) and 0.73μ (0.05 wt.%) standards. The R_f method indicates a polydisperse sample containing particles from less than 0.1μ to 1.0μ. The multiwavelength system indicates a distribution more closely resembling a bimodal blend of monodispersed components (Figure 38). The results still show more dispersity than what is actually present, but it is close to the actual composition.

E. Polydispersed Sample

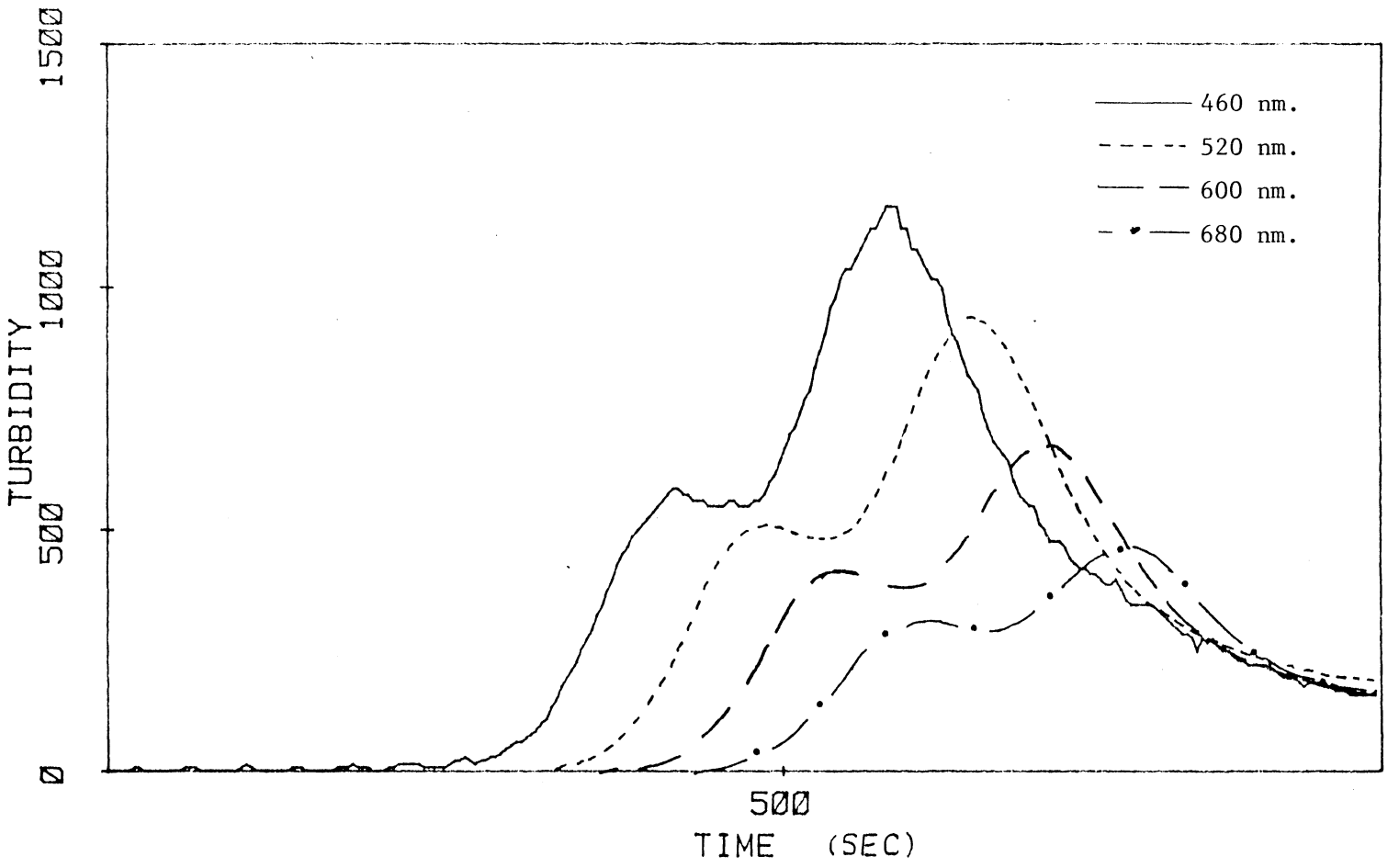

Figure 37. Chromatogram of bimodal mixture of 0.325μ - 0.73μ

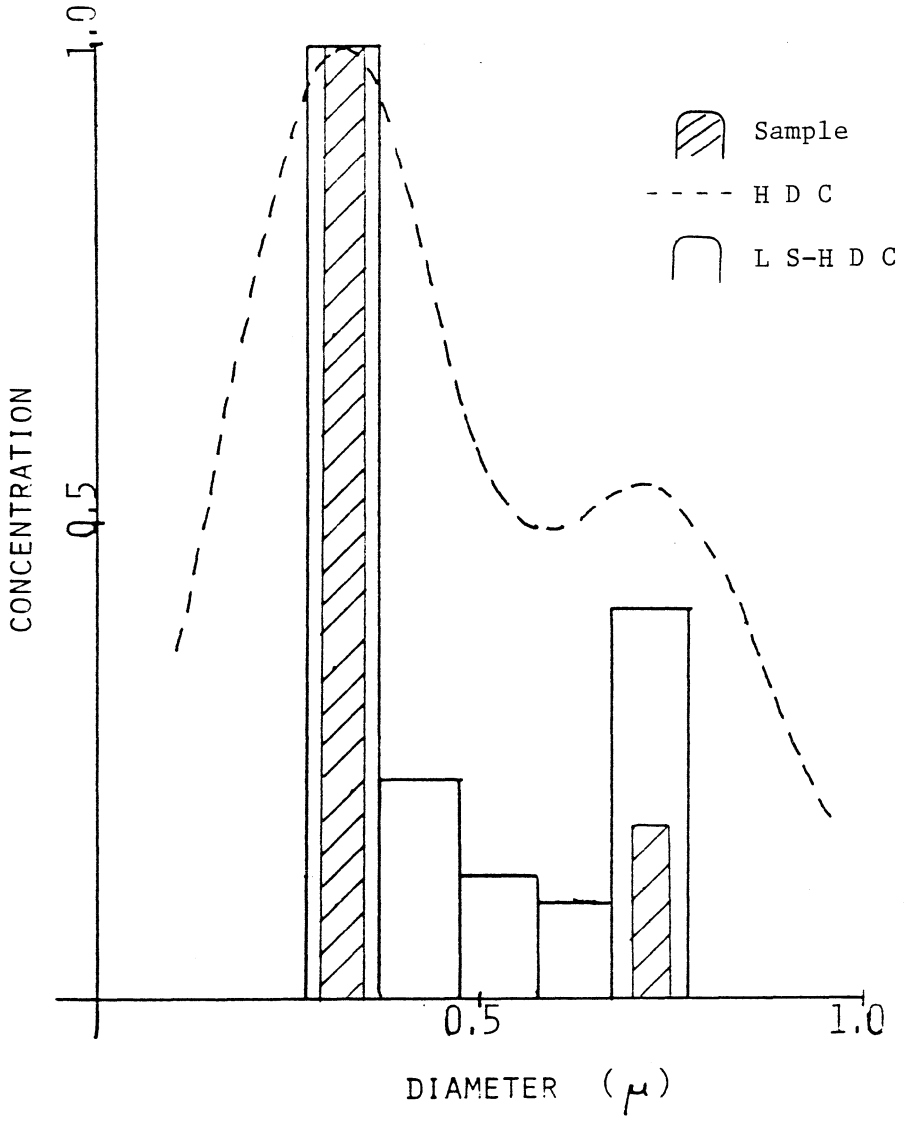

Size analysis of bimodal mixture of
0.325μ - 0.73μ

Figure 38.

An industrial polydispersed sample was studied. Dr. J. Hatfield of Union Carbide, Charleston, W. Va., supplied a typical latex sample produced by the Coating division. The sample was an acrylic with a refractive index of 1.55. The distribution of the sample was between 0.25μ and 1.5μ. Union Carbide analyzed the sample using a Joyce Loebl disc centrifuge. The same sample was analyzed using the multiwavelength detector and HDC. Figure 41 shows a comparison of the results of the various methods.

The chromatogram indicates a wider distribution than either the Joyce Loebl or the multiwavelength system. This was expected due to the band broadening characteristics of the column. The Joyce Loebl and the combined HDC multiwavelength detector system indicate comparable results. This analysis indicates that the combination of this new multiwavelength detector with a hydrodynamic chromatographic column can provide a satisfactory analytical tool for polydispersed samples.

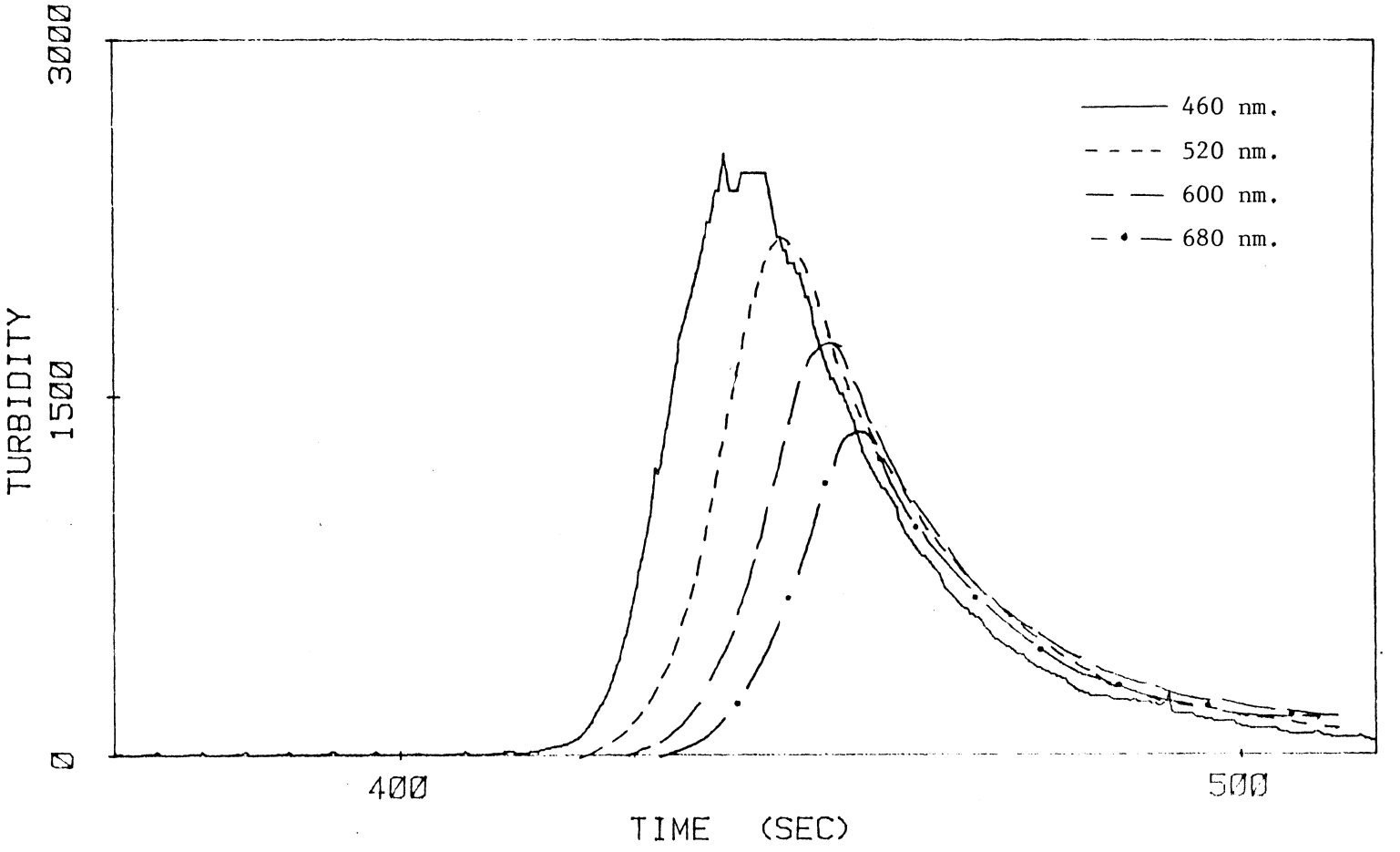

Figure 39. Chromatogram of Union Carbide 14FR10 latex

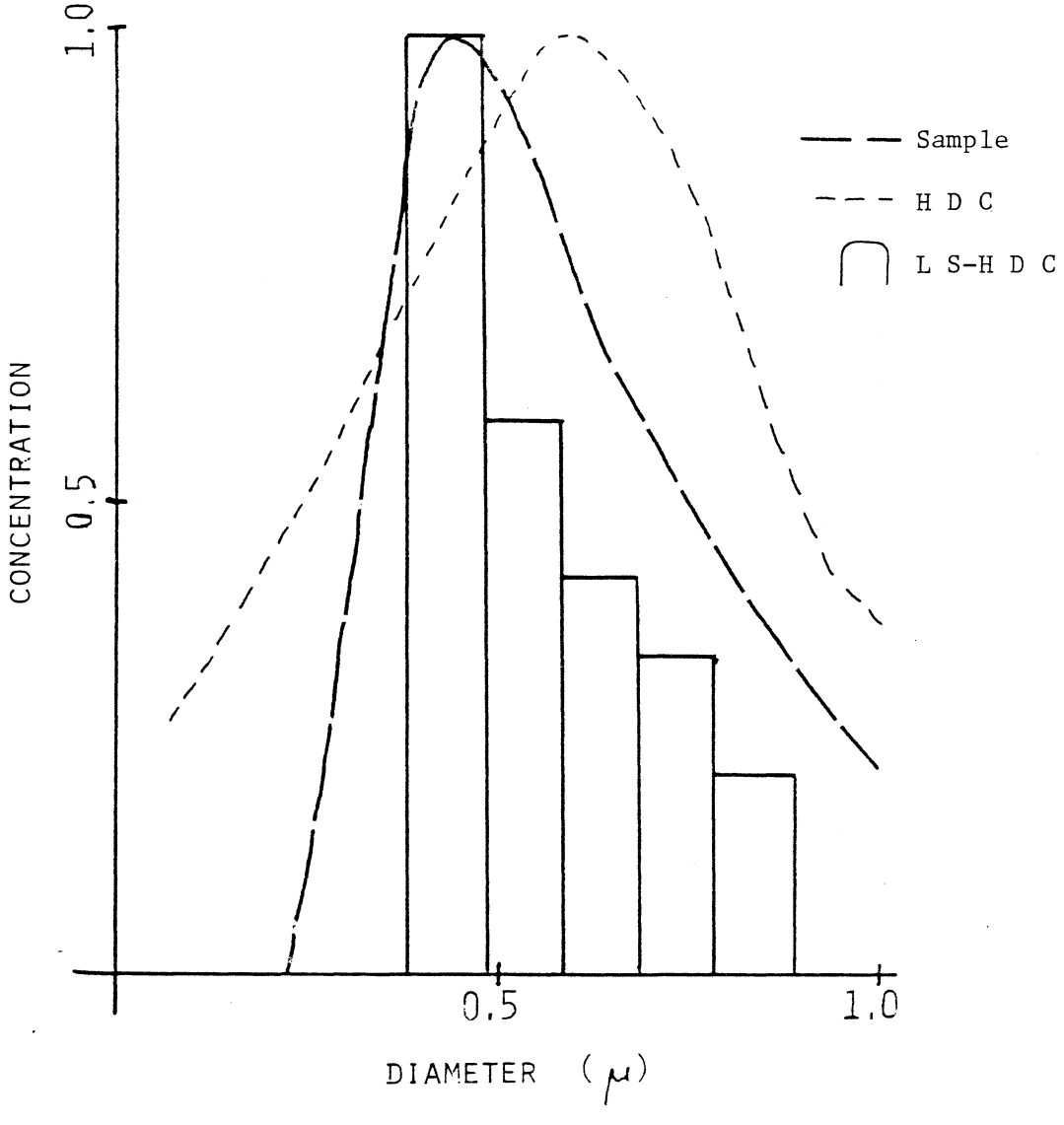

Size analysis of Union Carbide 14FR10

Figure 40.

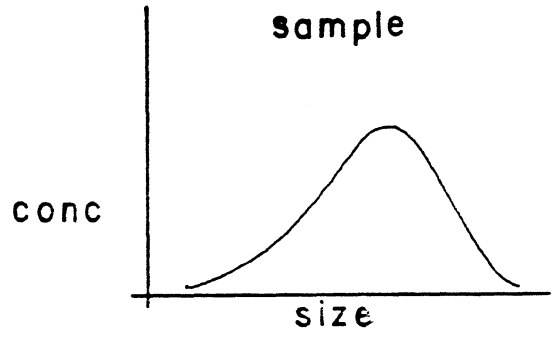

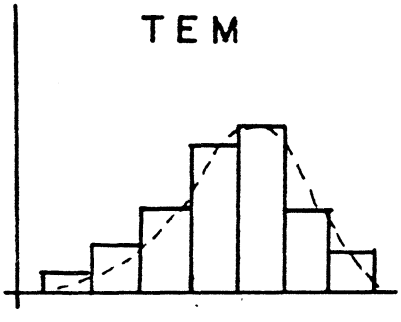

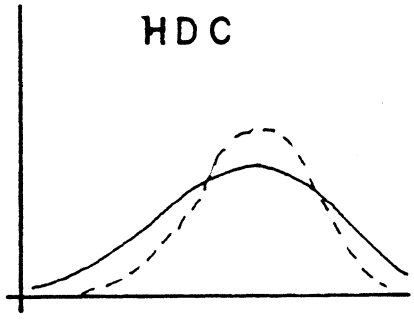

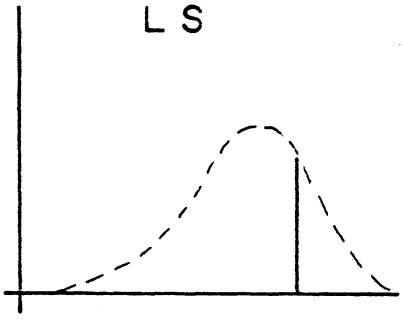

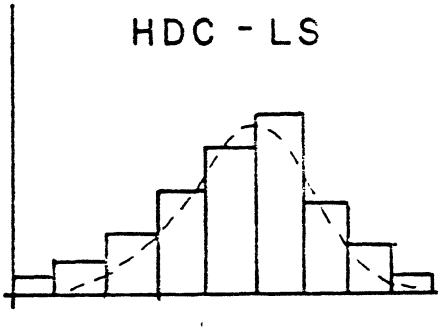

Comparison of techniques

Figure 41.

Summary

This work has shown the feasiblity of constructing a low cost, rugged system for rapid analysis of particle size and distribution. A major advantage of the design is the elimination of the need to model mathematically the distribution or the column parameters. Modeling the sample distribution requires knowledge of the sample before analysis, which may not be possible. Deconvolution of chromatograms in gel permeation chromatography have been reported but the approach is of limited use in HDC. The deposition of sample onto the column changes the axial dispersion characteristics of the column dynamically.

A limiting factor in HDC has been the overlap of the marker peak by the sample peaks. Delayed injection methods have been employed, adding complexity and decreasing sample throughput. The new detector system eliminates the need for such a marker. Even if a marker is used, as a check, wavelengths can be used to obtain the size information where the marker shows no absorption.

Using the R_f method requires good control of the flow rate. Variations in the flow rate may effect the elution times enough, that comparison of the R_f values with the calibration curve yields improper diameter values. The

multiwavelength system makes no assumptions concerning flow rates.

Analysis of particle sizes is limited to providing only average diameter values. Hydrodynamic chromatography using a single wavelength detector is characterized by a lack of resolution. This work shows that the coupling of a multiwavelength detector with hydrodynamic chromatography can provide information that normally requires complex and expensive equipment plus long analysis times. This work represents the combined state of the art for the two techniques.

Ideally one would like a system that yields absolute particle size and distribution information of a sample directly. The limiting factor at this time is the lack of resolution of the chromatographic step. Because of this lack of resolution, the solute in the flow cell is still polydispersed, but not as polydispersed as the original sample. The multiwavelength detection system gives an average diameter value for the sample present in the sample cell at each point in time. Ideally this detector system could provide information to decompose the chromatogram into the individual constituents present. Due to the limited spectral details demonstrated by these particles, the dispersions need to be very limited. The next generation of this system would require an improvement in

the column technology. As understanding increases about the actual forces operating within the column, this could be improved to the point that there would in fact be a narrow solute composition present in the sample cell at any point in time.

This project utilized wavelengths in the visible region of the spectrum. This makes it applicable to particles from 0.1μ to 5.0μ. To extend this technique to a larger particle size region requires the use of a larger wavelength range. Extension into the infrared region would be relatively straight forward. The detectors show good response in the infrared, but additional filters would be required. Extension into the ultraviolet region would be more difficult due to the poor response of these photodiodes to ultraviolet radiation. This could be overcome by using either UV-enhanced photodiodes or wavelength conversion compounds to absorb the ultraviolet radiation and then fluoresce or phosphoresce in the visible region.

Another aim of this work was to produce a rugged system. The present design requires some optical alignment. Attempts were made to use a bifurcated fiber optic bundle to direct the light directly to the two arrays. Because of the large numerical aperture of these bundles there was an inordinate amount of light scattered, and not focused on the detector arrays. With improved fiber technology

and design these difficulties could be overcome, eliminating most alignment problems.

References

1. H. Small, J. Colloid Interface Sci., 48, 147,(1974).

2. A. Hamielec, J. Liquid Chromatography, 1, 555, (1978).

3. Lord Rayleigh, Phil. Mag., 41, 107, (1871).

4. G. Mie, Ann. Physik, 25, 377, (1908).

5. V.K. LaMer, M. Barnes, J. Colloid Sci., 1, 71 (1946).

6. M. Barnes, V.K. LaMer, J. Colloid Sci., 1, 79 (1946).

7. R.M. Tabibian, W. Heller, and J.M. Epel, J. Colloid Sci., 11, 195, (1956).

8. J.B. Bateman, E.J. Weneck, and D.C. Eshler, J. Colloid Sci., 14, 308, (1959).

9. G. Dezelic, J.P. Kratohvil, J. Colloid Sci., 16, 561, (1961).

10. S.H. Maron, P.E. Pierce, and I.N. Ulevitch, J. Colloid Sci., 18, 470, (1963).

11. R.N. Dobbins, G.S. Jizmagian, J. Optical Soc. Am., 56, 1345, (1966).

12. G. Yamamoto, M. Tanaka, Appl. Opt., 8, 447, (1969).

13. K.L. Cashdollar, C. K. Lee, and J.M. Singer, Appl. Opt., 18, 1763, (1979).

14. L.R. Snyder, J.J. Kirkland, Introduction to Modern Liquid Chromatography, John Wiley and Sons Inc., N.Y., (1978).

15. R. Noel, K. Gooding, F. Regnier, D. Ball, C. Orr, M. Mullins, J. Chromat., 166, 373, (1978).

16. G.R. McGowan, M.A. Langhorst, J. Colloid Interface Sci., 89, 94, (1982).

17. L.H. Tung, J. Appl. Polym. Sci., 10, 375, (1966).

18. T. Provder, E.M. Rosen, Separ. Sci., 5, 437, (1970).

19. H.E. Pickett, M.S.R. Canton, J.F. Johnson, J. Appl. Polym. Sci., 21, 67, (1968).

20. T. Ishige, S.I. Lee, A.E. Hamielec, J. Appl. Polym. Sci., 15, 1607, (1968).

21. R.F. Stoisits, G.W. Poehlein, and J.W. Vanderhoff, J. Colloid Interface Sci., 57, 337, (1976).

22. C.A. Silebi, A.J. McHugh, J. Appl. Polym. Sci., 23, 1699, (1979).

23. Y. Talmi, Multichannel Image Detectors, American Chemical Society, Washington D. C., (1979).

24. R. Dessy, W. Nunn, C. Titus, W. Reynolds, J. Chrom. Sci., 14, 194, (1976).

25. M.M. Blouke, M.W. Cowens, J.E. Hall, J.A. Westphal, and A.B. Christensen, Appl. Opt., 19, 3318, (1980).

26. M.H. Crowell, T.M. Buck, E.E. Labunda, J.V. Dalton, and E.J. Walsh, Bell Sys. Tech. J., 46, 491, (1973).

27. Solid State Silicon Photodiodes, RCA Solid State Division Lancaster Penna., (1978).

28. H.A. Strobel, Chemical Instrumentation: A Systematic Approach, Addison-Wesley Co., Wesley Mass., (1973).

29. Optics Guide 2, Melles Griot, Irvine Calif., (1983).

30. J.V. Dave, Subroutines for Computing the Parameters of the Electromagnetic Radiation Scattered by a Sphere, IBM Research Center, Palo Alto, Calif., (1968)

31. T.A. Brubaker, R. Tracy, and C.L. Pomernacki, Anal. Chem., 50, 1017A, (1978).

32. H.C. van deHulst, Light Scattering by Small Particles, John Wiley and Sons, New York, (1963).

33. M. Kerker, The Scattering of Light and Other Electromagnetic Radiation, Academic Press, New York, (1969).

34. W. Heller, W.J. Pangonis, and A. Jacobson, Tables of Light Scattering Functions for Spherical Particles Wayne State University Press, Detriot (1957).

35. J.A. Davidson, J.S. Haller, J. Colloid Interface Sci., 47, 459, (1974).

36. D.J. Leggett, Anal. Chem., 49, 276, (1977).

37. C.L. Lawson, R.J. Hanson, Solving Least Squares Problems, Prentice-Hall, Englewood Cliffs, N.J., (1974).

Software Appendix

```
225 LIST

 0 ( MONOCHROMATOR CONTROL BLOCK                                  CRK)
 1 OCTAL
 2 VARIABLE   VOLTAGE                176760 CONSTANT   DACO
 3
 4 CODE   DACOUT   DACO VOLTAGE  MOV  NEXT
 5
 6 : +5VOLT   2000 VOLTAGE !  DACOUT ;
 7 : ZEROVOLT   0 VOLTAGE !   DACOUT ;
 8
 9 : MONOCONTROL   13560 0 DO +5VOLT  ZEROVOLT  LOOP ;
10
11 : NANOMETERS    0 DO  MONOCONTROL  LOOP ;
12
13 DECIMAL
14
15


226 LIST

 0 ( DATA AQUISITION ROUTINES                                     CRK)
 1 OCTAL
 2 176770  CONSTANT  ADCSR          176772  CONSTANT ADCBUF
 3 ( ADC EXPECTS A/D CHANNEL IN OCTAL )
 4 CODE   ADC  ADCBUF CLR ADCSR S ) MOV  BEGIN  ADCSR TST B
 5          0< END   S ) ADCBUF  MOV NEXT
 6 DECIMAL
 7 : STALL0   07500 0 DO '   LOOP  ;
 8 OCTAL
 9 2402 CONSTANT   D1 ( 460)         3402 CONSTANT   D2 ( 600)
10 1002 CONSTANT   D3 ( 520)         5002 CONSTANT   D4 ( 680)
11 DECIMAL
12 0 VARIABLE D1ARRAY  1000 ALLOT  0 VARIABLE D2ARRAY 1000 ALLOT
13 0 VARIABLE D3ARRAY  1000 ALLOT  0 VARIABLE D4ARRAY 1000 ALLOT
14 0 VARIABLE TEMP 2 ALLOT
15 231 LOAD


227 LIST

 0 ( DATA ACQUISITION ROUTINES BLOCK #2                           CRK)
 1 : RUN- A A  CR 1000    0 DO 0 TEMP ! D1 ADC  DROP
 2          10 0 DO D1 ADC TEMP @ + TEMP ! 2 +LOOP
 3          TEMP @ 5 / DUP .  D1ARRAY I + !  0 TEMP ! D2 ADC DROP
 4          10 0 DO  D2 ADC  TEMP @ + TEMP ! 2 +LOOP  TEMP @ 5 /
 5          DUP .   D2ARRAY I + !   0 TEMP ! D3 ADC DROP  10 0 DO
 6          D3 ADC TEMP @ + TEMP ! 2 +LOOP TEMP @ 5 / DUP .
 7          D3ARRAY I + !   0 TEMP ! D4 ADC DROP
 8          10 0 DO  D4 ADC TEMP @ + TEMP !   2 +LOOP
 9          TEMP @ 5 / DUP . D4ARRAY I + !  CR STALL0 2 +LOOP ;
10
11 : STORE-DATA   BLOCK  1000 MOVE UPDATE FLUSH ;
12
13
14
15
```

```
228 LIST

    0 ( CALCULATION OF TAU-VALUES                                  CRK)
    1 100 LOAD 108 L AD
    2 0 VARIABLE BLANK  2 ALLOT        0 VARIABLE DARK  2 ALLOT
    3 0 VARIABLE #BLOCK 2 ALLOT        0 VARIABLE Y     2 ALLOT
    4 0 VARIABLE Y-VALUE 1000 ALLOT    0 VARIABLE TBLANK
    5 0 VARIABLE TDARK                 0 VARIABLE 2Y  1000 ALLOT
    6
    7 : TAU-POINTS    TBLANK  !   0 FLOAT DARK F!   #BLOCK !
    8         TBLANK @ 0 FLOAT BLANK F! TBLANK @ DARK F@ FIX DROP
    9         -  TBLANK ! DARK F@ FIX DROP TDARK !
   10         BLANK F@ DARK F@ F- BLANK F!
   11         900  0 DO  #BLOCK @ BLOCK  040 + I + @ Y !
   12         Y @ TDARK @ - TBLANK @ < IF
   13         Y @ 0 FLOAT DARK F@ F-  BLANK F@ F/          LN -1E0 F*
   14         1000 0 FLOAT F* FIX DROP  Y-VALUE I + !
   15         ELSE  0 Y-VALUE I + ! THEN  2 +LOOP ;


229 LIST

    0 ( CALCULATE THE TAU RATIO                                    CRK)
    1 0 VARIABLE  IND                        0 VARIABLE  OFF
    2
    3
    4 : RATIO-TEST    TAU-POINTS  Y-VALUE 2Y 1000 MOVE   TAU-POINTS
    5      CR   200 0 DO 2Y I + IND @ + @ DUP 0 FLOAT F. 0 FLOAT
    6      Y-VALUE I + IND @ + OFF @ + @ DUP 0 FLOAT F. 0 FLOAT
    7      F/ F. CR  2 +LOOP ;
    8
    9      ( TO USE, LOAD "OFF" WITH THE NECESSARY OFFSET TO ACCOUNT
   10      FOR SPACIAL DIFFERENCE OF DIODES, AND LOAD "IND" WITH
   11      THE VALUE OF WHERE TO START CALCULATIONS IN THE ARRAYS.
   12      USAGE:  BLK# ARRAY 1, DARK VALUE ARRAY 1, SOLVENT BLANK
   13      ARRAY 1, BLK# ARRAY 2, DARK VALUE ARRAY 2, SOLVENT BLANK
   14      ARRAY 2,  RATIO-TEST)
   15


230 LIST

    0 ( EMPTY )
    1
    2
    3
    4
    5
    6
    7
    8
    9
   10
   11
   12
   13
   14
   15

Copyright VPI & SU  L.A.I.D. Group      NO DATE      LSI-11 polyFORTH

ok
```

FORTH GLOSSARY

WORD	BLOCK	STACK
+5VOLT	225	
	Puts the octal equivalent of +5 volts into the variable used by the digital-to-analog converter. Used to control the monochromator.	
ADC	226	(1-0)
	Given the analog-to-digital converter channel, does a conversion on that channel. The result is left in the ADC data buffer (ADCBUF).	
DACOUT	225	
	Outputs the voltage corresponding to value stored in the variable VOLTAGE. Either 0 or +5 volts is generally used.	
MONOCONTROL	225	
	Outputs 6000 pulses to the monochromator controller, which corresponds to one nanometer.	
NANOMETERS	225	(1-0)
	The number on the stack specifies the number of nanometers the monochromator will be advanced.	
RATIO-TEST	229	(6-0)
	Calculates the tau ratio from data obtained at two wavelengths. User supplies the blk#, dark value, and solvent blank values for each data array.	
RUN-DATA	227	
	Acquire data from the detectors and store in temporary data arrays. A five point box-car average is performed during this collection.	

STALLO 226

This loop determines how much time will elapse between the data collection from each individual diode. This determines the number of data points collected per minute.

STORE-DATA 227 (2-0)

Stores the data arrays, created by RUN-DATA in user specified blocks.

TAU-POINTS 228 (3-0)

Calculate the turbidity values. The user specifies the block number, background value, and the solvent blank value.

ZEROVOLTS 225

Puts a zero into the variable VOLTAGE, used by DACOUT. Used to pulse the monochromator controller.

SCAT.FOR

```
      SUBROUTINE SCAT
      COMMON WLA, DIAM, Q
      DIMENSION A(100),B(100),C(100),D(100)
      DIMENSION E(100),F(100)
      DIMENSION  BI(100), BJ(100),BK(100),BL(100),X(100)
      BM = 1.5683 + (10087.0 / (WLA*WLA))
      U = (1.7521 + 8110.0/(WLA*WLA))**0.5
      WLM = WLA/U
      AM = BM / U
      Z = DIAM * 3.1415927 / (WLM/1000)
      Y = AM * Z
      A(1) = SIN(Z)
      B(1) = COS(Z)
      C(1) = COS (Z)
      D(1) = -SIN(Z)
      E(1) = SIN(Y)
      F(1) = COS(Y)
      S = 0
      I = 2
      N = 1
      A(2) = A(1)/Z - B(1)
      B(2) = ( 1 - 1/Z**2)*A(1) + B(1)/Z
      C(2) = B(1)/Z + A(1)
      D(2) = (1 - 1/Z**2)*B(1) - A(1)/Z
      E(2) = E(1)/Y - F(1)
      F(2) = (1 - 1/Y**2)*E(1) + F(1)/Y
769   CONTINUE
      BI(N) = (AM*E(I)*B(I)-F(I)*A(I))/(F(I)*C(I)-
     &AM*E(I)*D(I))
      BJ(N) = (E(I)*B(I)-AM*F(I)*A(I))/(AM*F(I)*C(I)-
     &C(I)-E(I)*D(I))
      BK(N) = ATAN (BI(N))
      BL(N) = ATAN (BJ(N))
      X(N) = (2*N+1)*((SIN(BK(N)))**2+(SIN(BL(N)))**2)
      S = S + X(N)
      TA = X(N)/S
      IF (TA-0.0001) 1160,980,980
980   N = N + 1
      I = I + 1
      A(I) = ((2*I-3)/Z)*A(I-1) - A(I-2)
      B(I) = -((I-1)/Z)*A(I) + A(I-1)
      C(I) = (( 2*I-3)/Z)*C(I-1) - C(I-2)
      D(I) = -((I-1)/Z)*C(I) + C(I-1)
      E(I) = ((2*I-3)/Y)*E(I-1)-E(I-2)
      F(I) = -((I-1)/Y)*E(I)+E(I-1)
      GO TO 769
1160  Q = (2/Z**2)*S
```

```
RETURN
END
```

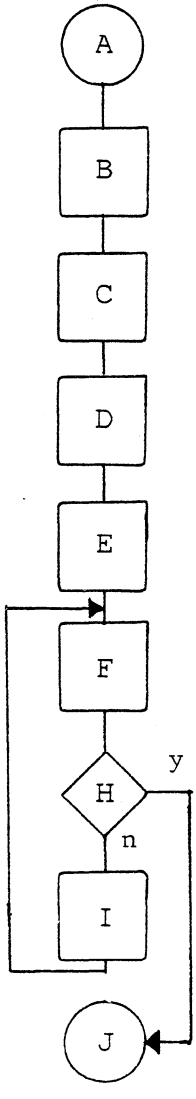

Q.FOR

A - Start

B - Enter the wavelength

C - Get beginning size for the calc.

D - Get ending size for the calc.

E - Get size increment of calc.

F - Calculate Q value

G - Output size and Q value

H - Done calculation for last size?

I - Increment size variable

J - End

Q.FOR

```
C       CALCULATE Q VALUES FOR SIZE REGION SPECIFIED
        COMMON WLA, DIAM, Q
        TYPE 100
C       GET WAVELENGTH
        ACCEPT 110, WLA
        TYPE 160
C       SMALLEST SIZE TO START Q CALCULATIONS
        ACCEPT 170, PSLO
        TYPE 180
C       LARGEST SIZE TO END Q CALCULATIONS
        ACCEPT 190, PSHI
        TYPE 200
C       INCREMENT OF CALCULATIONS
        ACCEPT 210, STEP
C       CALCULATE Q VALUE
        PS=PSLO
5       DIAM=PS
        CALL SCAT
        TYPE 240, PS, Q
        IF (PSHI-PS) 310,310,300
300     PS=PS + STEP
        GOTO 5
100     FORMAT ('WAVELENGTH -? ')
110     FORMAT (F10.3)
160     FORMAT ('SMALLEST PART. SIZE TO START CALC. - ? ')
170     FORMAT (F12.5)
180     FORMAT ('LARGEST PARTICLE SIZE TO END CALC. - ? ')
190     FORMAT (F12.5)
200     FORMAT ('INCREMENT FOR PARTICLE SIZE CALC. - ? ')
210     FORMAT (F10.5)
240     FORMAT(     F10.3,           F12.3)
310     END
```

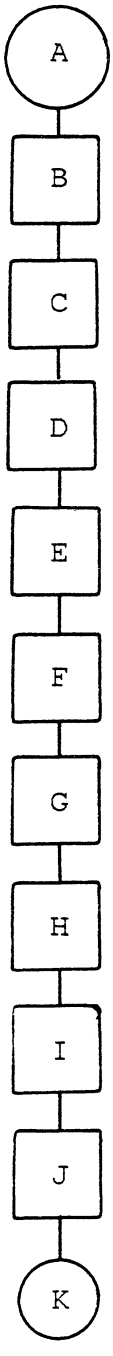

RATIO.FOR

A - Start

B - Enter the shortest wavelength

C - Enter the longest wavelength

D - Enter Tau ratio

E - Get beginning size for the calc.

F - Get ending size for the calc.

G - Get size increment of calc.

H - Calculate Q for first wavelength

I - Calculate Q for second wavelength

J - Calculate Q ratio store in TEMP

K - continued

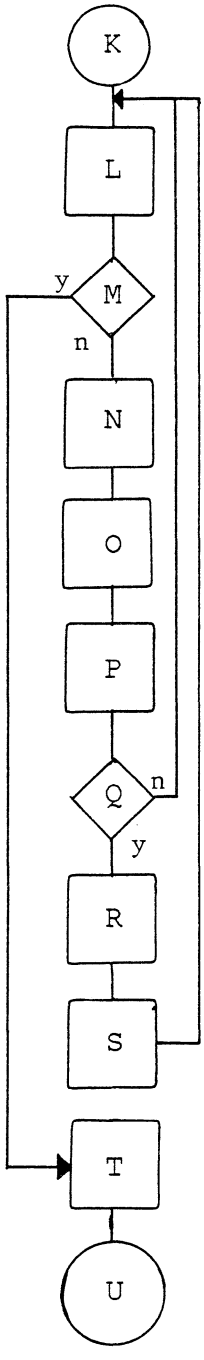

RATIO.FOR (cont.)

K - continue

L - Increment size

M - Done calc. for last size ?

N - Calculate Q for first wavelength

O - Calculate Q for second wavelength

P - Calculate new Q ratio

Q - New Q ratio closer to Tau ratio ?

R - Update TEMP

S - Store SIZE

T - Output SIZE

U - End

RATIO.FOR

```
C       FROM TWO SPECIFIED WAVELENGTHS AND THE
C       EXPERIMENTALLY DETERMINED TAU RATIO
C       FIND THE DIAMETER WHICH GIVES THE
C       CLOSEST Q RATIO
C
        COMMON WLA, DIAM, Q
C
C       ENTER THE SHORTEST WAVELENGTH
C
        TYPE 100
        ACCEPT 110, WLLO
C
C       ENTER THE LONGEST WAVELENGTH
C
        TYPE 120
        ACCEPT 130, WLHI
C
C       ENTER THE TAU RATIO
C
        TYPE 140
        ACCEPT 150, TAU
C
C       ENTER THE SMALLEST SIZE TO START CALC.
C
        TYPE 160
        ACCEPT 170, PSLO
C
C       ENTER THE LARGEST SIZE TO END CALC.
C
        TYPE 180
        ACCEPT 190, PSHI
C
C       ENTER THE SIZE INCREMENT FOR THE CALC.
C
        TYPE 200
        ACCEPT 210, STEP
        WLA=WLLO
        DIAM=PSLO
        PS = PSLO
        CALL SCAT
        Q1=Q
        WLA=WLHI
        CALL SCAT
        Q2=Q
        QRAT=Q1/Q2
        TEMP=ABS(QRAT-TAU)
        SIZE=PSLO
```

```
5       PS=(PS + STEP)
6       IF (PSHI-PS) 300,300,7
7       WLA=WLLO
        DIAM=PS
        CALL SCAT
        Q1=Q
        WLA=WLHI
        CALL SCAT
        Q2=Q
        QRAT=Q1/Q2
        DIFF=ABS(QRAT - TAU)
        IF (DIFF - TEMP) 8,8,5
8       TEMP = DIFF
        SIZE = PS
        GOTO 5
300     TYPE 220, SIZE
100     FORMAT ('WAVELENGTH WITH LARGEST TAU (WLLO) -? ')
110     FORMAT (F10.3)
120     FORMAT ('WAVELENGTH WITH SMALLEST TAU (WLHI) -? ')
130     FORMAT (F10.3)
140     FORMAT ('TAU RATIO CALCULATED FROM TAU VALUES -?)
150     FORMAT (F12.5)
160     FORMAT ('SMALLEST PART. SIZE TO START CALC. - ? ')
170     FORMAT (F12.5)
180     FORMAT ('LARGEST PARTICLE SIZE TO END CALC. - ? ')
190     FORMAT (F12.5)
200     FORMAT ('INCREMENT FOR PARTICLE SIZE CALC. - ? ')
210     FORMAT (F10.5)
220     FORMAT ('   DIAMETER =', F12.5)
310     END
```

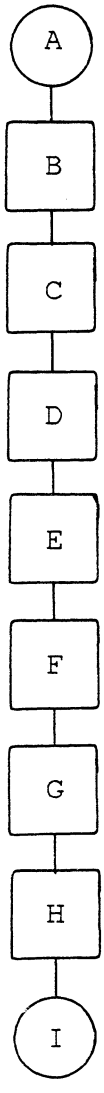

LPE.FOR

A - Start

B - Accept input of Q values

C - Take transpose of Q

D - Multiply Q by Q t = ATA

E - Invert ATA and return new ATA

F - Multiply ATA by Q t and return G

G - Multiply G by T to get N

H - Output N , the conc. vector.

I - End

LPE.FOR

```
C       DO THE LINEAR PARAMETER ESTIMATION LEAST
C       SQUARES CALCULATIONS GIVEN THE Q MATRIX, AND
C       THE TAU VALUE MATRIX.
        DOUBLE PRECISION A,TA,ATA,G,T,B
        DIMENSION A(9,3),TA(3,9),ATA(3,3),G(3,9),
        DIMENSION T(9,1),B(3,1)
C       TYPE IN THE Q MATRIX VALUES
        ACCEPT 3, A
3       FORMAT(D12.5)
        TYPE 5,A
5       FORMAT(9D12.5)
C
C       TAKE TRANSPOSE OF Q MATRIX
C
        CALL POSE (A,TA)
        TYPE 25, TA
25      FORMAT(3D12.5)
C
C       MULTIPLE Q TRANSPOSE BY Q
C
        CALL M1MUL2 (TA,A,ATA)
        TYPE 28, ATA
28      FORMAT(3D12.5)
C
C       INVERT Q TRANSPOSE  * Q RESULT
C
        CALL INVERT (ATA)
        TYPE 30,ATA
30      FORMAT(3D12.5)
C
C       MULTIPLE RESULT OF INVERSION BY Q TRANSPOSE
C
        CALL M2MUL2 (ATA,TA,G)
        TYPE 35,G
35      FORMAT(3D12.5)
        ACCEPT 40,T
40      FORMAT(1D12.5)
C
C       MULTIPLE (QTQ)-1QT RESULT BY TAU VECTOR
C
        CALL M3MUL2 (G,T,B)
C
C       OUTPUT FINAL RESULT OF LPE
C
        TYPE 50,B
50      FORMAT(3D12.5)
        END
```

POSE.FOR

```
C       SUBROUTINE TO TAKE TRANSPOSE OF Q MATRIX
        SUBROUTINE POSE (A,TA)
        DOUBLE PRECISION A, TA
        DIMENSION A(9,3),TA(3,9)
C       INITIALIZE TA MATRIX
        DO 15 I=1,3
        DO 10 J=1,9
        TA(I,J)=0
10      CONTINUE
15      CONTINUE
C       TRANSPOSE MATRIX AND STORE IN TA
        DO 60 I=1,9
        DO 55 J=1,3
        TA(J,I)=A(I,J)
55      CONTINUE
60      CONTINUE
        RETURN
        END
```

M1MUL.FOR

```
C       SUBROUTINE TO MULTIPLY TWO MATICES
C       MULTIPLY Q TRANSPOSE BY Q
        SUBROUTINE M1MUL2 (A,B,D)
        DOUBLE PRECISION A,B,D
        DIMENSION A(3,9),B(9,3),D(3,3)
C       INITIALIZE D MATRIX
        DO 30 I=1,3
        DO 35 J=1,3
        D(I,J)=0.
35      CONTINUE
30      CONTINUE
C       MULTIPLY AND LEAVE RESULTS IN D
        DO 100 I=1,3
        DO 100 J=1,3
        DO 100 L=1,9
        D(I,J)=A(I,L)*B(L,J)+D(I,J)
100     CONTINUE
        RETURN
        END
```

M2MUL.FOR

```
C       SUBROUTINE TO MULTIPLY TWO MATICES
C       MULTIPLY THE INVERTED RESULT BY Q TRANSPOSE
        SUBROUTINE M2MUL2 (A,B,D)
        DOUBLE PRECISION A,B,D
        DIMENSION A(3,3),B(3,9),D(3,9)
C       INITIALIZE D MATRIX
        DO 40 I=1,3
        DO 35 J=1,9
        D(I,J)=0.
35      CONTINUE
40      CONTINUE
C       MULTIPLY AND LEAVE RESULTS IN D
        DO 100 I=1,3
        DO 100 J=1,9
        DO 100 L=1,3
        D(I,J)=A(I,L)*B(L,J)+D(I,J)
100     CONTINUE
        RETURN
        END
```

M3MUL.FOR

```
C       SUBROUTINE TO MULTIPLY TWO MATICES
C       MULTIPLY (QTQ)-1QT RESULT BY TAU MATRIX
        SUBROUTINE M3MUL2 (A,B,D)
        DOUBLE PRECISION A,B,D
        DIMENSION A(3,9),B(9,1),D(3,1)
C       INITIALIZE D MATRIX
        J=1
        DO 40 I=1,3
        D(I,J)=0.
40      CONTINUE
C       MULTIPLY AND LEAVE RESULTS IN D
        J=1
        DO 100 I=1,3
        DO 100 L=1,9
        D(I,J)=A(I,L)*B(L,J)+D(I,J)
100     CONTINUE
        RETURN
        END
```

3INV.FOR

```
C       SUBROUTINE TO DETERMINE INVERSE OF A MATRIX
C       TAKE INVERSE OF Q TRANSPOSE Q PRODUCT
C       THIS ROUTINE WAS DEVELOPED BY SHAN S. KUO
C       AND APPEARED IN HIS BOOK "NUMERICAL METHODS AND
C       COMPUTERS", ADDISON-WESLEY, READING, MASS.
C       PP. 168-169 (1965)
        SUBROUTINE INVERT (A)
        DOUBLE PRECISION A,B,PIVOT,DET,T
        DIMENSION A(3 ,3),B(3,3),IPVOT(3)
        DIMENSION INDEX(3,2),PIVOT(3)
        COMMON IPVOT,INDEX,PIVOT
C       INITIALIZE IPVOT
        DO 10 J=1,3
10      IPVOT(J)=0
        DO 100 I=1,3
C       SEARCH FOR PIVOT ELEMENT
        T=0.
        DO 13 J=1,3
        IF (IPVOT(J)-1) 11,13,11
11      DO 23 K=1,3
        IF (IPVOT(K)-1) 21,23,31
21      IF (ABS(T)-ABS(A(J,K))) 33,23,23
33      IROW=J
        JCOL=K
        T=A(J,K)
23      CONTINUE
13      CONTINUE
        IPVOT(JCOL)=IPVOT(JCOL)+1
C       PUT PIVOT ELEMENT ON THE DIAGONAL
        IF (IROW-JCOL) 73,109,73
73      DET=-DET
        DO 30 L=1,3
        T=A(IROW,L)
        A(IROW,L)=A(JCOL,L)
30      A(JCOL,L)=T
109     INDEX(I,1)=IROW
        INDEX(I,2)=JCOL
        PIVOT(I)=A(JCOL,JCOL)
C       DIVIDE PIVOT ROW BY PIVOT ELEMENT
        A(JCOL,JCOL)=1.
        DO 50 L=1,3
50      A(JCOL,L)=A(JCOL,L)/PIVOT(I)
C       REDUCE NON-PIVOT ROWS
        DO 100 LI=1,3
        IF (LI-JCOL) 65,100,65
65      T=A(LI,JCOL)
        A(LI,JCOL)=0.
```

```
        DO 70 L=1,3
70      A(LI,L)=A(LI,L)-A(JCOL,L)*T
100     CONTINUE
C       INTERCHANGE COLUMNS?
        DO 80 I=1,3
        L=3-I+1
        IF (INDEX(L,1)-INDEX(L,2)) 85,80,85
85      JROW=INDEX(L,1)
        KCOL=INDEX(L,2)
        DO 90 K=1,3
        T=A(K,JROW)
        A(K,JROW)=A(K,KCOL)
        A(K,KCOL)=T
90      CONTINUE
80      CONTINUE
31      RETURN
        END
```

NNLS.FOR

```
C       THIS PROGRAM WILL SOLVE A LEAST SQUARES PROBLEM
C       WITH THE CONSTRAINT THAT THE SOLUTION VECTOR MUST
C       CONTAIN VALUES GREATER THAN OR EQUAL TO 0.
C       THIS PROGRAM AND THE SUBPROGRAMS THAT THIS ROUTINE
C       CALL WERE OBTAINED FROM DR. DAVID LEGGETT AT
C       DOW CHEMICAL, FREEPORT TEXAS.
C       THESE PROGRAMS WERE ORIGINALLY DEVELOPED AND
C       WRITTEN BY C.L. LAWSON AND R.J. HANSON
C       "SOLVING LEAST SQUARES PROBLEMS",
C       PRENTICE-HALL, ENGLEWOOD CLIFFS, N. J.
C       PP. 304-330 (1974)
        SUBROUTINE NNLS (A,MDA,M,N,B,X,RNORM,W,ZZ,DUMMY,
     &INDEX,MODE,NSOLNS,NETACL,NWVLS)
        DIMENSION A(NSOLNS,NETACL),INDEX(NETACL),
        DIMENSION W(NETACL), X(NETACL), DUMMY(NSOLNS),
        DIMENSION B(NWVLS),ZZ(NSOLNS)
        ZERO=0.
        ONE=1.
        TWO=2.
        FACTOR=0.01
        MODE=1
        IF(M.GT.0.AND.N.GT.0) GO TO 10
        MODE=2
        RETURN
10      ITER=0
        ITMAX=3*N
C
C       INITIALIZE THE ARRAYS INDEX() AND X()
C
        DO 20 I=1,N
        X(I)=ZERO
20      INDEX(I)=I
        IZ2=N
        IZ1=1
        NSETP=0
        NPP1=1
C
C       MAIN LOOP BEGINS HERE
C
30      CONTINUE
C
        IF(IZ1.GT.IZ2.OR.NSETP.GE.M) GO TO 350
        DO 50 IZ =IZ1,IZ2
        J=INDEX(IZ)
        SM=ZERO
        DO 40 L=NPP1,M
40      SM=SM+A(L,J)*B(L)
```

```
50      W(J)=SM
C
C       FIND LARGEST POSITIVE W(J)
C
60      WMAX=ZERO
        DO 70 IZ=IZ1,IZ2
        J=INDEX(IZ)
        IF(W(J)-WMAX)70,70,71
71      WMAX=W(J)
        IZMAX=IZ
70      CONTINUE
C
C       IF WMAX.LE.0. GO TO TERMINATION
C
        IF(WMAX)350,350,80
80      IZ=IZMAX
        J=INDEX(IZ)
C
C       THE SIGN OF W(J)
C
        ASAVE=A(NPP1,J)
        CALL H12 (1,NPP1,NPP1+1,M,A(1,J),1,UP,
     &DUMMY, 1,1,0,NSOLNS,NETACL,NSOLNS)
        UNORM=ZERO
        IF(NSETP.EQ.0) GO TO 100
        DO 90 L=1,NSETP
90      UNORM=UNORM+A(L,J)**2
100     UNORM=SQRT(UNORM)
        DIFF1=UNORM+DABS(A(NPP1,J))*FACTOR-UNORM
        IF(DIFF1)130,130,110
110     DO 120 L=1,M
120     ZZ(L)=B(L)
        CALL H12 (2,NPP1,NPP1+1,M,A(1,J),1,UP,ZZ,
     &1,1,1,NSOLNS,NETACL,NSOLNS)
        ZTEST=ZZ(NPP1)/A(NPP1,J)
C
C       SEE IF Z TEST IS POSITIVE
C
        IF(ZTEST)130,130,140
C
130     A(NPP1,J)=ASAVE
        W(J)=ZERO
        GO TO 60
C
140     DO 150 L=1,M
150     B(L)=ZZ(L)
        INDEX(IZ)=INDEX(IZ1)
        INDEX(IZ1)=J
        IZ1=IZ1+1
        NSETP=NPP1
        NPP1=NPP1+1
```

```
      IF(IZ1.GT.IZ2) GO TO 170
      DO 160 JZ=IZ1,IZ2
      JJ=INDEX(JZ)
160   CALL H12 (2,NSETP,NPP1,M,A(1,J),1,UP,A(1,JJ),
     &1,MDA,1,NETACL,NETACL,NSOLNS)
170   CONTINUE
      IF(NSETP.EQ.M) GO TO 190
      DO 180 L=NPP1,M
180   A(L,J)=ZERO
190   CONTINUE
      W(J)=ZERO
C
C     SOLVE THE TRIANGULAR SYSTEM
C
      ASSIGN 200 TO NEXT
      GO TO 400
200   CONTINUE
C
C     SECONDARY LOOP BEGINS HERE
C
210   ITER=ITER+1
      IF(ITER.LE.ITMAX) GO TO 220
      MODE=3
      TYPE 440
      GO TO 350
220   CONTINUE
      ALPHA=TWO
      DO 240 IP=1,NSETP
      L=INDEX(IP)
      IF(ZZ(IP))230,230,240
230   T=-X(L)/(ZZ(IP)-X(L))
      IF(ALPHA-T)240,240,241
241   ALPHA=T
      JJ=IP
240   CONTINUE
      IF(ALPHA-TWO)242,330,242
242   DO 250 IP=1,NSETP
      L=INDEX(IP)
250   X(L)=X(L)+ALPHA*(ZZ(IP)-X(L))
C
C     MODIFY A AND B AND THE INDEX
C
      I=INDEX(JJ)
260   X(I)=ZERO
      IF(JJ.EQ.NSETP) GO TO 290
      JJ=JJ+1
      DO 280 J=JJ,NSETP
      II=INDEX(J)
      INDEX(J-1)=II
      CALL G1 (A(J-1,II),A(J,II),CC,SS,A(J-1,II))
      A(J,II)=ZERO
```

```
      DO 270 L=1,N
      IF(L.NE.II) CALL G2 (CC,SS,A(J-1,L),A(J,L))
270   CONTINUE
280   CALL G2 (CC,SS,B(J-1),B(J))
290   NPP1=NSETP
      NSETP=NSETP-1
      IZ1=IZ1-1
      INDEX(IZ1)=I
C
C     SEE IF THE REMAINING COEFCIENTS
C
      DO 300 JJ=1,NSETP
      I=INDEX(JJ)
      IF(X(I))260,260,300
300   CONTINUE
C
C     COPY B() INTO ZZ()
C
      DO 310 I=1,M
310   ZZ(I)=B(I)
      ASSIGN 320 TO NEXT
      GO TO 400
320   CONTINUE
      GO TO 210
C
C     END OF SECONDARY LOOP
C
330   DO 340 IP=1,NSETP
      I=INDEX(IP)
340   X(I)=ZZ(IP)
C
C     ALL NEW
C
      GO TO 30
C
C     END OF MAIN LOOP
C
350   SM=ZERO
      IF(NPP1.GT.M) GO TO 370
      DO 360 I=NPP1,M
360   SM=SM+B(I)**2
      GO TO 390
370   DO 380 J=1,N
380   W(J)=ZERO
390   RNORM=SQRT(SM)
      RETURN
C
C     THE FOLLOWING
C
400   DO 430 L=1,NSETP
      IP=NSETP+1-L
```

```
      IF(L.EQ.1) GO TO 420
      DO 410 II=1,IP
410   ZZ(II)=ZZ(II)-A(II,JJ)*ZZ(IP+1)
420   JJ=INDEX(IP)
430   ZZ(IP)=ZZ(IP)/A(IP,JJ)
      GO TO NEXT,(200,320)
440   FORMAT(//2X' NNLS QUITTING ON ITERATION COUNT.')
      END
```

H12.FOR

```
C     HOUSEHOLDER TRANSFORMATION SUBROUTINE FOR
C     THE NON-NEGATIVE LEAST SQUARES PROGRAM
C     C. L. LAWSON, R. J. HANSON, "SOLVING LEAST SQUARES
C     PROBLEMS", PRENTICE-HALL, ENGLEWOOD CLIFFS, N. J.
C     PP. 304-330 (1974).
      SUBROUTINE H12 (MODE,LPIVOT,L1,M,U,IUE,UP,C,
     &ICE,ICV,NCV,NDIM,NETACL,NSOLNS)
      DIMENSION U(1,NETACL),C(NSOLNS)
      ONE=1.0
      IF(0.GE.LPIVOT.OR.LPIVOT.GE.L1.OR.L1.GT.M)RETURN
      CL=DABS(U(1,LPIVOT))
      IF(MODE.EQ.2) GO TO 60
C
C     CONSTRUCT THE TRANSFORM
C
      DO 10 J=L1,M
10    CL=DMAX1(DABS(U(1,J)),CL)
      IF(CL)130,130,20
20    CLINV=ONE/CL
      SM=((U(1,LPIVOT))*CLINV)**2
      DO 30 J=L1,M
30    SM=SM+((U(1,J))*CLINV)**2
      SM1=SM
      CL=CL*SQRT(SM1)
      IF(U(1,LPIVOT))50,50,40
40    CL=-CL
50    UP=U(1,LPIVOT)-CL
      U(1,LPIVOT)=CL
      GO TO 70
C
C     APPLY THE TRANSFORM
C
60    IF(CL)130,130,70
70    IF(NCV.LE.0)RETURN
      B=(UP)*U(1,LPIVOT)
C
C     B MUST BE NONPOSTIVE HERE
C
      IF(B)80,130,130
80    B=ONE/B
      I2=1-ICV+ICE*(LPIVOT-1)
      INCR=ICE*(L1-LPIVOT)
      DO 120 J=1,NCV
      I2=I2+ICV
      I3=I2+INCR
      I4=I3
      SM=C(I2)*(UP)
```

```
      DO 90 I=L1,M
      SM=SM+C(I3)*(U(1,I))
90    I3=I3+ICE
      IF(SM)100,120,100
100   SM=SM*B
      C(I2)=C(I2)+SM*(UP)
      DO 110 I=L1,M
      C(I4)=C(I4)+SM*(U(1,I))
110   I4=I4+ICE
120   CONTINUE
130   RETURN
      END
```

G1.FOR

```
C     COMPUTE ORTHOGONAL ROTATION MATRIX
C     C. L. LAWSON, R. J. HANSON, "SOLVING LEAST SQUARES
C     PROBLEMS", PRENTICE-HALL, ENGLEWOOD CLIFFS, N. J.,
C     PP. 304-330, (1974).
      SUBROUTINE G1 (A,B,COS,SIN,SIG)
C
      ZERO=0.0
      ONE=1.0
      IF(DABS(A).LE.DABS(B)) GO TO 10
      XR=B/A
      YR=SQRT(ONE+XR*XR)
      COS=SIGN(ONE/YR,A)
      SIN=COS*XR
      SIG=DABS(A)*YR
      RETURN
10    IF(B)20,30,20
20    XR=A/B
      YR=SQRT(ONE+XR*XR)
      SIN=SIGN(ONE/YR,B)
      COS=SIN*XR
      SIG=DABS(B)*YR
      RETURN
30    SIG=ZERO
      COS=ZERO
      SIN=ONE
      RETURN
      END
```

G2.FOR

```
C     APPLY THE ROTATION COMPUTED BY G1
C     C. L. LAWSON, R. J. HANSON, "SOLVING LEAST SQUARES
C     PROBLEMS", PRENTICE-HALL, ENGLEWOOD CLIFFS, N. J.
C     PP. 304-330, (1974).
C
      SUBROUTINE G2 (COS,SIN,X,Y)
C
      XR=COS*X+SIN*Y
      Y=-SIN*X+COS*Y
      X=XR
      RETURN
      END
```

The vita has been removed from the scanned document